FINAL REPORT OF A SCALABLE, AUTOMATED, SEMIPERMANENT SEISMIC ARRAY (SASSA) METHOD FOR DETECTING CO_2 EXTENT DURING GEOLOGIC CO_2 INJECTION

Deliverable D4 – Final Report
Task 3

(for the period October 1, 2016 – October 31, 2017)

Prepared for:

AAD Document Control

National Energy Technology Laboratory
U.S. Department of Energy
626 Cochrans Mill Road
PO Box 10940, MS 921-107
Pittsburgh, PA 15236-0940

Cooperative Agreement No. DE-FE0012665

Prepared by:

Shaughn A. Burnison
Amanda J. Livers-Douglas
Cesar Barajas-Olalde
Lu Jin
Olarinre Salako
Heidi M. Vettleson
John A. Hamling
Charles D. Gorecki

Energy & Environmental Research Center
University of North Dakota
15 North 23rd Street, Stop 9081
Grand Forks, ND 58202-9018

2017-EERC-12-02

December 2017

EERC DISCLAIMER

LEGAL NOTICE This research report was prepared by the Energy & Environmental Research Center (EERC), an agency of the University of North Dakota, as an account of work sponsored by the U.S. Department of Energy (DOE) National Energy Technology Laboratory. Because of the research nature of the work performed, neither the EERC nor any of its employees makes any warranty, express or implied, or assumes any legal liability or responsibility for the accuracy, completeness, or usefulness of any information, apparatus, product, or process disclosed or represents that its use would not infringe privately owned rights. Reference herein to any specific commercial product, process, or service by trade name, trademark, manufacturer, or otherwise does not necessarily constitute or imply its endorsement or recommendation by the EERC.

ACKNOWLEDGMENT

This material is based upon work supported by the U.S. Department of Energy, National Energy Technology Laboratory under Award Number DE-FE0012665.

DOE DISCLAIMER

This report was prepared as an account of work sponsored by an agency of the United States Government. Neither the United States Government, nor any agency thereof, nor any of their employees, makes any warranty, express or implied, or assumes any legal liability or responsibility for the accuracy, completeness, or usefulness of any information, apparatus, product, or process disclosed, or represents that its use would not infringe privately owned rights. Reference herein to any specific commercial product, process, or service by trade name, trademark, manufacturer, or otherwise does not necessarily constitute or imply its endorsement, recommendation, or favoring by the United States Government or any agency thereof. The views and opinions of authors expressed herein do not necessarily state or reflect those of the United States Government or any agency thereof.

FINAL REPORT OF A SCALABLE, AUTOMATED, SEMIPERMANENT SEISMIC ARRAY (SASSA) METHOD FOR DETECTING CO_2 EXTENT DURING GEOLOGIC CO_2 INJECTION

ABSTRACT

The scalable, automated, semipermanent seismic array (SASSA) project led and managed by the Energy & Environmental Research Center (EERC) was designed as a 3-year proof-of-concept study to evaluate and demonstrate an innovative application of the seismic method. The concept was to use a sparse surface array of 96 nodal seismic sensors paired with a single, remotely operated active seismic source at a fixed location to monitor for CO_2 saturation changes in a subsurface reservoir by processing the data for time-lapse changes at individual, strategically chosen reservoir reflection points. The combination of autonomous equipment and modern processing algorithms was used to apply the seismic method in a manner different from the normal paradigm of collecting a spatially dense data set to produce an image. It was used instead to monitor individual, strategically chosen reservoir reflection points for detectable signal character changes that could be attributed to the passing of a CO_2 saturation front or, possibly, changes in reservoir pressure.

Data collection occurred over the course of 1 year at an oil field undergoing CO_2 injection for enhanced oil recovery (EOR) and focused on four overlapping "five-spot" EOR injector–producer patterns. Selection, procurement, configuration, installation, and testing of project equipment and collection of five baseline data sets were completed in advance of CO_2 injection within the study area. Weekly remote data collection produced 41 incremental time-lapse records for each of the 96 nodes. Validation was provided by two methods: 1) a conventional 2-D seismic line acquired through the center of the study area before injection started and again after the project ended and processed in a time-lapse manner and 2) by CO_2 saturation maps created from reservoir simulations based on injection and production history matching.

Interpreted results were encouraging but mixed, with indications of changes likely due to the presence of CO_2 on some node reflection points where and when effects would be expected and noneffects where no CO_2 was expected, while results at some locations where simulation outputs suggested CO_2 should be present were ambiguous. Acquisition noise impacted interpretation of data at several locations. Many lessons learned were generated by the study to inform and improve results on a follow-up study. The ultimate aim of the project was to evaluate whether deployment of a SASSA technology can provide a useful and cost-effective monitoring solution for future CO_2 injection projects. The answer appears to be affirmative, with the expectation that lessons learned applied to future iterations, together with technology advances, will likely result in significant improvements.

TABLE OF CONTENTS

Continued . . .

TABLE OF CONTENTS (continued)

LIST OF FIGURES

Continued . . .

LIST OF FIGURES (continued)

Continued . . .

LIST OF FIGURES (continued)

LIST OF TABLES

FINAL REPORT OF A SCALABLE, AUTOMATED, SEMIPERMANENT SEISMIC ARRAY (SASSA) METHOD FOR DETECTING CO_2 EXTENT DURING GEOLOGIC CO_2 INJECTION

EXECUTIVE SUMMARY

The scalable, automated, semipermanent seismic array (SASSA) project led and managed by the Energy & Environmental Research Center (EERC) was designed as a 3-year proof-of-concept study to evaluate and demonstrate an innovative application of the seismic method. This was accomplished by using a sparse surface array of nodal seismic sensors paired with a single, remotely operated active seismic source at a fixed location to monitor for CO_2 saturation changes in a subsurface reservoir by monitoring for time-lapse changes at individual, strategically chosen reservoir reflection points. The application differs from the normal paradigm of collecting a spatially dense data set to produce an image. Instead, standard time-lapse processing and innovative displays of incremental monitor trace data for individual receiver locations were analyzed for signal character changes that could be attributed to the passing of a CO_2 saturation front or, possibly, changes in reservoir pressure. Monitoring was done in a low-impact, cost-effective manner, remotely, with the future intention of automating as many of the processes as possible.

Data collection occurred over the course of 1 year at the Bell Creek oil field in southeastern Montana, an oil field undergoing CO_2 injection for enhanced oil recovery (EOR), and focused on four overlapping "five-spot" EOR injector–producer patterns. Selection, procurement, configuration, installation, and testing of project equipment and collection of five baseline data sets were completed in advance of CO_2 injection within the study area. Weekly remote data collection produced 41 incremental time-lapse records for each of the 96 nodes.

CO_2 injection data and the reservoir simulation results showed that saturation distributions in the study area progressed unevenly and that only a subset of the 96 node midpoints could be expected to show character changes due to the presence of CO_2. While all node data were processed, data from twenty-six nodes were selected for in-depth analysis. The data sets were affected by several types of seismic noise which presented processing and interpretation challenges. Weather and the cultural noise associated with an active oil field were the most challenging because of their temporal and spatial variability.

Interpretation results were encouraging, but mixed. Several nodes appear to show seismic reflection character changes indicative of the presence of CO_2, while other nodes with corresponding reflection points where no CO_2 was expected showed no effect. However, there are nodes where a CO_2 effect is expected but not forthcoming and one where no effect is expected that exhibits a compelling positive response (Figure ES-1). Validation methods from reservoir simulations and a time-lapse 2-D line acquired through the middle of the study area helped the interpretation but have not fully removed ambiguity.

The ultimate aim of the project was to evaluate whether deployment of SASSA technology can provide a cost-effective monitoring solution for future CO_2 injection projects.

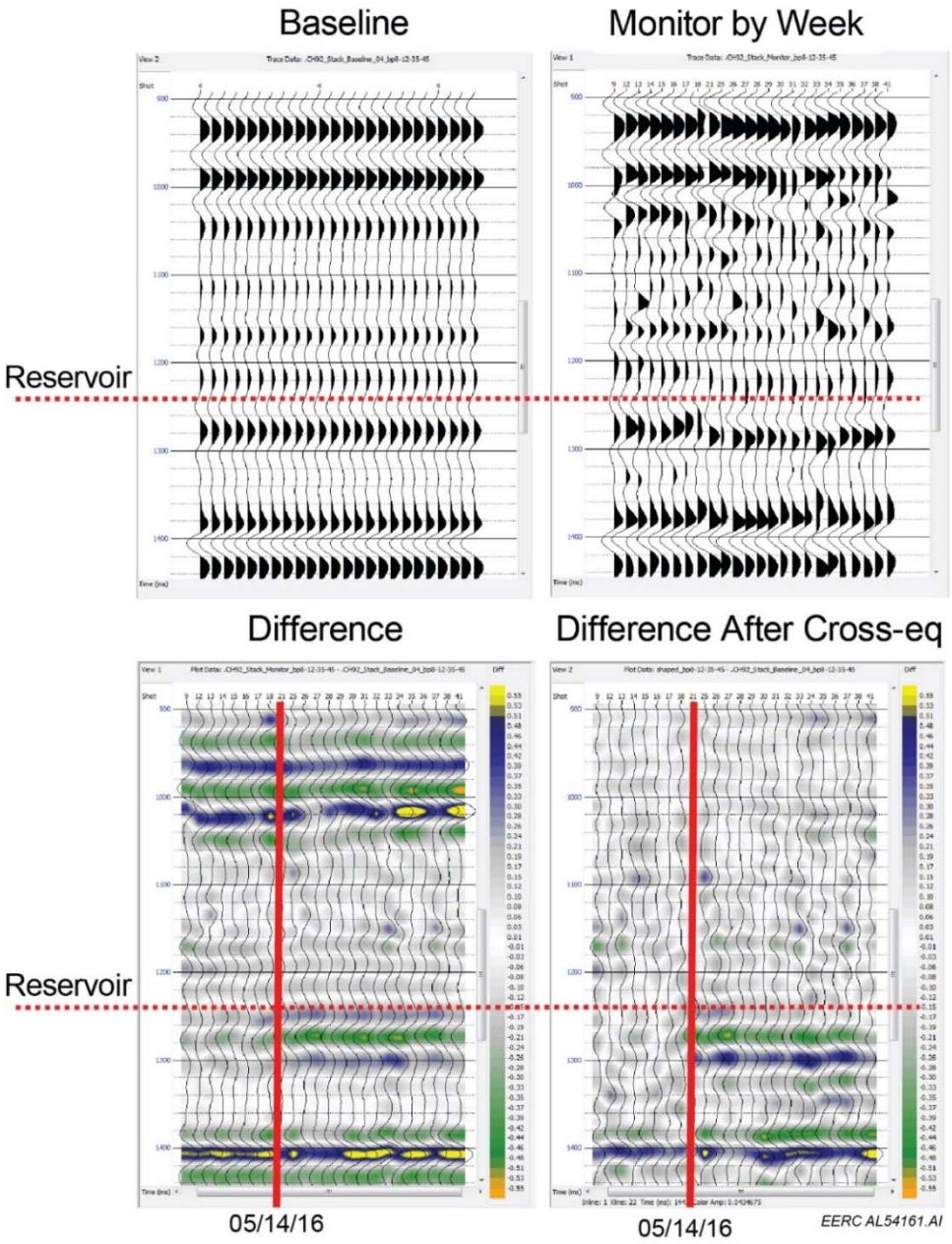

Figure ES-1. Time-lapse difference results for Channel 92 before and after cross equalization. The interpreted reservoir level is indicated. The monitored location is 1000 feet south of a well that started CO_2 injection in January 2016. The vertical red line marks May 14, 2016, when a visible change at the reservoir is observed. The difference corresponds to a decrease in amplitude of a seismic reflection, which matches expectations of what a CO_2 effect would look like.

Current results and expected improvements from future application of the many lessons learned from this pilot study suggest that SASSA is a viable monitoring technology for certain geologic settings. Future iterations and technology advances will likely produce significant improvements and efficiencies in the SASSA method.

FINAL REPORT OF A SCALABLE, AUTOMATED, SEMIPERMANENT SEISMIC ARRAY (SASSA) METHOD FOR DETECTING CO_2 EXTENT DURING GEOLOGIC CO_2 INJECTION

BACKGROUND AND OVERVIEW

The scalable, automated, semipermanent seismic array (SASSA) project led and managed by the Energy & Environmental Research Center (EERC) was designed as a 3-year proof-of-concept study to evaluate and demonstrate an innovative way of deploying a sparse surface array of flexible nodal seismic sensors paired with a single, remotely operated active seismic source at a fixed location. The objective was to incrementally monitor the course of CO_2 saturation fronts in a subsurface reservoir from the surface at an oil field undergoing CO_2 injection for enhanced oil recovery (EOR) and do so in a low-impact, cost-effective manner remotely, with the future intention of automating as many processes as possible. The combination of flexible autonomous equipment and sophisticated modern processing algorithms was used to apply the seismic method in a manner different from the normal paradigm of collecting a spatially dense data set to produce an image. The SASSA method instead monitors individual, strategically chosen reservoir reflection points for detectable signal character changes that could be attributed to the passing of a CO_2 saturation front (Figure 1). Data collection and processing occurred over the course of a year to see when and where the CO_2 saturation front had progressed was to provide actionable information to the field operator, as well as data that could be used to improve the accuracy of reservoir simulations. This incremental information would then be used to help decide the timing of larger and more expensive, higher-impact monitoring methods such as 3-D seismic surveys. The ultimate aim of the project was to evaluate whether the deployment of SASSA technology could provide an effective solution for monitoring CO_2 in geologic environments.

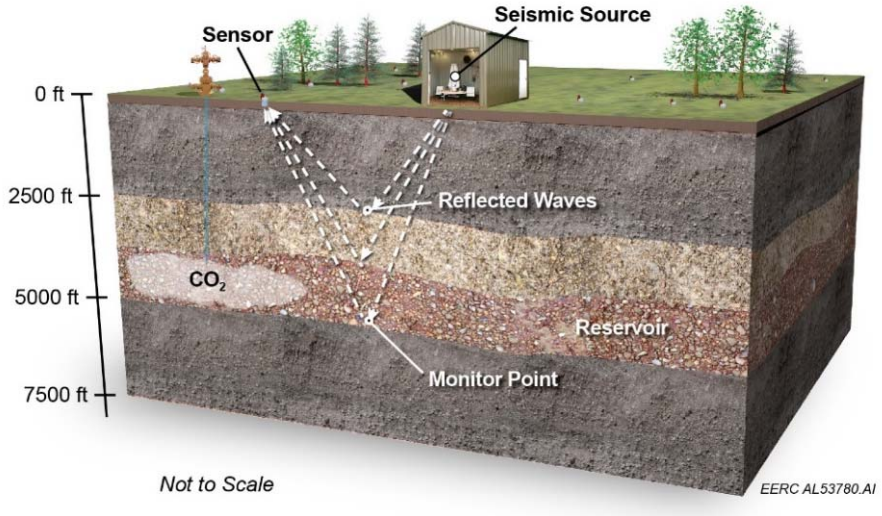

Figure 1. Schematic illustrating the SASSA concept. Seismic wave raypaths are depicted from the fixed source to a single receiver at the surface. If injected CO_2 moves across the raypaths, the character of data recorded at the surface receiver will change (Livers and others, 2017).

Project Structure

Project execution commenced on October 1, 2013. The scope of work can be separated into two main parts and is summarized as follows:

1) Selection and procurement of project equipment, modeling to determine how the field experiments will be conducted, deployment and testing of the field system, acquisition of at least one baseline data set prior to the start of CO_2 injection in the study area, and documenting the technical design.

2) Data acquisition for 1 year while CO_2 injection in the field progressed, processing and interpretation of the collected data, comparison with reservoir simulations and the time-lapse 2-D survey validation methods, analysis of the applicability of the method, and reporting.

The scope is formalized into the project tasks:

Task 1.0 – Project Management, Planning, and Reporting

Task 2.0 – Evaluation, Planning, Optimization, and Deployment:
- Subtask 2.1 – Equipment Selection
- Subtask 2.2 – Modeling the Seismic Source with the Permanent Vertical Receiver Array
- Subtask 2.3 – Modeling the Seismic Source with the Surface Receiver Array
- Subtask 2.4 – Modeling with Both the Permanent and Semipermanent Receiver
- Subtask 2.5 – Source Location Preparation and Equipment Installation
- Subtask 2.6 – Testing and Optimization
- Subtask 2.7 – Predictive Simulation of CO_2 Plume Migration

Task 3.0 – Data Collection, Data Processing, and Interpretation:
- Subtask 3.1 – Continuous Data Collection
- Subtask 3.2 – Processing and Interpretation of the Collected Data
- Subtask 3.3 – Review of Results of the Case Study

This document, Deliverable D4 – Final Report, focuses on the data collected and its acquisition, processing, and interpretation. The technical design document, Deliverable D2 – Interim Report on Completion of Technical Design (Burnison and others, 2015) submitted at the end of Budget Period 1 and closing out the first part of the project scope described above, serves as a companion document. It describes in detail the design of the project data acquisition plan, the physical basis behind the concept, equipment selected and how it was installed, geophysical model building and array design, and the study area and its geology. When topics overlap, the reader is referred to the companion document for detail.

Project Study Area

The project study area was the Bell Creek oil field in southeastern Montana (Figure 2). The reservoir in the field is a clean sandstone within the Muddy Formation at a depth of about 4500 feet. The sandstone generally varies in thickness from 20 to 30 feet and is encased by siltstones and shales within the Muddy Formation, which is about 55 to 70 feet thick. The Muddy Formation acts as a thin-bed reflector, with the appearance of an entering trough followed immediately by an exiting peak and is easily interpretable in most areas of the field (Salako and others, 2017). However, in the SASSA study area, this reflection has very low amplitude, making interpretation of the reservoir challenging (Figure 3). Reservoir reflection time in the study area often must be inferred by measuring up or down from a higher amplitude reference reflector. A more complete description of the study area geology and reservoir reflection character is provided in Burnison and others (2014).

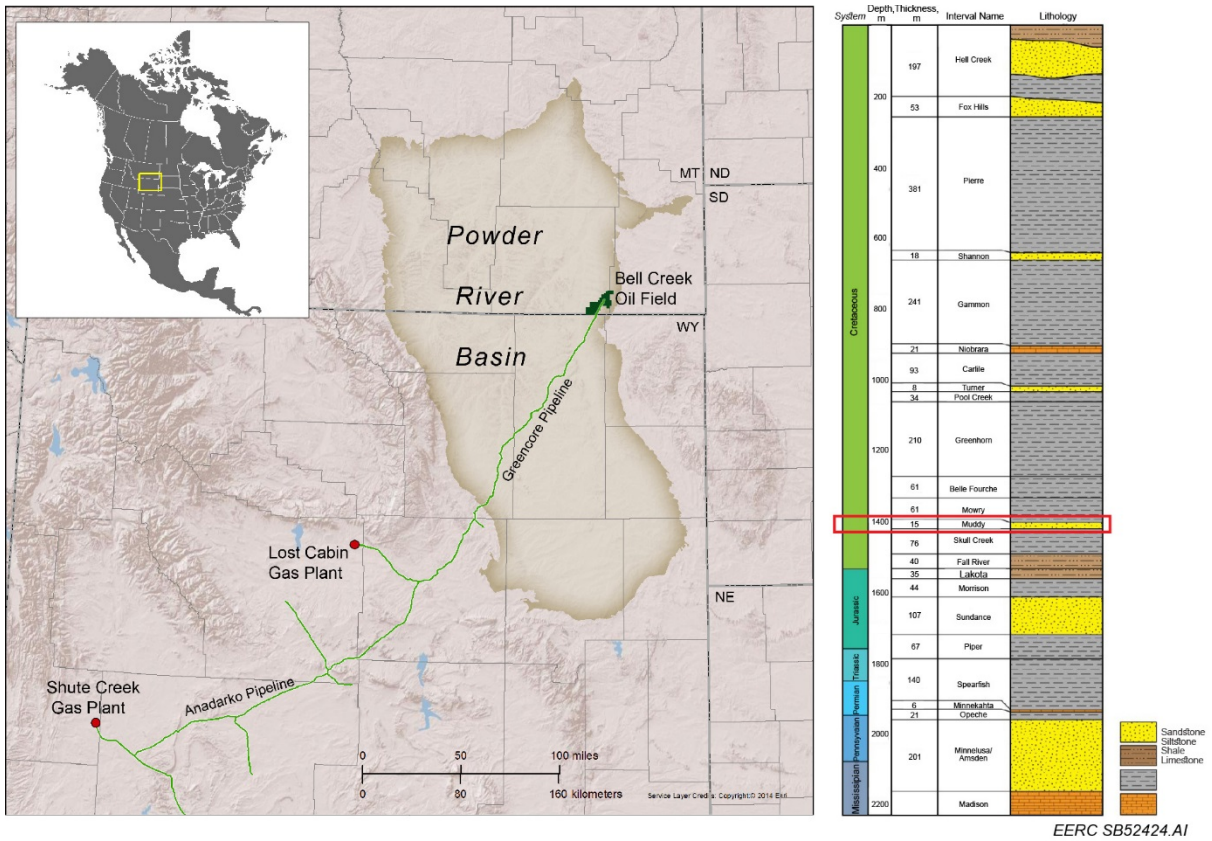

Figure 2. The Bell Creek oil field in southeastern Montana lies on the eastern edge of the Powder River Basin. CO_2 used for EOR is transported to the field by pipeline from ExxonMobil's Shute Creek and ConocoPhillips' Lost Cabin natural gas-processing plant (Burnison and others, 2017a). The target reservoir is within the Lower Cretaceous Muddy Formation as indicated by the red box on the stratigraphic column.

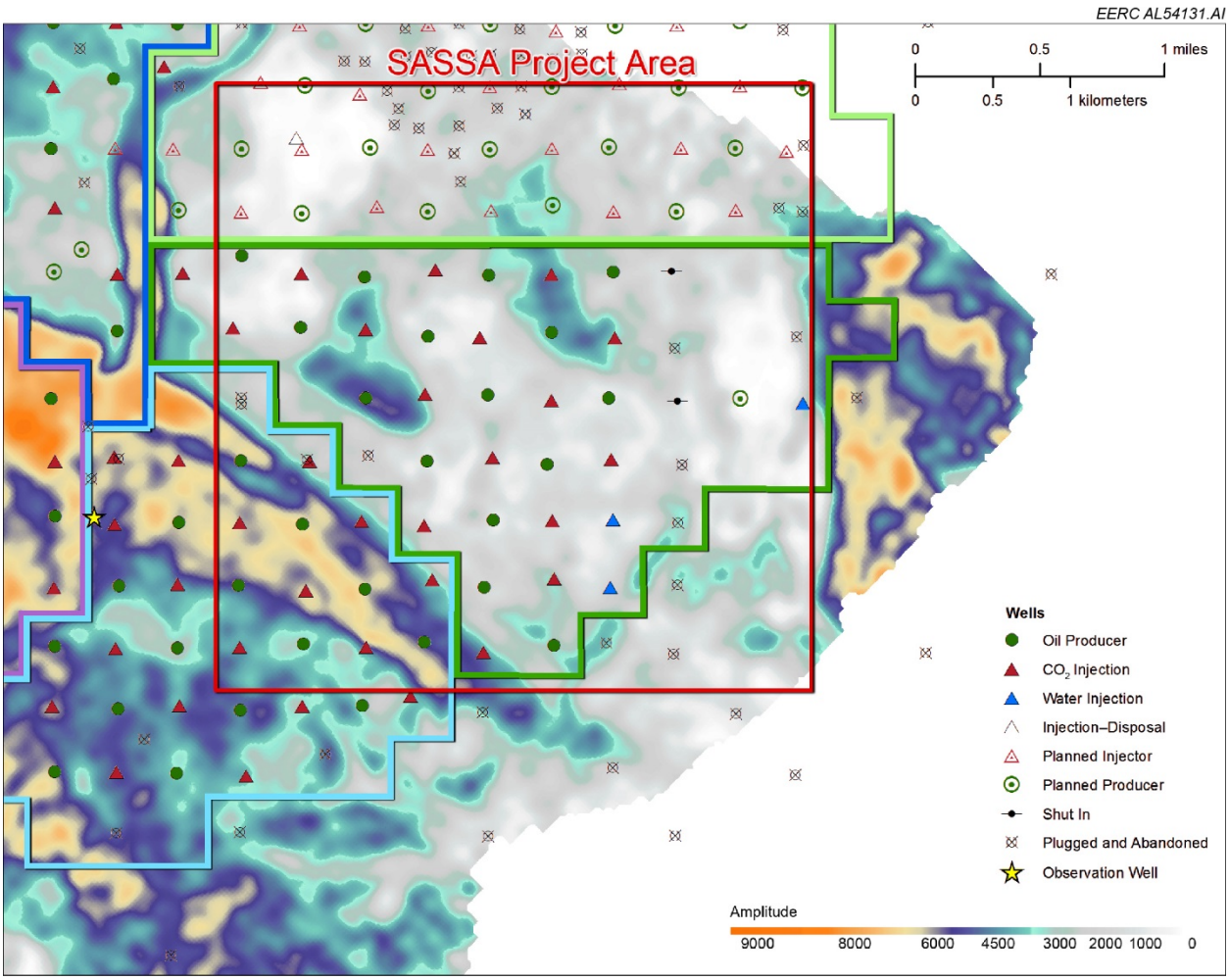

Figure 3. A map of the Muddy Formation seismic reflection amplitude over part of the Bell Creek oil field. Warmer colors indicate higher amplitudes, with white indicating near-zero amplitude. The SASSA project area is indicated by the red box. Reservoir reflection amplitude is close to zero in most of the project area. Reservoir reflection time on SASSA gathers must be determined by measuring from a visible reference reflector.

Initially, the project team was uncertain as to whether the injected CO_2 in the relatively thin Bell Creek reservoir would be visible on surface seismic data. This uncertainty was resolved when a 2-D line originally acquired in the first field development area was reacquired in July 2014 after 14 months of CO_2 injection. After processing the two lines with conventional time-lapse methods, CO_2 in the reservoir was clearly visible on difference displays (Figure 4). Subsequent investigations at Bell Creek have shown that the effect due to CO_2 is visible and highly interpretable using time-lapse seismic methods (Bossart and others, 2016; Salako and others, 2017).

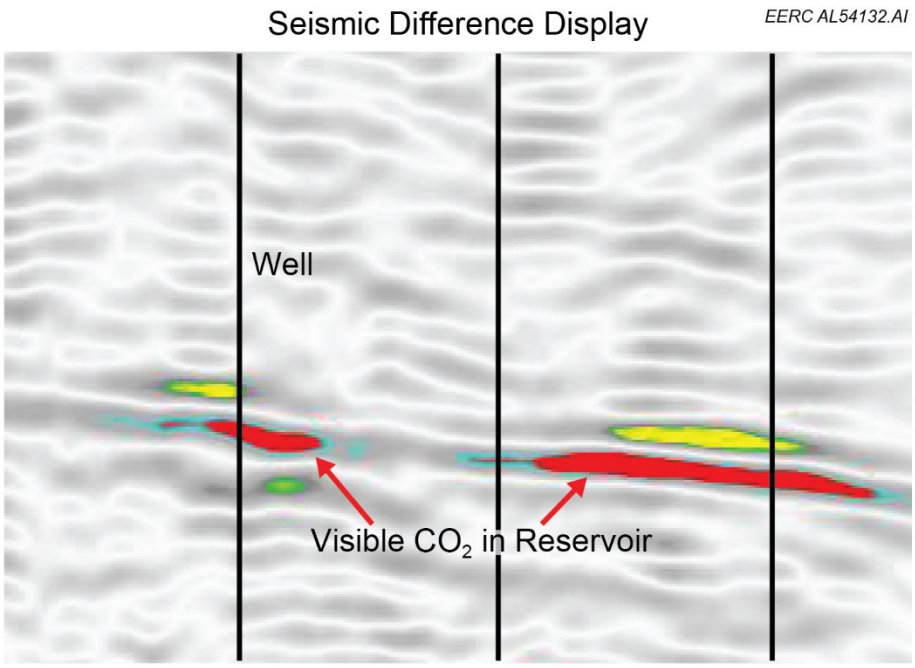

Figure 4. A portion of the time-lapse difference display from a preinjection baseline and subsequent repeat 2-D line acquired in Development Phase 1 after 14 months of injection, which proved that CO_2 would be visible on the reservoir reflector (Salako and others, 2017).

The SASSA project was originally envisioned to be deployed in the second development phase of the field where an existing 50-level geophone array cemented in a monitor well could provide a conventional means of data collection and processing to compare with the unconventional data collected with the sparse array. However, injection in this phase of the field started before the SASSA array could be deployed. An important requirement of the SASSA system field test is that it be deployed and acquire baseline data prior to the start of injection in the study area because the interpretation method requires time-lapse differencing between data acquired at later times after CO_2 injection has been ongoing. To meet this requirement, the array was relocated to Development Phase 4, which was too far away from the borehole array to include it in the study. An alternative means of validation, acquiring a time-lapse 2-D surface seismic survey through the study area similar to the previously mentioned 2-D baseline and repeat in Phase 1, was devised. Modeling efforts were updated to the new Phase 4 location. A more complete description of the SASSA modeling is provided in the technical design document (Deliverable D2).

Project Equipment Selection

A remotely operated seismic source was crucial to project economics, given the distance from the office to the field, and remote monitoring was a key project objective. The GISCO ESS850 accelerated weight drop source was chosen for several reasons: the firing cycle could be operated remotely with a simple electrical contact closure provided by a Web-enabled relay; safe remote operation was possible with the source secured in a locked structure; the accelerated 850-pound weight produced sufficient energy for the distances required; and the source was mobile.

Choosing a recording system was also part of the equipment selection task. The SASSA concept requires nodal geophone and recording units for flexible field deployment. The FairfieldNodal system offered a compact, self-contained node without exposed wiring and many user-friendly features associated with the server, software, and charging system. A 96-node system was procured.

Source mobility together with a flexible 96-node recording system provided the opportunity to acquire a 2-D seismic line through the study area at the beginning and end of the project, with time-lapse processing similar to the 2-D seismic lines collected in Phase 1. The time-lapse 2-D lines would serve as a validation method for the SASSA project.

Equipment Installation and Baseline Data Collection

Installation of system components proceeded from September 28 to October 8, 2015, and is documented in detail in the technical design document (Deliverable D2). Before the nodes were installed in the main array, the initial preinjection 2-D line was acquired on the weekend of October 3 and 4 to avoid noise from weekday work traffic. On October 6, nodes were installed across the study area in the main array configuration by placing them stake-in on the surface as they had been for the 2-D line, and the first baseline data were acquired the same evening by firing the source 100 times (Figure 5). The following day nodes were retrieved and recharged, and the baseline data were harvested. Common receiver gathers from the harvested data were observed on the Fairfield server display to verify that data had been collected. A key operational objective, to acquire baseline data prior to the start of CO_2 injection in the study area, had been met. Three additional baseline data sets would be acquired before injection began in late December 2015.

Semipermanent Installation of the Array and Seismic Source

On the second SASSA trip (October 26–30, 2015) the semipermanent array was installed, and the source was set up for remote operation. Semipermanent installation of nodes required them to be dug into the ground about 8 inches, so that the top of the node was at grade. A housing was installed to protect the nodes from cattle and people, and prevent the ground from collapsing or ice forming and making node retrieval difficult during periodic trips to harvest data and recharge the batteries. This housing for each node comprised a 9-inch section of PVC (polyvinylchloride) pipe large enough to fit over the node and a PVC cap that covered the node and pipe (Figure 6). The PVC cap was transparent to the GPS (global positioning system) antenna signals, ensuring the node could maintain GPS time.

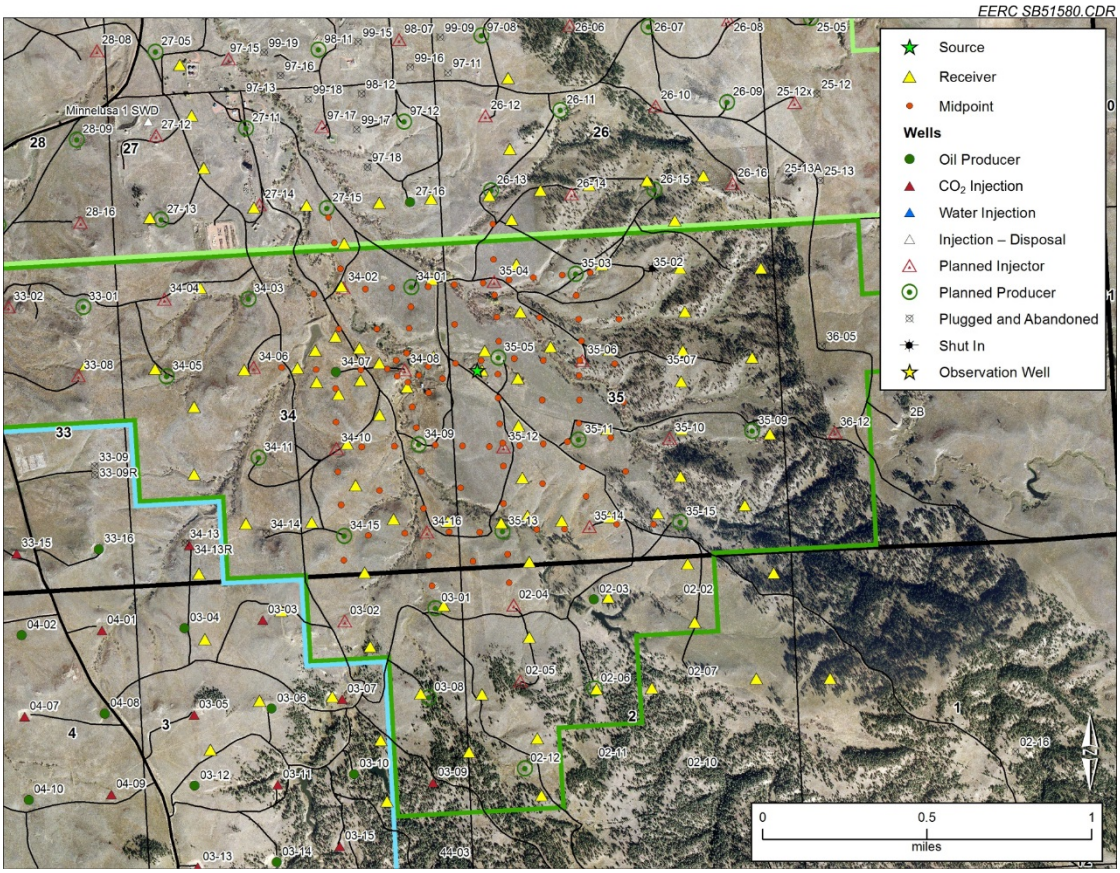

Figure 5. The SASSA preplan receiver layout used to acquire the first baseline is shown with topography of the study area.

Figure 6. Semipermanent installation of the node array: nodes were placed within dug-in PVC sleeves and protected by a PVC cap.

After the initial field data collection, some nodes were relocated from their initial planned location by tens or hundreds of feet to avoid placement by power lines, trees, or high traffic areas. This was part of the testing and optimization effort as survey design was not able to anticipate all obstacles. New coordinates, different reflection points, and changes in elevation were determined for the new locations. A map and table with location data for the array are provided in Main Array Data Acquisition Detail (Appendix A).

To ensure safe and secure operation of the GISCO source, a steel-walled shed was procured and installed near the center of the SASSA nodal array. A 1500-pound engineered steel footing for the source to strike was embedded in the floor of the source shed to ensure a consistent source signature over the duration of the project. Semipermanent installation of the source involved centering it over the engineered steel footing in the floor of the source shed with tie-downs to the four corner anchors to prevent back and forth movement. Side-to-side motion was prevented with 2×6s held against the outside of the wheels by long steel stakes (Figure 7). Batteries that power the electric motor were hooked to intelligent trickle chargers. The remote control system was configured and made operational, and the first remote control acquisition occurred from Grand Forks on the afternoon of October 30, 2015.

Figure 7. The seismic source was secured in a semipermanent manner to minimize movement and ensure a consistent source signature.

ONE YEAR OF DATA COLLECTION

Data Acquisition by Remote Control of the Source

The SASSA project was designed for weekly data acquisition by remotely operating the source via an Internet connection. The custom remote control system developed by the EERC is described in detail in the technical design document (Deliverable D2). The nodes were programmed to wake and record during a window from 7:00 a.m. to 5:00 p.m. Central Standard Time on Saturdays and Sundays, with a shorter 4-hour window on Mondays from 3:00 to 7:00 p.m. These times were chosen because the field typically had less human activity and was seismically quieter on weekends. The Monday time window allowed for troubleshooting and data acquisition if problems were experienced during the weekend. Examples of data acquisition problems included poor trigger switch sensitivity settings, Internet connection outages, and an intermittent Web relay. Acquisition window times were adjusted as needed later in the project to accommodate source firing twice each week.

Remote operation of the source was via a log-in to an Internet-connected computer in the source shed, which was connected to the source by a Web-enabled relay. The Web-enabled relay controlled internal lighting, warning lights, and controlled firing of the source. An IP (internet protocol) camera provided a view of the source while it fired. A waveform window plotted the output of an accelerometer attached to the source weight (Figure 8). After weekly firing was completed, the source weight was rested on the strike plate to minimize stretch on the acceleration elastomer. Initially, when the fire button was pressed, firing would continue automatically until the stop button was pressed. It was realized later that a sudden loss of the Internet connection would leave the source in an uncontrolled firing cycle, so automatic firing was disabled. Subsequently, each shot required a button push.

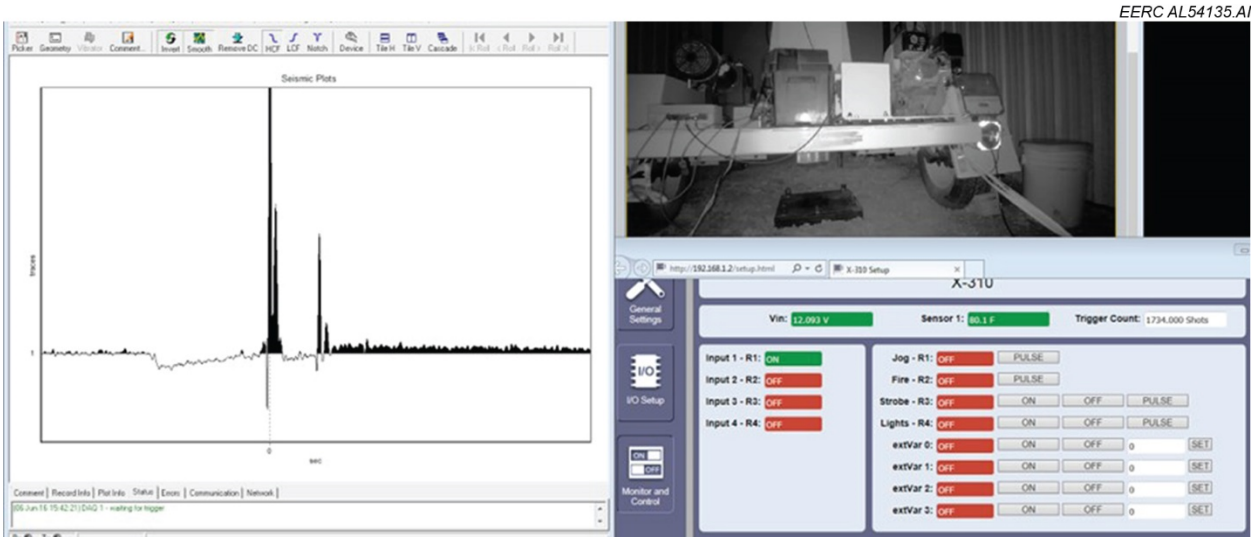

Figure 8. Screen shot of the source remote controls. Accelerometer waveform on the left, camera view of the source upper right, and Web relay controls lower right.

For shot quality assurance, the waveform from an accelerometer attached to the source weight was plotted immediately after each shot and recorded by the source signature recorder (SSR). The waveform had a characteristic shape that gave a visual indication of shot consistency. Waveform timing confirmed that a piezoelectric switch on the strike plate had triggered the recording of the GPS shot time correctly in an SSR file. The GPS shot time file was essential to harvesting the recorded shots from the nodes. Getting the trigger switch properly attached to the strike plate so that it triggered consistently over time was a challenge early on in the project, which was later resolved.

Data acquisitions were attempted on 55 occasions from October 6, 2016, to October 25, 2017. All but two acquisitions were performed remotely. Forty-one data sets were harvested and used for monitoring. Unsuccessful acquisitions were because of several causes; four data sets were not recorded because a setup error in defining the node recording times; four were compromised or incomplete as a result of the trigger switch coming loose from the strike plate; five were lost when the SSR shot time file was corrupted by a voltage surge. Firing was intentionally postponed on one date because of waterlogged surface conditions, once as the footing awaited additional plates to compensate for being pounded into the ground, and once when the satellite Internet dish antenna became misaligned by the weather. A table listing each acquisition date and providing more detail can be found in Appendix A.

Mobilizations to Bell Creek

The Bell Creek oil field in Powder River County, Montana, is 600 miles from the EERC offices in Grand Forks, North Dakota, and 87 miles north of Gillette, Wyoming. In addition to the installation efforts described above, execution of the fieldwork portion of the project occurred over 13 months from October 2015 to October 2016. Field efforts were needed to recharge the node batteries. Recorded data were harvested during recharge. Nodes were then redeployed and acquisition continued until batteries needed to be recharged again. There was also travel to solve source triggering issues and attend to service calls to restore the Internet connection, which was sensitive to wind effects.

Major mobilizations involving five or more field crew members and three vehicles occurred on eight multiday trips. After the data collection effort had been completed, the nodes and source were stored at the Bell Creek oil field. A decommissioning trip returned the nodes, data server, and source to the EERC in July 2017. A final trip in October 2017 brought the source shed back to Grand Forks, North Dakota, which closed out all fieldwork needed for the project (Table 1).

Data Acquisition Challenges

Data acquisition was done remotely from 600 miles away. If something went wrong, a drive to the field involved significant effort and expense. Some problems could be fixed in processing, such as trigger switch misses. Other problems that involved hardware failures, such as loss of Internet connectivity due to physical movement of the antenna by the weather or electronics damage due to overvoltage on the main power lines required a physical visit to resolve.

Table 1. SASSA Project Mobilizations from Grand Forks, North Dakota, to Bell Creek Oil Field, Montana

Date Out	Days	Purpose	Crew
September 28, 2015	11	Install systems and shed, acquire 2-D and array baseline data	6 to 8
October 26, 2015	5	Semipermanent install of array and source, set up remote control	6
December 7, 2015	5	Recharge note batteries and harvest data	6
January 7, 2016	2	Repair source trigger switch	2
January 25, 2016	5	Recharge node batteries and harvest data	6
April 4, 2016	5	Recharge node batteries and harvest data	6
April 28, 2016	2	Internet fix, waterlogged site	2
May 23, 2016	5	Recharge node batteries and harvest data	6
July 25, 2016	4	Recharge node batteries and harvest data	6
September 8, 2016	3	Internet fix, discovered lighting strike damage to source	2
September 19, 2016	5	Repair source, charge node batteries, and harvest data	6
October 24, 2016	5	Harvest data, acquire monitor 2-D line, charge and store nodes	6
July 10, 2017	4	Retrieve SASSA equipment and source, decommission	5
October 9, 2017	3	Retrieve source shed	3

The trigger switch is a piezoelectric device held in contact with the source strike plate by a hold-down bracket and large bolts. When the source weight strikes the footing, the shock wave deforms the switch slightly, inducing a voltage "trigger" signal that causes the source signature recorder to capture and record the GPS time of the strike. The bolts could not be highly torqued, as that would constrain the switch and keep it from deforming in response to a strike. As they could not be tightened, repeated shocks tended to loosen the bolts, causing missed triggers or triggering that occurred with a time delay. Many shots acquired during the early acquisitions had trigger delays. The delays caused the trace data on all nodes to be misaligned. Eventually, the issues with the bolts loosening over time were resolved with the use of a threadlocker compound and lock washers.

Traces recorded with trigger delays were shifted in time by the length of the delay. The amount of the time shift varied with each shot and affected the data recorded on every node. A fix was applied during processing by using the first breaks recorded on a node that had been placed next to the source shed. This "time zero" node was there to allow recovery of data if something happened to the SSR. In this case, by picking the first breaks on the time zero node, the proper time interval to correct the data on all nodes was determined and applied, salvaging many shots (Figure 9).

A 1500-pound engineered steel footing for the source to strike was embedded in the floor of the source shed to help ensure a consistent source signature for the duration of the project. Even with a base area of 9 square feet, the footing was driven into the ground by the source over time. By January 2016, the footing had been driven about 2 inches deeper. The footing was constructed of half-inch steel plates, so three additional plates were added in January to account for initial settling. Another technique applied later was to dig dirt out beneath the tires to lower the source platform.

The rate of settling was greatest when the soil was wet. To avoid driving the footing deeper, on May 1 source firing was omitted because of extremely wet ground conditions to give the ground time to drain after a week of spring storms. Wet ground also affected the source signature. An analysis measuring the normalized RMS (root mean square, NRMS) of the source signature on Channel 70, at 344 feet offset from the source, showed a consistent source signature for the entire project, except 3 weeks in May when the ground was very wet (Figure 10).

Sometime after 52 shots were fired on August 27, 2016, the Internet connection at the source shed became inactive. During an Internet service call to the site on September 9, 2016, it was determined that the Internet modem had been damaged. The modem was replaced, and service was renewed. However, other items were also discovered to be out of service, including the remote control computer, the monitor, and the UPS; in addition, the batteries on the source were dead. Equipment known to be damaged was brought back to Grand Forks for repair with plans to return and reinstall on September 19, 2016, for the next battery recharge and data harvest trip. After returning to the field on September 19, 2016, it was discovered that major damage had also been done to the source electronics and the SSR, so while the usual fieldwork proceeded to recharge nodes and harvest data, other activities were happening in parallel to get replacement equipment purchased or borrowed and shipped to Gillette for installation to repair the source and continue data acquisition. Repairs were completed and acquisition continued on September 23, 2016, static time shift was computed to salvage the shots by picking with subsequent acquisitions occurring twice each week until the end of acquisition on October 25, 2016.

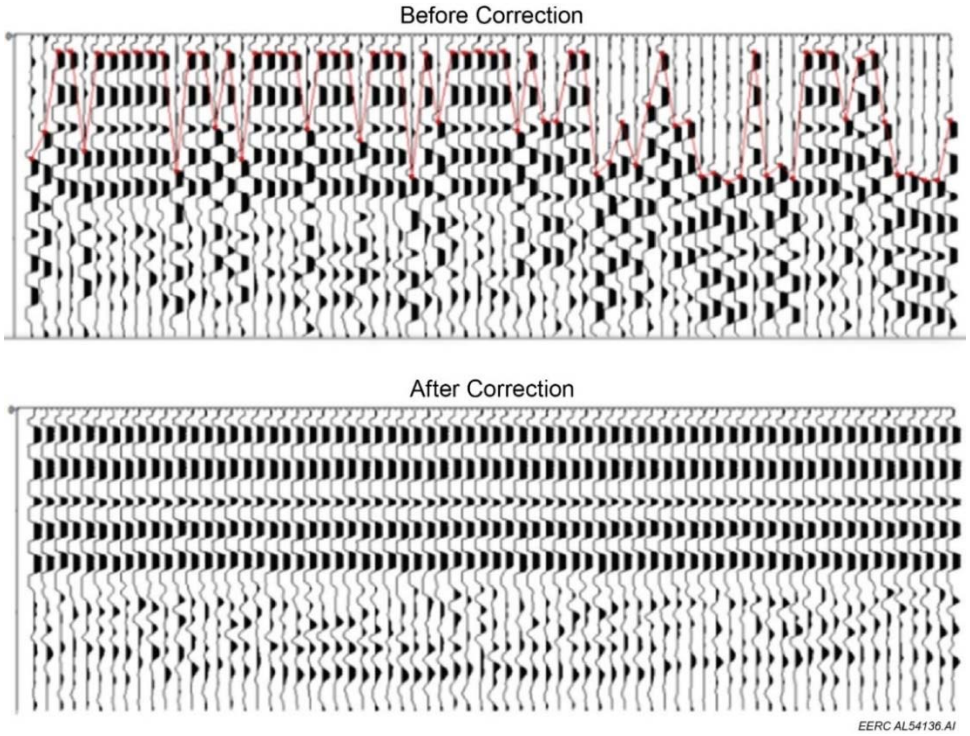

Figure 9. Data recorded on the “time-zero” node next to the source shed during 1 week’s data acquisition exhibit delays due to intermittent triggering. Rather than removing affected shots, a first break times on the time-zero node records and applying the time shift to align them on all traces affected by that shot.

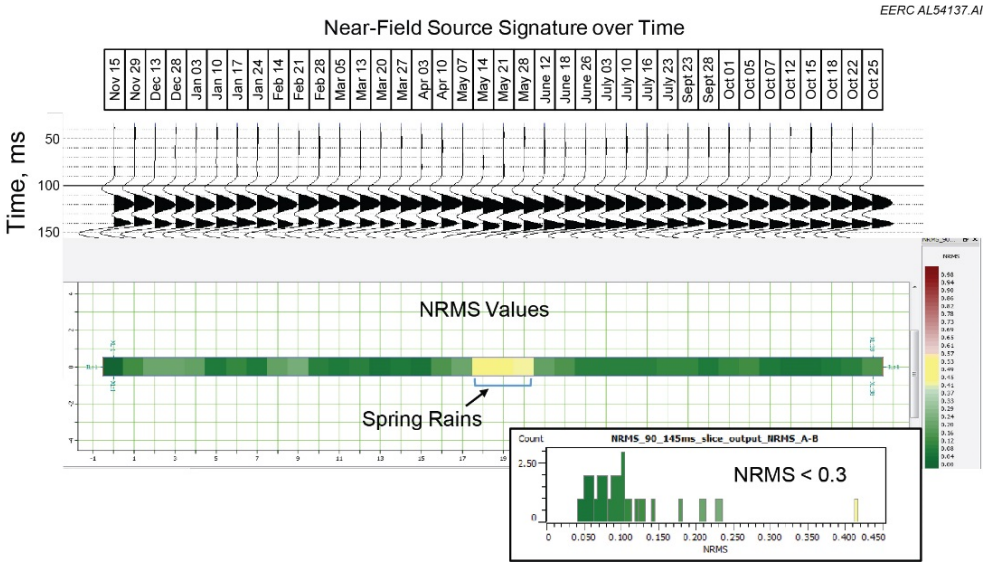

Figure 10. NRMS comparison of the first arrival waveforms at Channel 70, the second nearest channel to the source. Each trace is the vertically stacked result of the labeled day's acquisition, with nominally 50 traces stacked to create each trace shown. A very consistent source signature is indicated except for changes in May because of wet ground.

There is evidence that an electrical surge of unknown origin came to the source shed causing the previously described equipment damage. The apparent path of the electrical surge was through the main power lines. Fuses that are sensitive to high current surges were intact, suggesting the surge was of high voltage. The surge tripped one side of a two-sided breaker at the power drop on the nearby power pole, making it through the other side to the shed on the power lines, traveling through and damaging the battery chargers to get to the source batteries. From the battery terminals, the source control board was accessible, where components were damaged (Figure 11), as well as the SSR, where boards were damaged and the shot time file was corrupted. From the SSR, the surge passed through the ethernet circuit to the remote control computer, frying the ethernet cards and VGA (video graphics array) DisplayPort, and ruining the IP camera, the Internet modem, and the wireless router that were also connected to the ethernet. The surge also entered the UPS from the power plug and damaged the batteries in that unit. The GPS antenna and an accelerometer were also damaged. Evidence supporting this path includes burn marks on some plugs and one pushed out of its outlet (Figure 12). The lesson was that if the battery chargers had been plugged into the UPS (uninterruptible power and supply), the damage may have been avoided as the path to equipment would have halted at the UPS.

Although the shot time file in the SSR was corrupted, none of the actual seismic data collected by the nodes was lost. Harvesting the data is still possible by recreating the shot time file using information from the time zero-node (attempts to do this before the end of the project were unsuccessful). A change in procedure was implemented to prevent the loss of subsequent GPS time-stamped data by downloading the file from the SSR immediately after the source was fired each week.

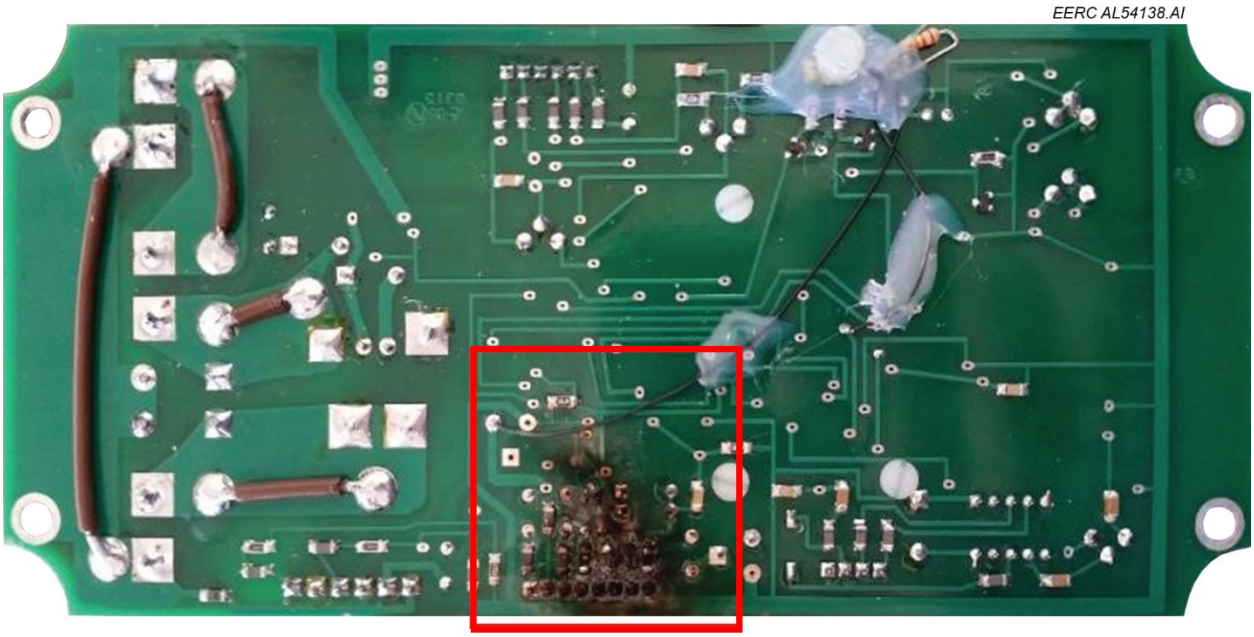

Figure 11. Burn marks on the back of the source control board indicated by the red box as a consequence of a destructive voltage surge at the source shed.

Figure 12. Melted metal observed on equipment plugs after the surge at the source shed.

VALIDATIONS AND VERIFICATION

Dynamic Reservoir Simulation

Dynamic reservoir simulations were performed to model and map the expected distribution of CO_2 saturation change over time in the SASSA study area during the project period. If history-matching results are good and there is confidence in the underlying geologic model, then the CO_2 saturation distribution maps generated by the simulations can be used as one form of validation for the SASSA results. A cautionary note is that the history match can only be as good as the data being matched. If the primary history-matching controls are production, injection, and pressure data, as in the SASSA project area, then there are multiple possible CO_2 saturation realizations that could result in a match. This fact leads to some ambiguity when using the simulated data as a validation method for SASSA.

Computer Modelling Group Ltd. (CMG) GEM, a general compositional reservoir simulator, was used because of its ability to predict the composition change of fluids and CO_2 distribution for large-scale CO_2 flooding. As an input to GEM, the sophisticated third version of the Bell Creek reservoir static geologic model created as part of another DOE project was leveraged for the predictive modeling task (Jin and others, 2016). History matching of available production/injection data from Phase 4 wells was conducted to ensure the simulation model would represent the real reservoir behavior and make reasonable predictions under the known operational conditions. There were 37 active wells in the Phase 4 model used for history matching, including 18 production wells, ten water attributing gas (WAG) injection wells, and nine water injection wells. After history matching was completed, CO_2 saturation distributions were calculated for each month of the data acquisition period up to the end of SASSA data collection, October 2016 (Figure 13). More details about history matching the wells in the study area for dynamic reservoir simulation can be found in Appendix B.

History matching and reservoir simulation are sometimes said to be as much of an art as a science, as the reservoir engineer makes adjustments to geologic model parameters in order to best match the measured production and injection data. The adjustments compensate for reservoir heterogeneities that were not captured in the underlying geologic model. The initial intent of the field test was to use SASSA results to inform the history-match process by alerting the reservoir engineer to locations where CO_2 saturation had been detected. Data processing and interpretation challenges made this intent unrealizable as originally planned. Instead, the CO_2 saturation distribution map helped to concentrate data processing and interpretation efforts on channels with monitored midpoints that intersected with modeled CO_2 saturations, with the understanding that there may be monitored midpoints that have encountered changes due to CO_2 that are outside of CO_2 distributions as mapped from the simulations.

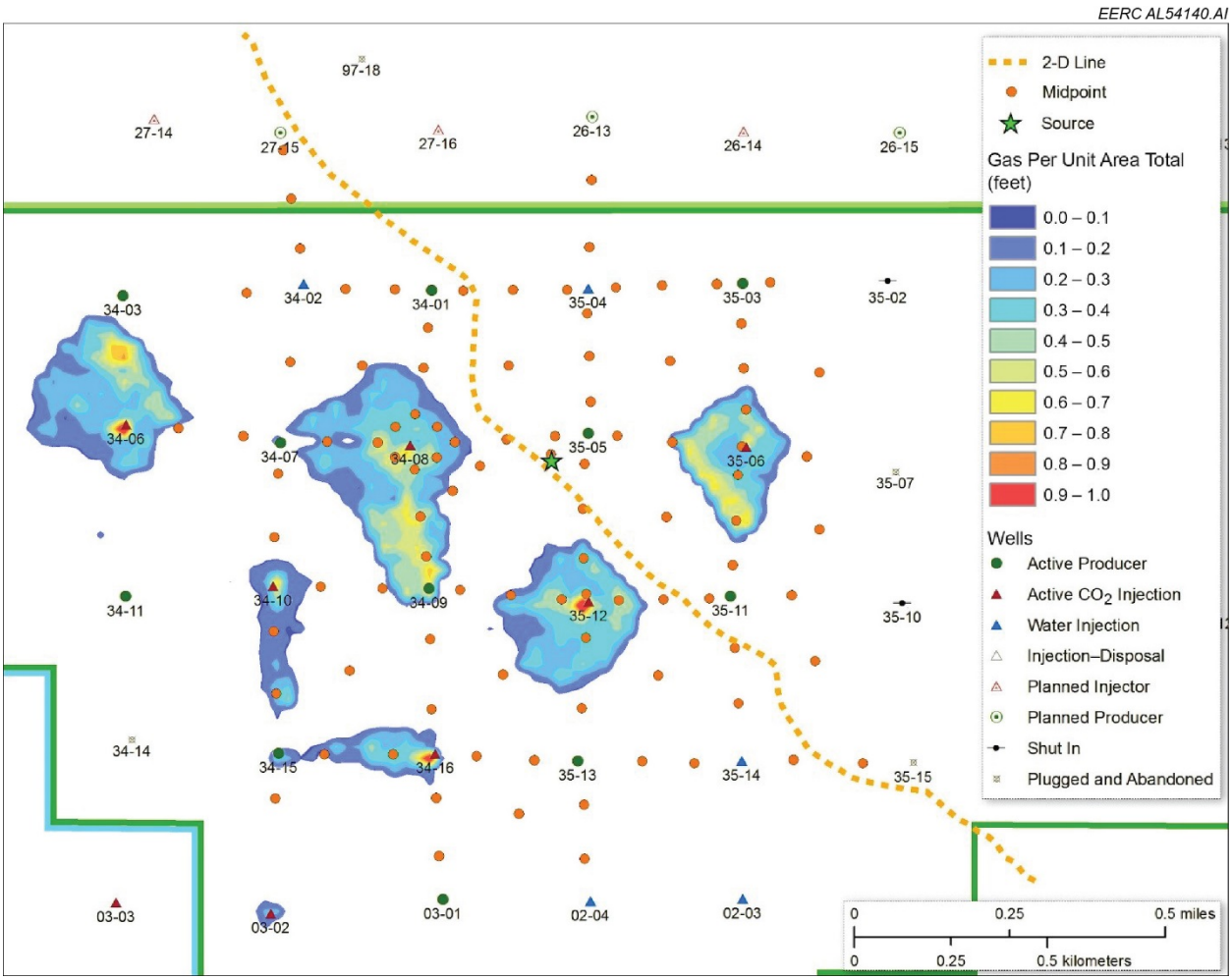

Figure 13. One reservoir simulation realization of CO_2 distribution in units of gas saturation per unit area at the completion of SASSA data acquisition. Compared to this simulation output, most of the main array monitor points do not appear to have encountered CO_2, nor has the 2-D line.

2-D Time-Lapse Seismic Line

The 2-D time-lapse seismic line provided a second means of validation in the form of a conventional seismic survey to compare with the unconventional data gathered by the main SASSA array. The line was acquired before and after CO_2 injection in October 2015 and October 2016, respectively. Acquisition was conducted along an existing roadway that traversed the study area diagonally from southeast to northwest (Figure 14). The same 96 3C FairfieldNodal Zland nodes and the accelerated weight drop seismic source Gisco ESS 850 used in the SASSA array were utilized for the 2-D survey. Acquisition parameters mimicked those of the test line acquired in Phase 1, with receiver nodes deployed every 110 feet along the road to form a crooked 2-mile line. The source was fired between receivers every 220 feet along the line. The elevation change and irregular topography of the field road were considerable (Figure 15).

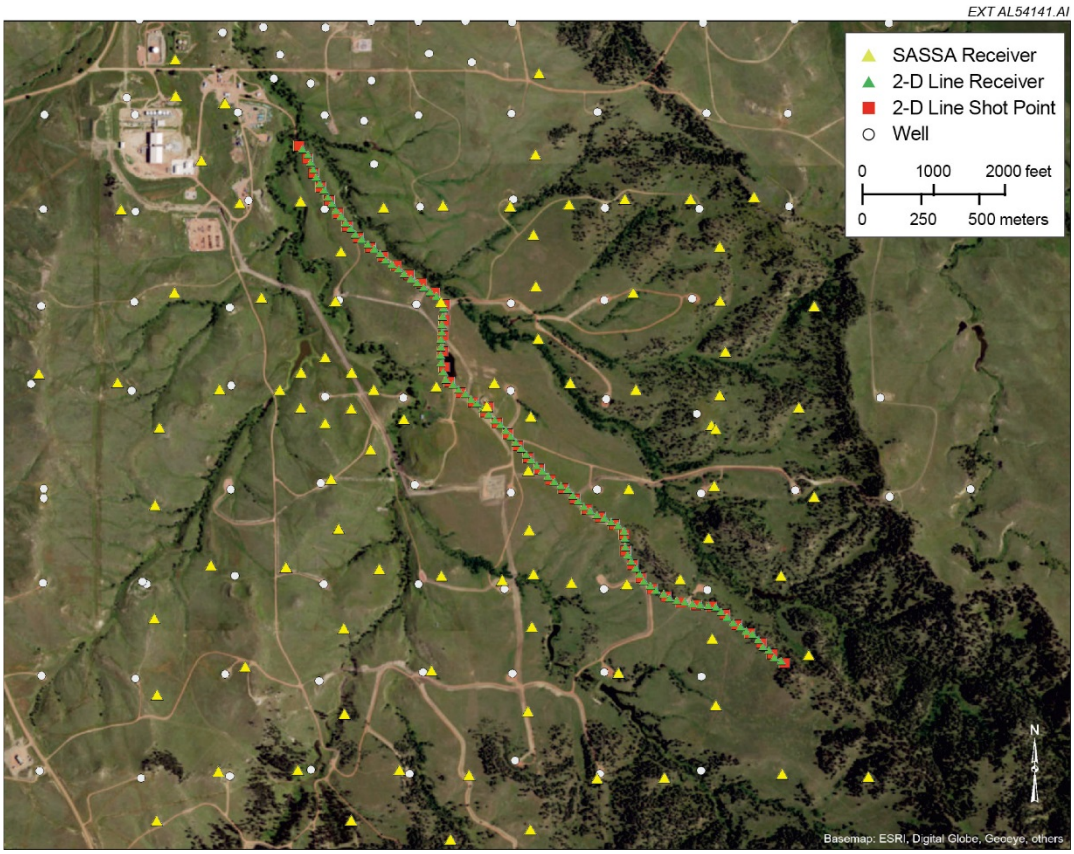

Figure 14. Location of 2-D survey and permanent SASSA receivers.

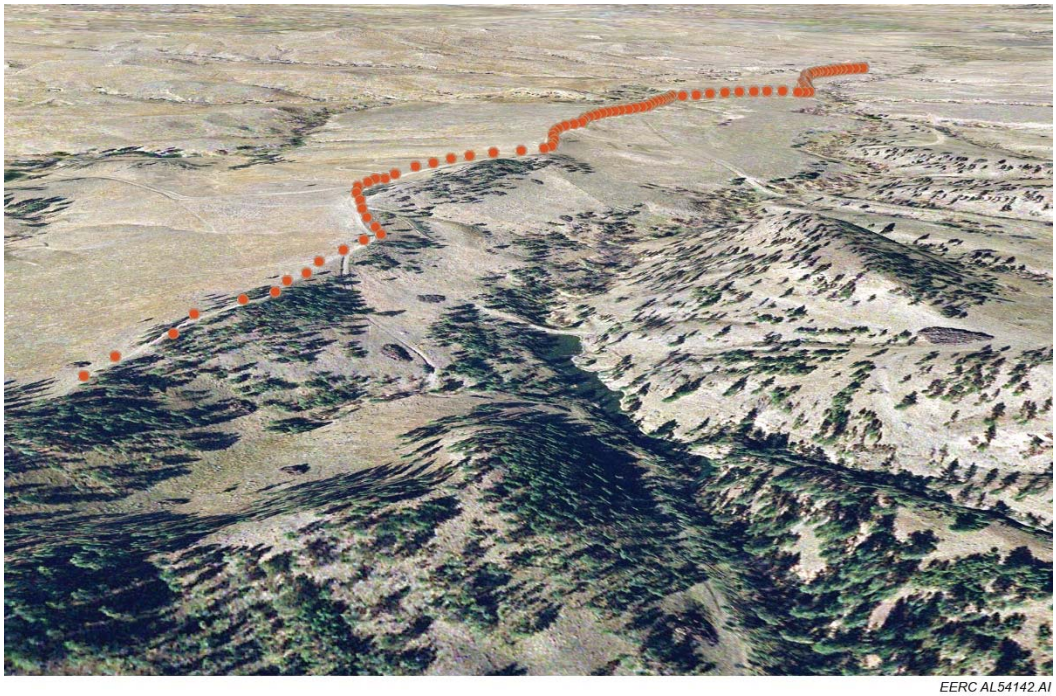

Figure 15. Elevations of 2-D SASSA survey. Left to right: northwest to southwest of the 2-D survey. Yellow points: receiver locations; red point: source locations.

To ensure repeatability of the time-lapse data, the source and receivers were deployed in the same locations for both the pre- and postinjection surveys within a small margin of error. The weight drop source was fired 16 times at each shot location to improve the signal-to-noise ratio by stacking the shots. Interestingly and for reasons unknown, the baseline and monitor surveys were affected by different types of high-amplitude noise, which presented a challenge for data processing and time-lapse analysis. The monitor data also have a lower signal-to-noise ratio than the baseline survey on most of the shot gathers.

The baseline and monitor surveys were processed following standard conventions of time-lapse surveys. A similar workflow was applied to the two surveys with the exception of the static corrections and noise attenuation steps which were applied differently to address the differences between the two data sets. Seismic data processing was done with GeoTomo GeoThrust 2-D seismic data-processing software, which has sophisticated noise attenuation algorithms that were applied. More detail on the considerable data-processing effort applied in 2-D Line Data Processing can be found in Appendix C.

A summary of the data processing workflow is as follows:

1. Upload data
2. Apply geometry
3. Estimate near-surface model
4. Determine replacement velocity and static corrections and pick floating datum
5. Edit traces
6. Performance time resampling
7. Correct geometrical spreading
8. Attenuation monochromatic noise
9. Perform surface consistent scaling
10. Do ground roll attenuation and muting
11. Perform surface-consistent deconvolution
12. Perform = first break mute
13. Apply bandpass filter (Ormsby filter: 5, 8, 56, 65 Hz)
14. Apply to mostatics corrections
15. Apply residual statics corrections
16. Attenuate random noise
17. Perform second pass of surface consistent scaling
18. Pick velocity
19. Migrate prestack time
20. Resample time
21. Muting
22. Stack
23. Bandpass filter (Ormsby filter: 8, 12, 25, 35 Hz)
24. Output SEGY files

The final seismic sections produced show coherent events for both the baseline and monitor survey and have characteristics consistent with events on nearby inlines from the 3-D seismic data collected as part of a separate project (Figure 16). There is a phase difference attributable to the different type of seismic source. The line is in an area where the reservoir reflector is very difficult to pick, so the reservoir location is inferred by its time difference above a reference reflector.

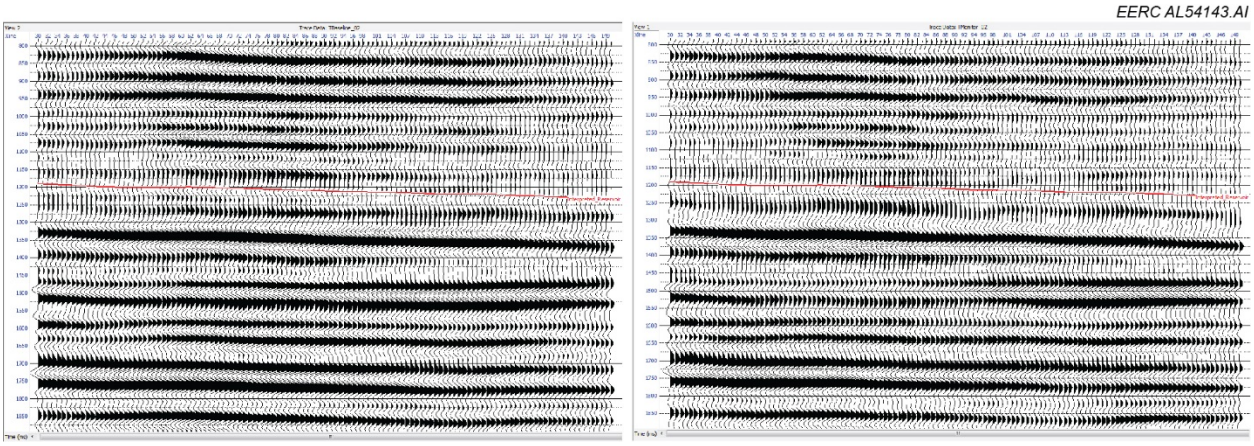

Figure 16. Stack of Kirchhoff prestack time common image point (CIP) gathers after muting migration artifacts and stretching effects, and the application of a band pass filter (8,12-25,35 Hz). Left: baseline survey; Right: monitor survey. CIP gathers from 30 to 150 are shown. The red line represents the interpreted location of the reservoir.

2-D Line Time-Lapse Differencing

Conventional time-lapse analysis involves interpretation of difference displays created by subtracting the pre-CO_2 injection data from the post-CO_2 injection data. The method requires minimizing the general differences between data sets while being careful to avoid impacting real differences that are associated with injection into the reservoir. Calibration is accomplished with a cross-equalization workflow designed to minimize time, phase and amplitude differences between the data sets where they are not expected to occur, such as above an injection zone. After the corrections, differences between data sets are more likely to represent the real changes that have occurred.

Typical cross-equalization processes use a design window to calculate corrections which are then applied to the entire trace. To preserve changes on the reservoir reflection due to CO_2, the design windows are commonly chosen to exclude the reservoir reflection, so knowing the location of the reservoir reflection is key. Identifying the reservoir reflector on the 2-D data was difficult as the amplitude is very low with poor continuity. An attempt was made to tie sonic logs of nearby wells to the 2-D line, but the sonic logs available from wells in Phase 4 are very short, so this method was not productive. Instead, the nearest inline from the 3-D data collected in the same area was used to compare previously interpreted horizons to the 2-D data after bandpass filtering to match bandwidths.

After identifying the reservoir location, a cross-equalization workflow was designed and applied. The workflow included steps to assess the repeatability of the data sets and an iterative approach based on phase and time shifts, shaping filters and quality control (QC) steps to match frequency, content, phase, time, and amplitude of the two data sets in areas away of the target reservoir. The workflow applied to the 2-D time-lapse data consisted of the following steps:

1. Estimation of correlation coefficients and shifts
2. Estimation of predictability
3. Estimation and application of phase and time shifts
4. Application of shaping filter
5. Estimation of time-variant time shifts
6. Preconditioning and application of time-variant shifts

Time-lapse difference displays were created by subtracting the baseline survey from the monitor data for the 2-D line data prior to and after cross equalization. Prior to cross equalization, there are several high-amplitude differences above and below the reservoir. Differences in the reservoir are present but have a lower amplitude and are not easily interpretable. After cross equalization, the high-amplitude differences above and below the reservoir are attenuated, and the differences in and directly below the reservoir are enhanced (Figure 17). These differences in the reservoir correspond to an area along the 2-D line that is near an injector that started injecting CO_2 in January 2016 and continued injecting through October 2016 when the 2-D monitor data were acquired (Figure 18). The realization from dynamic reservoir simulation that is shown does not indicate that CO_2 has migrated to this area during the course of the project, but it is possible that a different realization that matches the same control data would indicate the presence of CO_2. In addition, confidence is high that these results indicate time-lapse changes in the reservoir because of the presence of CO_2. This interpretation also appears to be confirmed by SASSA array data interpretations shown later in this document.

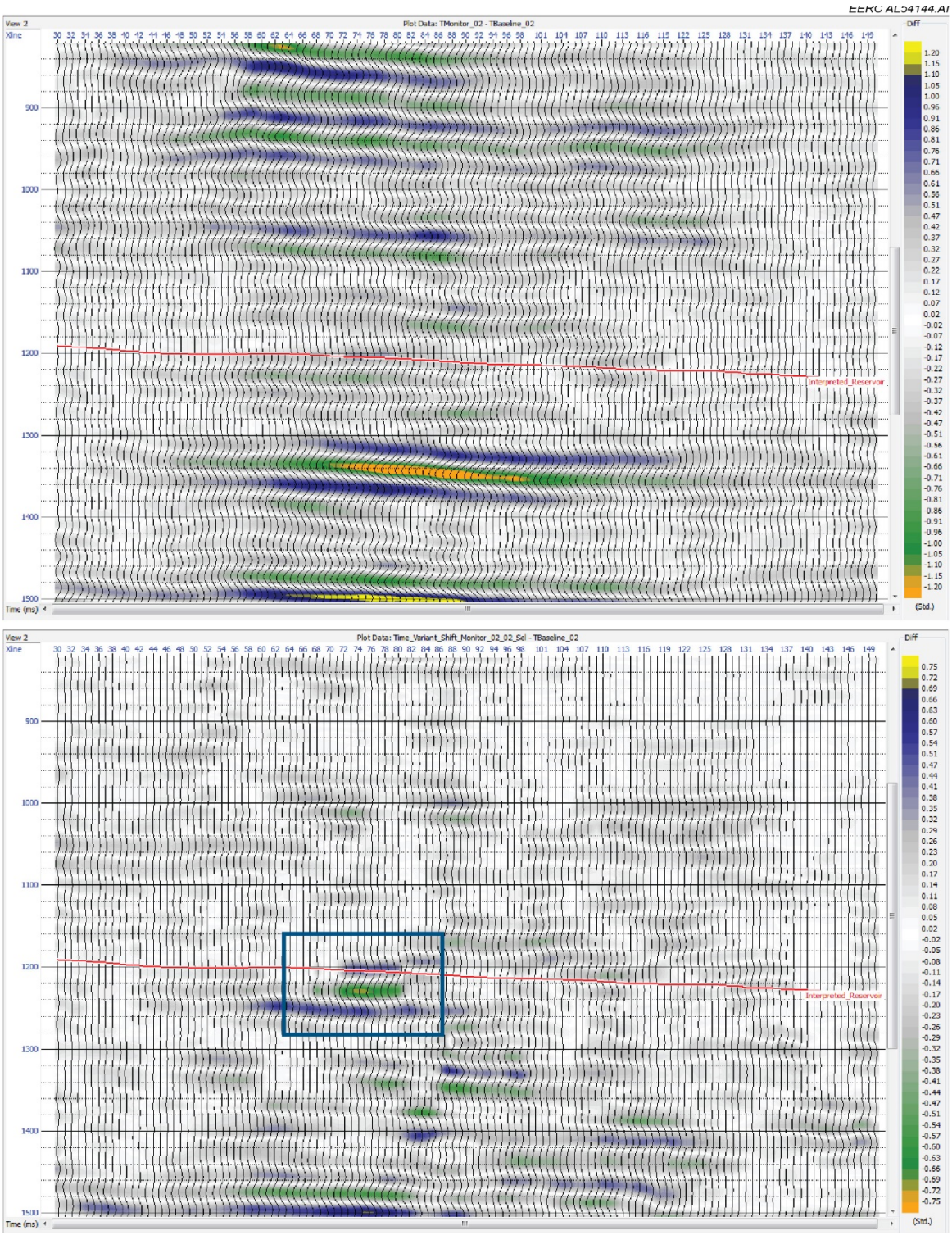

Figure 17. Top: difference display of monitor minus baseline PSTM (prestack time migration) stacks. Bottom: difference display after cross equalization. Time window from 980 and 1420 ms. CIP gathers from 30 to 150 (horizontal axis). The red line represents the interpreted location of the target reservoir. A significant difference at the reservoir level between CIPs 70 and 80 (outlined in blue) indicates a possible time-lapse change related to the presence of CO_2.

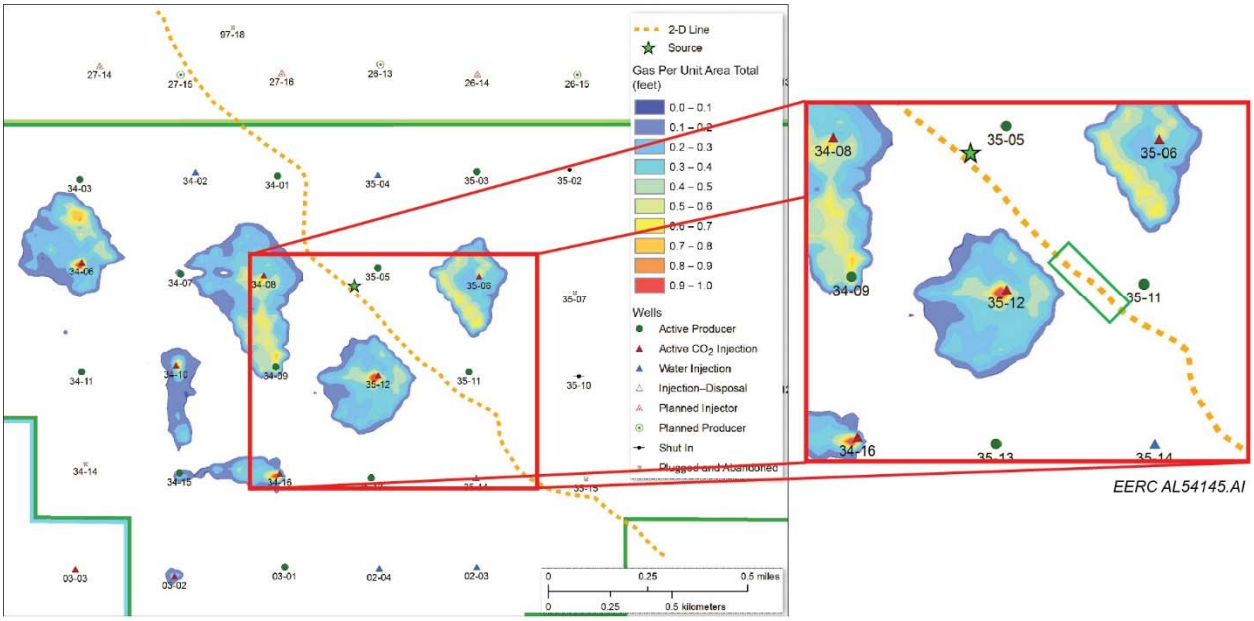

Figure 18. One mapped realization of gas saturation per unit area in the reservoir from the simulation at the SASSA project end. The light orange line indicates the 2-D seismic line location. The green box highlights the area corresponding to time-lapse differences in the reservoir interpreted between CIPs 70 and 80 on the 2-D time-lapse data in Figure 17 above.

MAIN ARRAY DATA QUALITY

Seismic data acquisition, data processing, and interpretation are interrelated activities. In general, the results of interpreting available geologic and geophysical information drive the seismic data acquisition and processing. These two activities, in turn, are highly dependent. The acquisition environment, the type of signal and noise sampling in time and space, and the achieved signal-to-noise ratio will have a direct impact on the selection of algorithms that can be used in data processing.

Seismic data acquired on onshore environments are generally affected by meteorological noise, cultural noise generated by human activities, and noise generated by the seismic source, which is highly affected by the conditions of the near surface. Conventional land seismic data acquisition systems try to minimize the noise using analog sensor arrays or a high-density configuration of individual sensors, sometimes combined with a high channel count. These types of configurations can be used to attenuate some noise components in the field or in simulated arrays in data processing.

The SASSA configuration does not allow the attenuation of noise in the field, nor the design of simulated arrays in data processing. However, the type of individual sensors used in the SASSA array can acquire high-fidelity signal and noise. Recorded high-fidelity noise can be used to create filters to attenuate noise on data with both signal and noise.

When land seismic data are acquired in a time-lapse manner, data processing should compensate not only for time variations of the recorded noise, but also for near-surface velocity fluctuations to correctly estimate the changes at the level of the reservoir. The cultural noise variations over time from active oil fields can be very challenging because of the expected variety of human activities. The recorded noise during the SASSA project at the Bell Creek oil field confirmed the diversity of the noise and near-surface conditions. The source of the time-lapse noise can be attributed to the industrial installations located in the northwestern part of the study area (Figure 14), the electromechanical equipment at the wells, the pipelines of CO_2 and water, power lines, the movement of vehicles, and cattle in the area. The change of meteorological conditions in the form of wind, rain, and the frozen near-surface layer was also observed in the SASSA data. Some examples of the challenging noise conditions during the SASSA data acquisition are discussed below.

There are differences in the spatial noise conditions in the area where the SASSA data were acquired that can be illustrated by computing the power spectra of noise records obtained during one day of acquisition (Figure 19). High-level noise (yellow and orange squares) is clearly shown at sensors in the northwest part of the field from the industrial installations where the CO_2 pipeline comes into the field. Other sensors with high-level noise that are not located near the main industrial installations were discovered to be located close to small sources of electromagnetic noise such as wells and power lines.

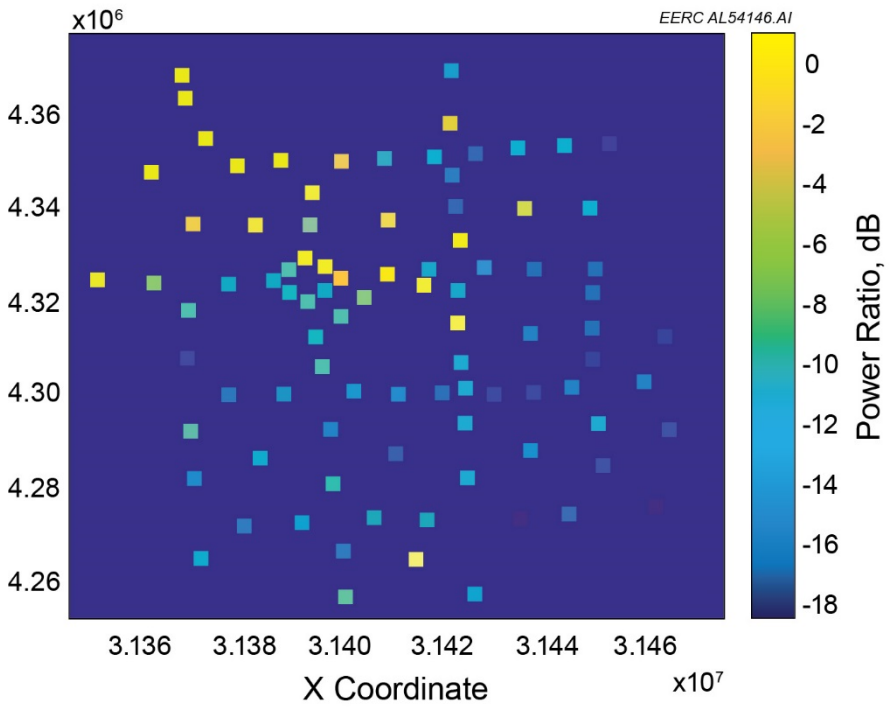

Figure 19. Trace energy level estimated from ambient noise recordings. The squares represent the locations of the 96 SASSA sensors. The colors show the estimated energy of ambient noise recorded at each sensor location, with yellow representing high levels of noise and blue lower levels. Notice the large difference between the sensors near the industrial installations where the CO_2 pipeline comes into the field (yellow color on the left top corner).

Monochromatic noise (noise affecting only one frequency) was observed throughout the field. Each sensor exhibited a unique combination of monochromatic noise depending on its spatial location with respect to infrastructure. For example, sensors near producers exhibited high-amplitude 30-Hz noise that may be associated with chemical pumps. In the northwest portion of the study area near the gas plant, sensors showed a combination of 10-, 15-, 20-, 30-, 40-, 50-, 60-, 70-, 80-, and 90-Hz monochromatic noise (Figure 20). Temporal variations of monochromatic noise were also observed during the few minutes of the weekly data acquisitions. A common receiver gather from a sensor located near a pumping station shows 15-Hz monochromatic noise at the beginning of the acquisition, disappearing during the acquisition of some shots, and then reappearing at the end of the acquisition (Figure 21).

Coherent noise generated from human activities was recorded by some SASSA sensors. The irregular distribution in time and space of this noise during the recording represents an additional challenge for data processing. This type of noise had similar amplitude and frequency characteristics as the signal and was recorded at similar arrival times. Because of these similarities, the separation of signal and noise can be more complicated in data processing.

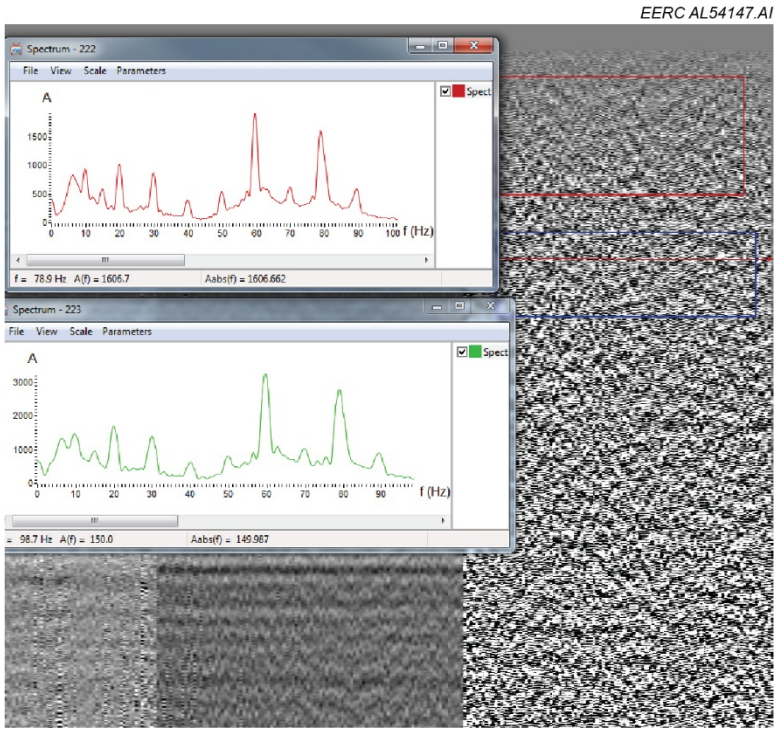

Figure 20. Example of monochromatic noise on common receiver gather (CRG) (Sensor 33). Amplitude spectra of the red and blue windows from the third gather from the left show monochromatic noise at 10, 15, 20, 30, 40, 50, 60, 70, 80, and 90 Hz.

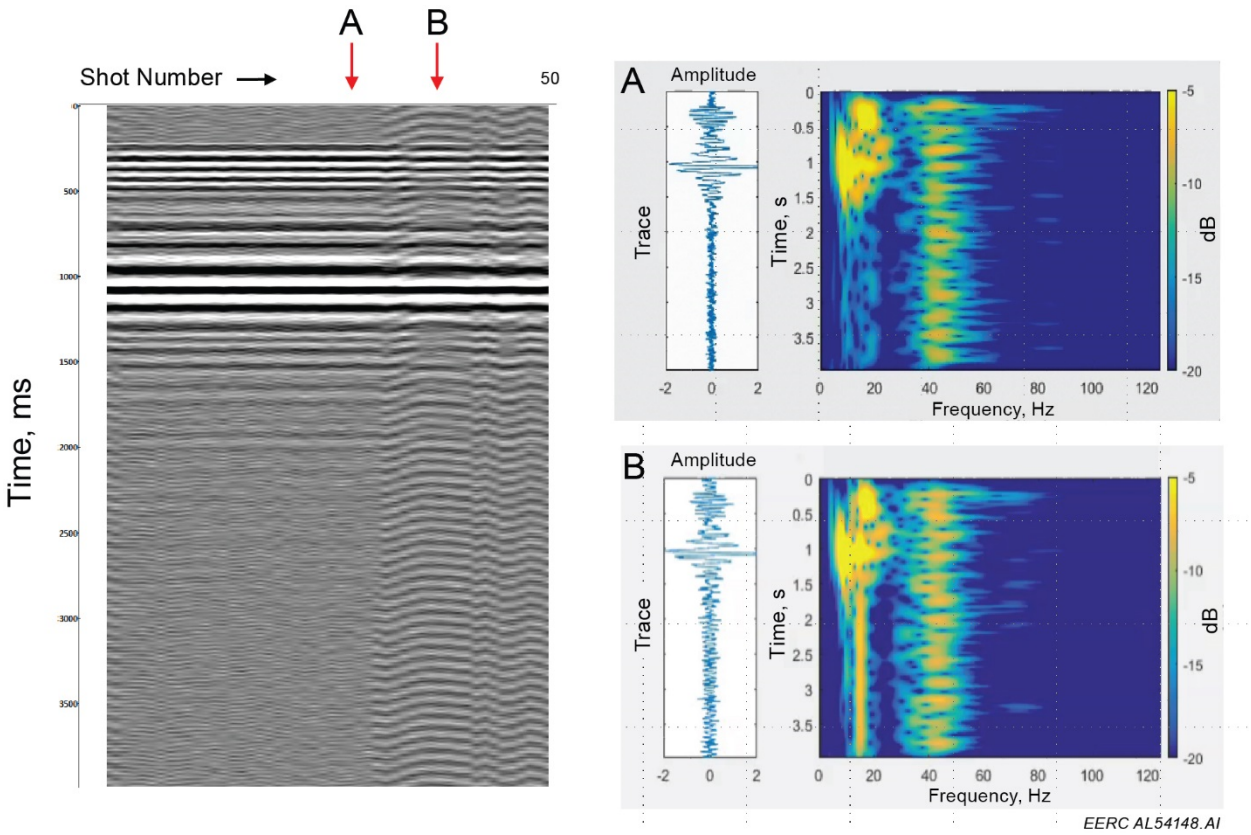

Figure 21. Cultural noise. Left: CRG showing the effect of a pump on a channel's data during one morning's acquisition. Right: time-frequency representation of two traces marked by A and B on CRG. The intermittent pump noise can be observed at approximately 15 Hz (B).

The changes of wind and rain conditions affected the SASSA data. Whereas strong wind overwhelmed the signal in some acquisition records, the rain affected some traces during the weekly acquisitions (Figure 22). In standard commercial data acquisitions, the options to minimize the effect of wind are changes of the seismic source parameters to increase the seismic energy or stoppage of data acquisition activities until the wind noise decreases. Rain noise is normally associated to high-amplitude noise. Depending on the intensity and frequency of the rain and the number of sensors affected, the seismic operations can be continued or delayed until the meteorological conditions improve.

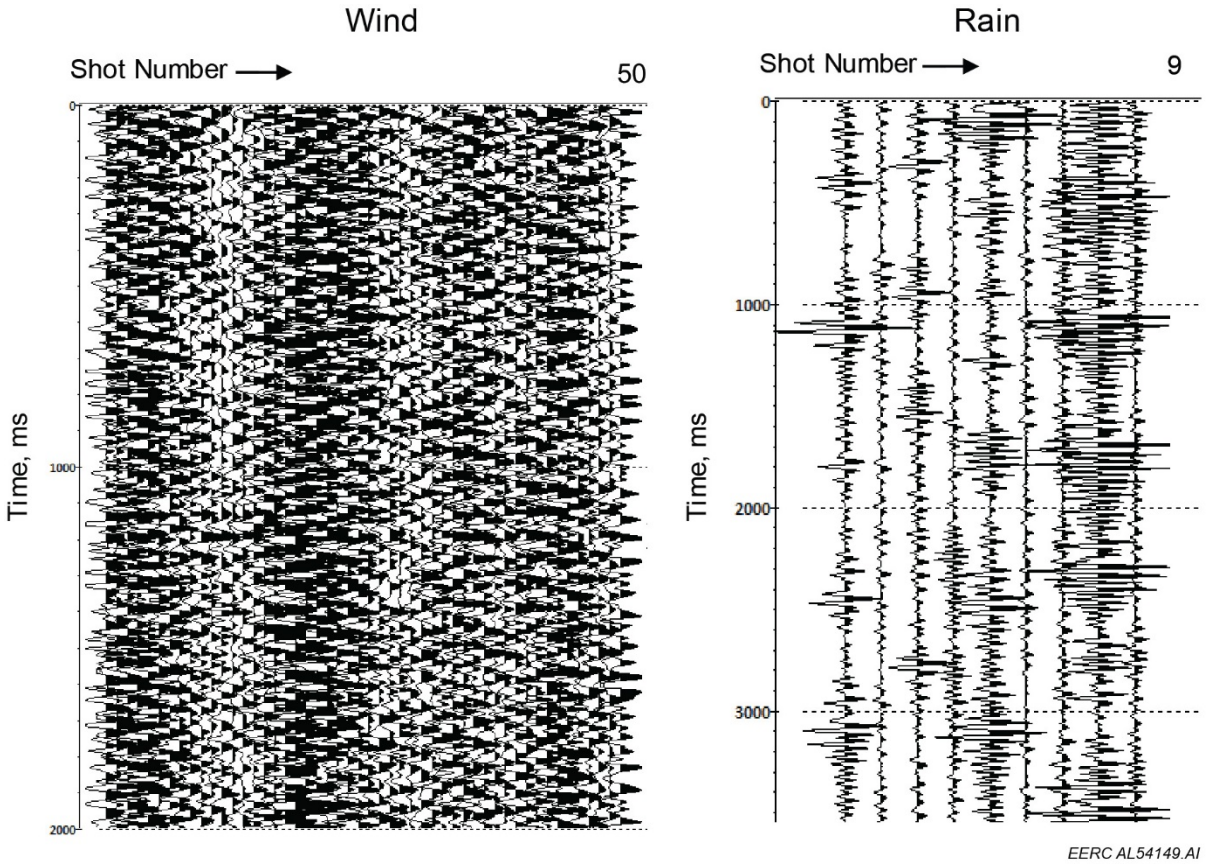

Figure 22. Example of meteorological noise. Left: wind noise. Notice the high-amplitude noise during most of the shots. Some bands of the high-amplitude noise are also observed. They can be associated to gusts. The seismic signal at approximately 1200 ms is overwhelmed in almost the complete receiver gather. Right: rain noise recorded passively while the nodes were on, but the source was not being actively fired.

The effect of the near-surface seasonal changes was clearly visible in the SASSA data. Temperatures measured at Broadus, Montana (wunderground.com), a nearby location, during the 1-year of acquisition correlate to the character change of near-surface guided waves recorded at the nearest offset sensor (Figure 23). The seismic amplitudes shown in the 300–400-ms time window clearly change from window to window. These changes can be associated to the temporal variations of the sediments forming the near-surface environment.

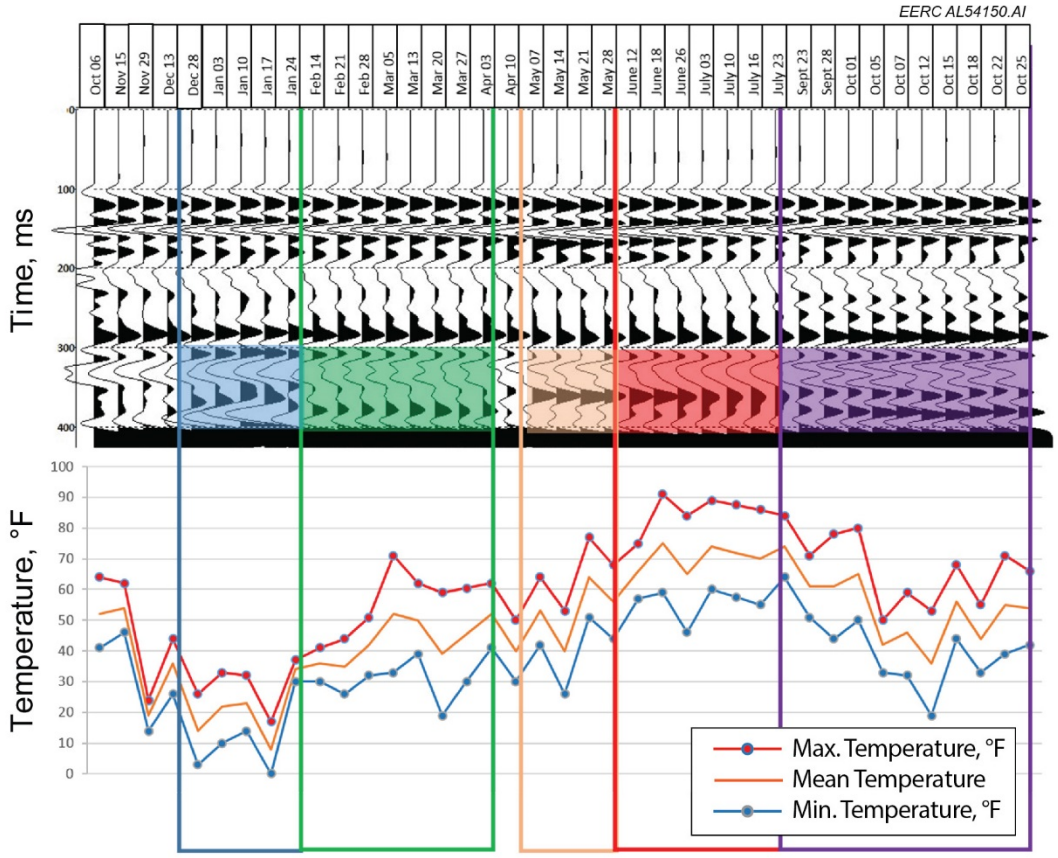

Figure 23. Near-surface seasonal changes affecting seismic data. Top: 0–400-ms time window of stacked traces for each week of acquisition of Sensor 70. The horizontal axis is the date of acquistion. The vertical axis is the two-way travel time of the recorded seismic events. Bottom: historical temperature data from nearby Broadus, Montana (wunderground.com). The colored time windows from 300 to 400 ms indicate changes to waveform shapes associated with the near-surface conditions that are relatable to the temperature data below. The 100–200-ms window shows the first breaks and guided waves.

Ground roll noise affected the sensors close to the seismic source. At these near-offset sensors, ground roll arrived at the same time as the reservoir reflection (Figure 24). Because of the sparse and irregular data acquisition, conventional noise attenuation algorithms such as frequency-wavenumber filters and radial filters were not possible to use or their use was too limited. Other types of guided waves observed in the data did not arrive at the same time as the reservoir reflections, but standard muting of these waves during processing limited the size of the data-conditioning design window for far offset sensors.

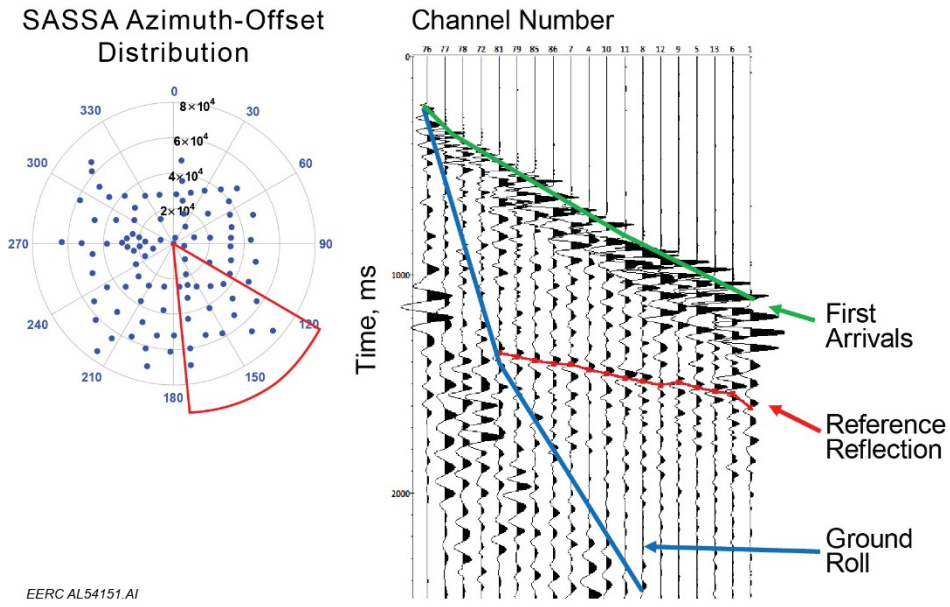

Figure 24. Ground roll noise shown on a common azimuth gather (right). The sensors contributing to this gather are shown by the red polygon on the diagram of the SASSA azimuth-offset distribution (left).

MAIN ARRAY DATA PROCESSING

Processing Flow Development

Several signal-processing routines were tested and applied to the SASSA array data. These routines included a variety of standard and advanced signal-processing algorithms applied to enhance signal and attenuate noise without artificially changing the amplitude of the recorded signal. The commercially available seismic data-processing software packages used in these tests were developed to process data with conventional 2-D and 3-D geometries and presented a challenge for processing the SASSA data given the unconventional sparse geometry of the array; however, processing in multiple domains provided a means to test advanced processing methods applied in conventional 3-D seismic data processing. Processing in multiple domains including shot gathers, pseudo inlines and crosslines, common azimuth gathers, and common receiver gathers was explored. Custom headers and strategic sorting were also used to overcome limitations of the predefined algorithms in these commercial software packages.

After testing several possible processing domains, the common receiver domain appeared to be the optimal domain to apply processing. For each day of data acquisition, a common receiver gather for a single channel consists of one trace for every time the source was fired. Because of the fact that the source is stationary, seismic events are recorded at the same time on each trace, resulting in horizontal events. These common receiver gathers with horizontal events allowed for the application of advanced noise attenuation algorithms that use windows spanning multiple traces to distinguish and differentiate noise and signal based on dip, coherency, and frequency content.

Simple Processing Flow

A simple processing flow was applied to common receiver gathers for each of the 96 receivers using RadExPro™ seismic data-processing software, and time-lapse differencing and cross equalization were accomplished with CGG's HampsonRussell™ software to assess the time-lapse changes present and determine how to focus advanced noise attenuation efforts. In total, data from 39 different days of data collection consisting of over 220,000 traces were processed. The simple processing flow applied is outlined below and discussed in more detail in Appendix D:

1. Upload raw field data
2. Apply geometry to headers
3. Save data from the vertical geophone to a separate file
4. Sort vertical component data into common receiver gathers
5. Apply bandpass filter (Ormsby filter: 2, 5, 75, 90 Hz)
6. Correct geometrical spreading
7. Perform trace edits
8. Attenuate of strong noise (e.g., burst noise)
9. Perform time and frequency domain filtering
10. Perform vertical stack of common receiver gathers
11. Apply bandpass filter (Ormsby filter: 4, 8, 56, 64 Hz)
12. Create monitor stack section
13. Create baseline stack sections
14. Output SEG-Y (Society of Exploration Geophysicists-Y) files of monitor and baselines

Based on this initial time-lapse analysis of the simply processed data from all 96 receivers, dynamic reservoir simulations, and associated production and injection data, a subset of 26 receivers was selected for in-depth analysis, including reprocessing with more advanced algorithms.

Advanced Processing Flow

The emphasis of the advanced processing workflow is noise attenuation on the common receiver gathers. The input data to this workflow are edited common receiver gathers with field geometry in SEG-Y format. Traces with highly anomalous amplitudes were killed in the editing process. The VISTA seismic data-processing software was used to develop this workflow as outlined below (more details of this workflow can be found in Appendix D).

1. Upload data
2. Condition header for VISTA seismic data-processing software
3. Perform geometrical spreading correction: Exponential gain constant: 1
4. Apply bandpass filter (Ormsby filter: 2, 7, 55, 60 Hz)
5. Attenuate monochromatic noise
6. Attenuate strong noise (e.g., burst noise)
7. Attenuate white noise
8. Perform vertical stack of common receiver gathers
9. Set time window: 0–2000 ms

10. Trace selection of baseline and monitor
11. QC of baseline and monitor stacked traces.
12. Mute first-breaks and guided waves
13. Create monitor stack section
14. Create baseline stack sections
15. Output SEG-Y files of monitor and baselines

Time-Lapse Calibration

As with the 2-D line, identifying the reservoir reflection or its approximate time was required prior to the time-lapse calibration. Interpreting the reservoir on the SASSA array data set was a challenge given the low-amplitude nature of the reservoir reflection and was also complicated by the fact that interpretation was across different data domains: conventional stacked data vs. SASSA common receiver gathers. As with the 2-D line, the common receiver gathers from the array were compared to 3-D data collected as part of the Plains CO_2 Reduction (PCOR) partnership. For this comparison, static and moveout corrections were applied to the array data. Because of the far offset of many of the array sensors, this comparison was not fruitful. The method that proved to be the best option for interpreting the reservoir reflection was to locate an easily identifiable high-amplitude reflection and calculate the expected time difference between this reflection and the reservoir reflection on the 3-D data to determine the approximate time of the reservoir reflection on the SASSA data. The reference reflection is interpreted to be the Piper Formation and is easily identifiable on pseudo inline and crosslines and azimuth gathers (Figure 25). This reference reflection is approximately 150 ms and 870 feet below the reservoir reflection based on analysis of the 2-D line data.

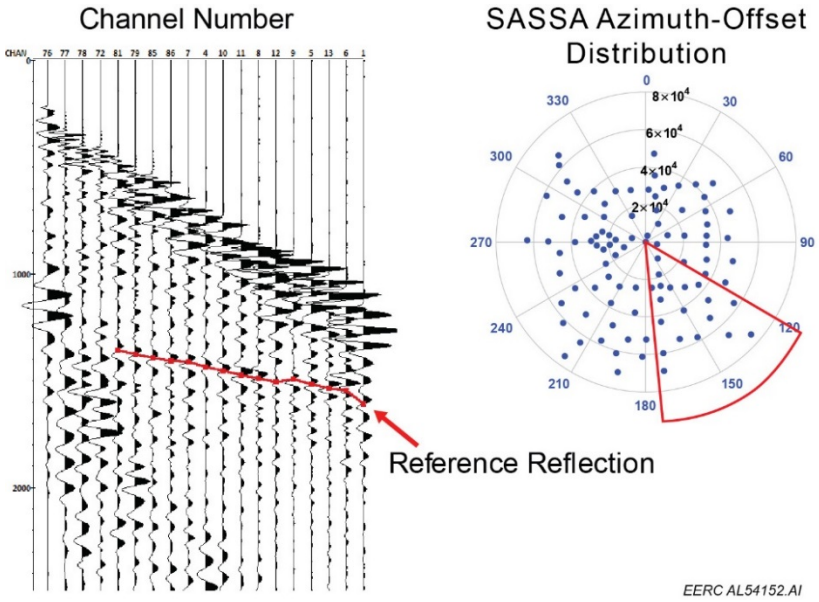

Figure 25. Common azimuth gather for the azimuth range outlined on the azimuth-offset distribution map. High-amplitude reference reflection is visible between 1350 and 1550 ms.

After the approximate time of the reservoir reflection was identified, a cross-equalization workflow was applied to the data. The input data for the cross-equalization workflow are a baseline

and monitor CRG. The baseline CRG is the stacked baseline trace repeated so that the number of traces in the baseline CRG match the number of traces in the monitor CRG (Figure 26). The monitor CRG has one stacked trace for each week that has been selected for time-lapse analysis and is ordered chronologically (Figure 26). Each trace is a stack of the 50 to 100 traces acquired that week, minus those that were removed as part of noise editing. An initial time-lapse difference display was created by subtracting the baseline data from the monitor data to assess differences and choose a design window (Figure 27). Given the uncertainty of the exact reservoir location, design windows for cross equalization were chosen to exclude data within 40 ms of the reservoir pick. Window selections were based on test results. Once a design window was chosen, phase and time correction were calculated and applied to the monitor data. The effectiveness of these corrections was analyzed by calculating QC factors such as NRMS to assess the improvement in repeatability of the two data sets and comparing the initial difference display to the difference display created using the corrected monitor data. If repeatability was improved, the corrected monitor data were used as an input to compute a shaping filter to further improve the repeatability. If repeatability was not improved, the original monitor data were used as an input to compute a shaping filter. This was only common for far offset channels where muting of first arrivals and guided waves limited the size of the design window. After the shaping filter was applied to the monitor data, a final difference display was created, and time-lapse changes were interpreted (Figure 27). For each channel discussed in this report, only results obtained using the baseline data with waveforms that are the most consistent with the monitor data are shown.

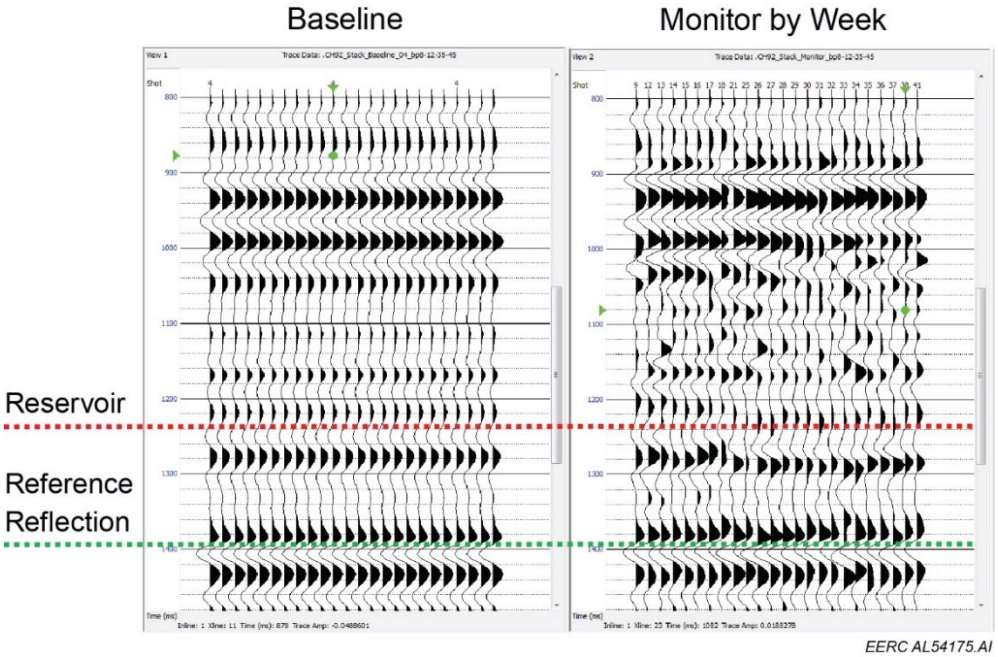

Figure 26. Left panel: repeated baseline stacked common receiver gather trace for Channel 92. Right panel: time-lapse display of stacked common receiver gather traces for Channel 92. The red dashed line indicates the approximate time corresponding to the interpreted reservoir reflection time, and the green dashed line indicates the interpreted reference reflection.

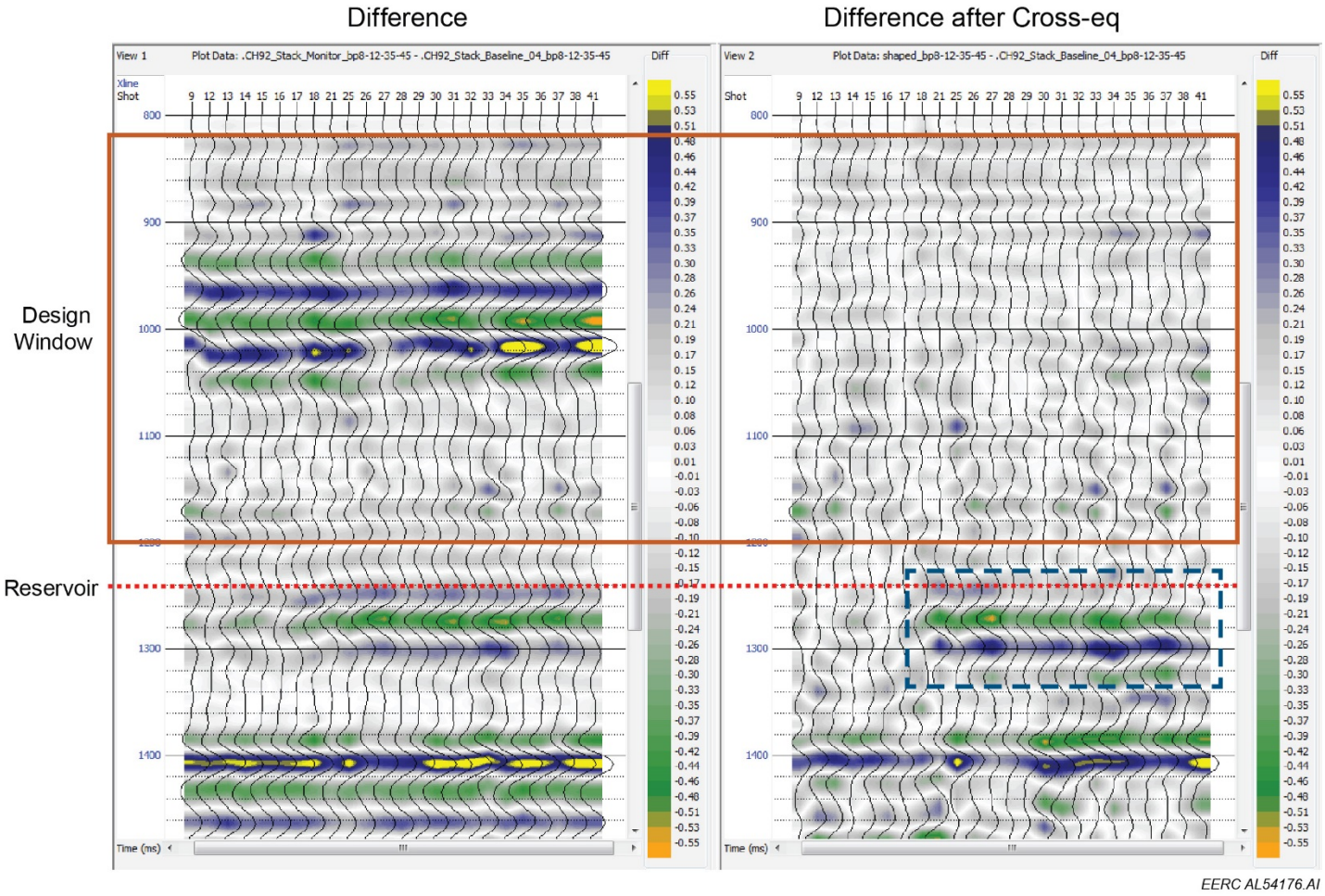

Figure 27. Left panel: difference display for Channel 92 created by subtracting baseline CRG traces from time-lapse monitor CRG traces. The colors represent the magnitude of the difference between the two data sets. Right panel: difference display after cross-equalizing the monitor with the baseline data, which corrects for phase, time, and amplitude differences. Corrections are computed over a design window above the reservoir indicated by the orange box (820–1200 ms) but applied to the entire trace. The red dashed line indicates the interpreted reservoir reflection time. A persistent difference starting at Week 18 just below the reservoir level is indicated by the dashed blue box.

RESULTS AND INTERPRETATION

This section includes results and discussion for six channels from the 26-channel subset on which advanced processing was applied. Results for the other 20 channels can be found in Appendix E – Interpretation Results. The six channels in this section correspond to monitor locations near a single injection well (Figure 28) and are a representative subset of the results obtained from time-lapse analysis.

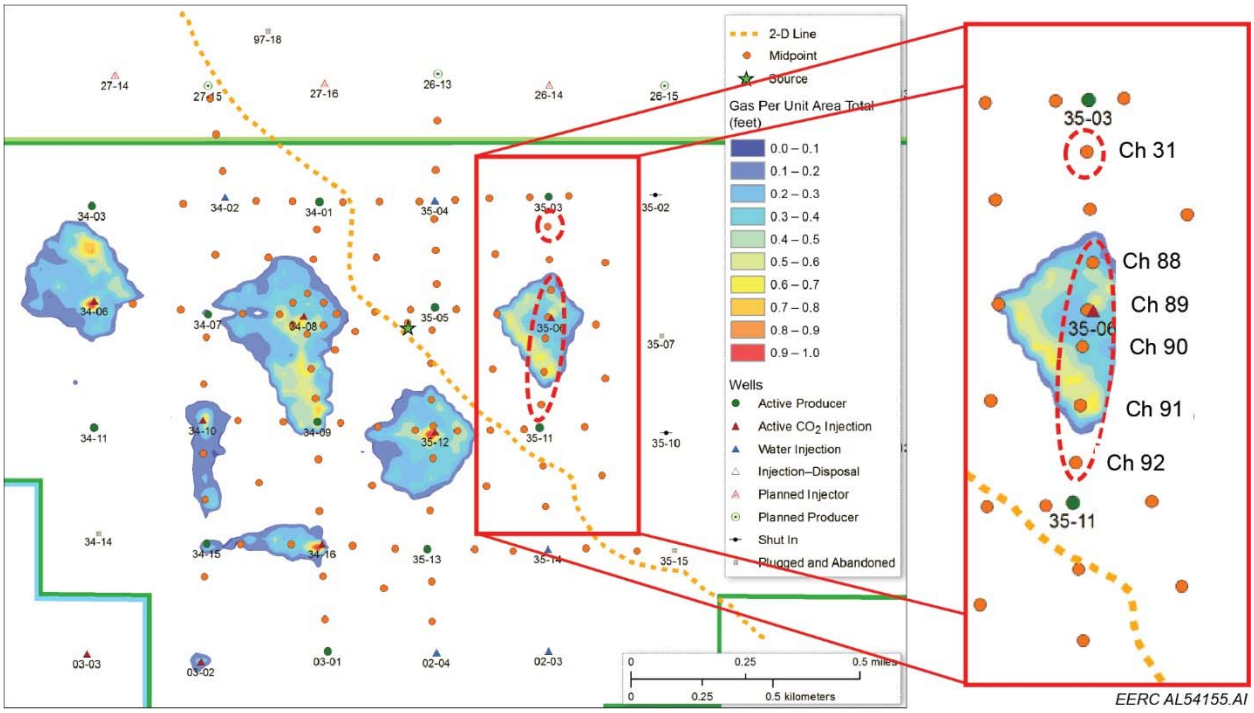

Figure 28. Map of gas saturation per unit area total generated from one possible dynamic reservoir simulation realization. The dashed red areas highlight the monitor locations corresponding to the channels discussed in this section. The orange dots depict the monitor locations. The light orange dashed line corresponds to the 2-D line.

Channel 31 (Figure 29)

- Channel 31 is offset 3961 feet from the source with the monitor point located ~1000 feet north of a CO_2 injection well that started injecting in January 2016. There is no CO_2 effect expected at this location. Baseline 3 (November 29, 2015) is used as the reference.

- Prior to cross equalization, there are differences across all weeks on several reflection events. After cross equalization, differences are corrected on almost every trace. Differences that remain appear to be due to noise. The presence of CO_2 is not indicated, as expected.

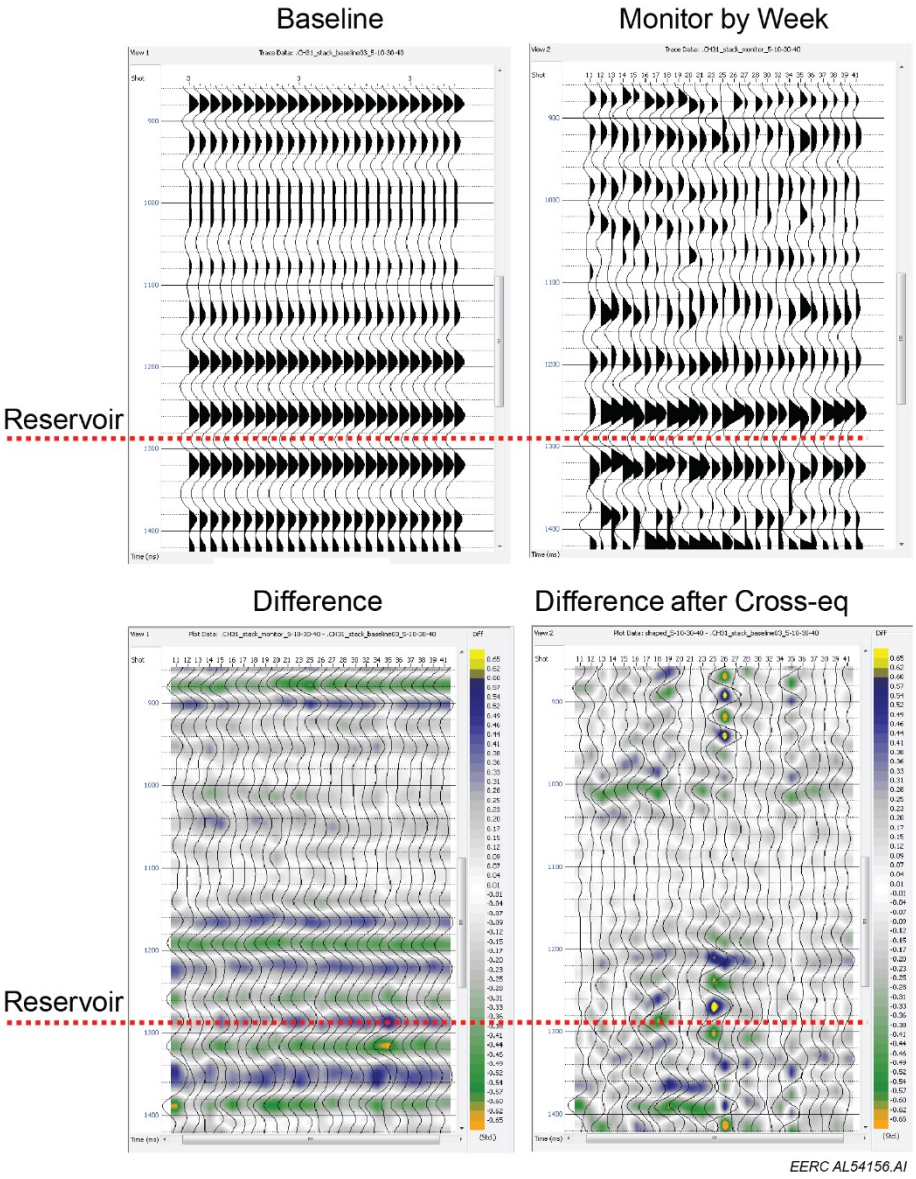

Figure 29. Time-lapse difference results for Channel 31 before and after cross equalization. The dotted red line indicates the interpreted reservoir location. The differences indicated at Week 26 are due to noise.

Channel 88 (Figure 30)

- Channel 88 is offset 3430 feet from the source with the monitor point located ~320 feet north of the 35-06 CO_2 injection well that started injecting in January 2016. A CO_2 effect is expected at this location as early as February (Weeks 10–13). Baseline 4 (December 13, 2015) is the reference.

- Prior to cross equalization, differences above and near the reservoir level are visible, but their interpretation is ambiguous. After cross equalization, the differences near the reservoir remain but are ambiguous. The difference could be due to the early arrival of CO_2.

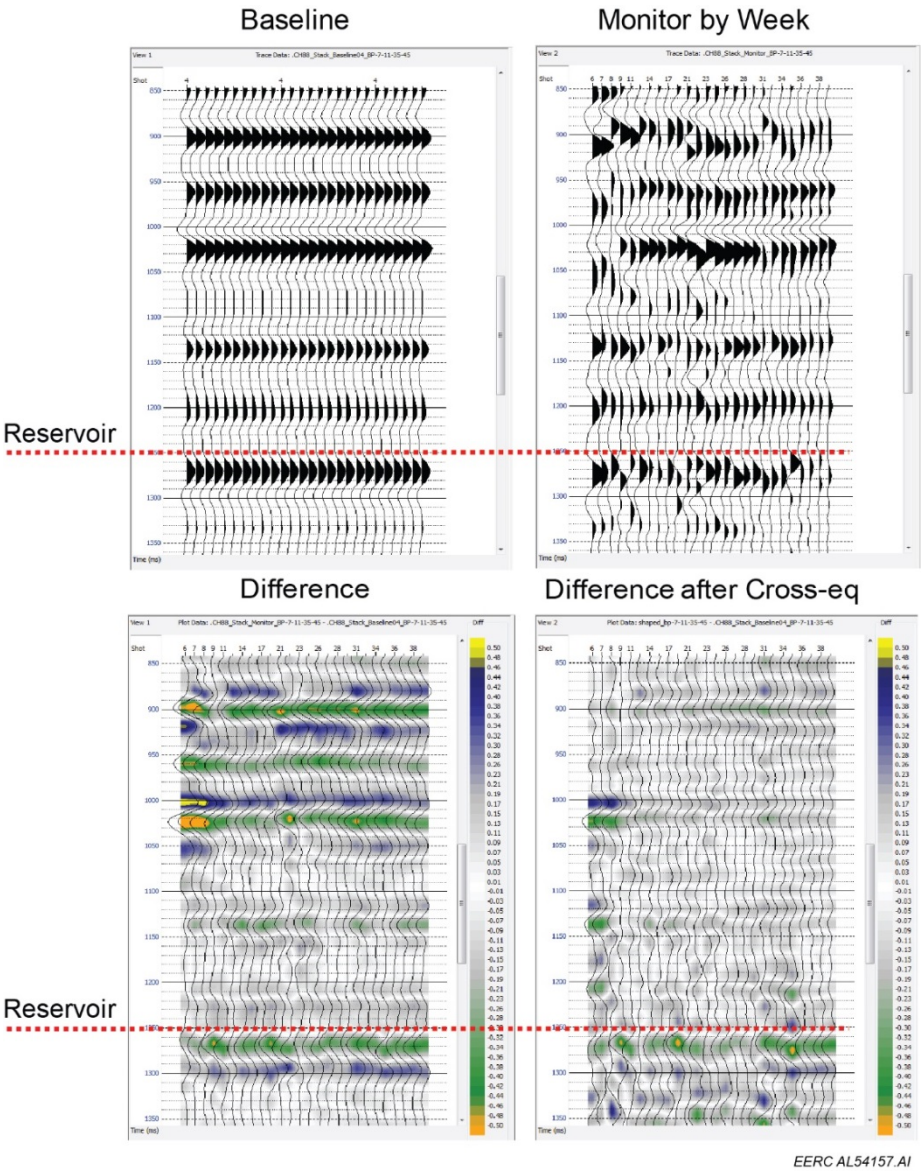

Figure 30. Time-lapse difference results for Channel 88 before and after cross equalization. Differences that remain at the reservoir level could be due to the early arrival of CO_2.

Channel 89 (Figure 31)

- Channel 89 is offset 3272 feet from the source with the monitor point located ~55 feet from injector 35-06. A CO_2 effect is expected at this location on all monitor traces recorded after January 2016, which includes all traces shown below. Baseline 4 (December 13, 2015) was the reference.

- Prior to cross equalization, the differences between monitor and baseline traces are continuous and appear to increase in magnitude with time. After cross equalization, the changes are preserved at the reservoir level, but noisy traces interfere, making the interpretation ultimately ambiguous.

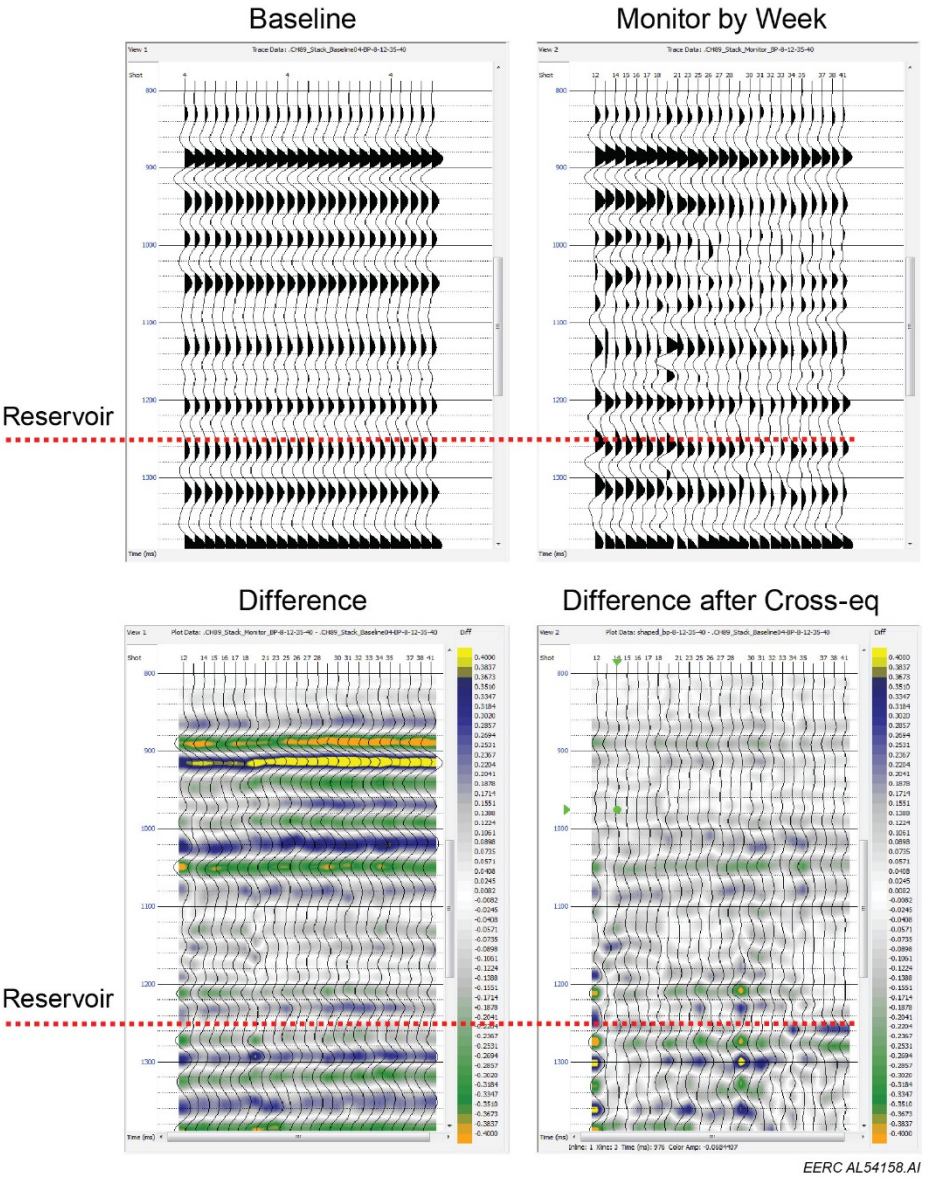

Figure 31. Time-lapse difference results for Channel 89 before and after cross equalization.

Channel 90 (Figure 32)

- Channel 90 is offset 3226 feet from the source with the monitor location ~260 feet south and cross-dip of CO_2 Injector 35-06. A CO_2 effect is expected on the data in February or March (Weeks 10–17). Baseline 4 (December 13, 2015) is the reference.

- Prior to cross equalization, the differences near the reservoir level are ambiguous. After cross equalization, a lasting change, interpreted to be due to CO_2, occurs at Week 17 (March 27, 2016).

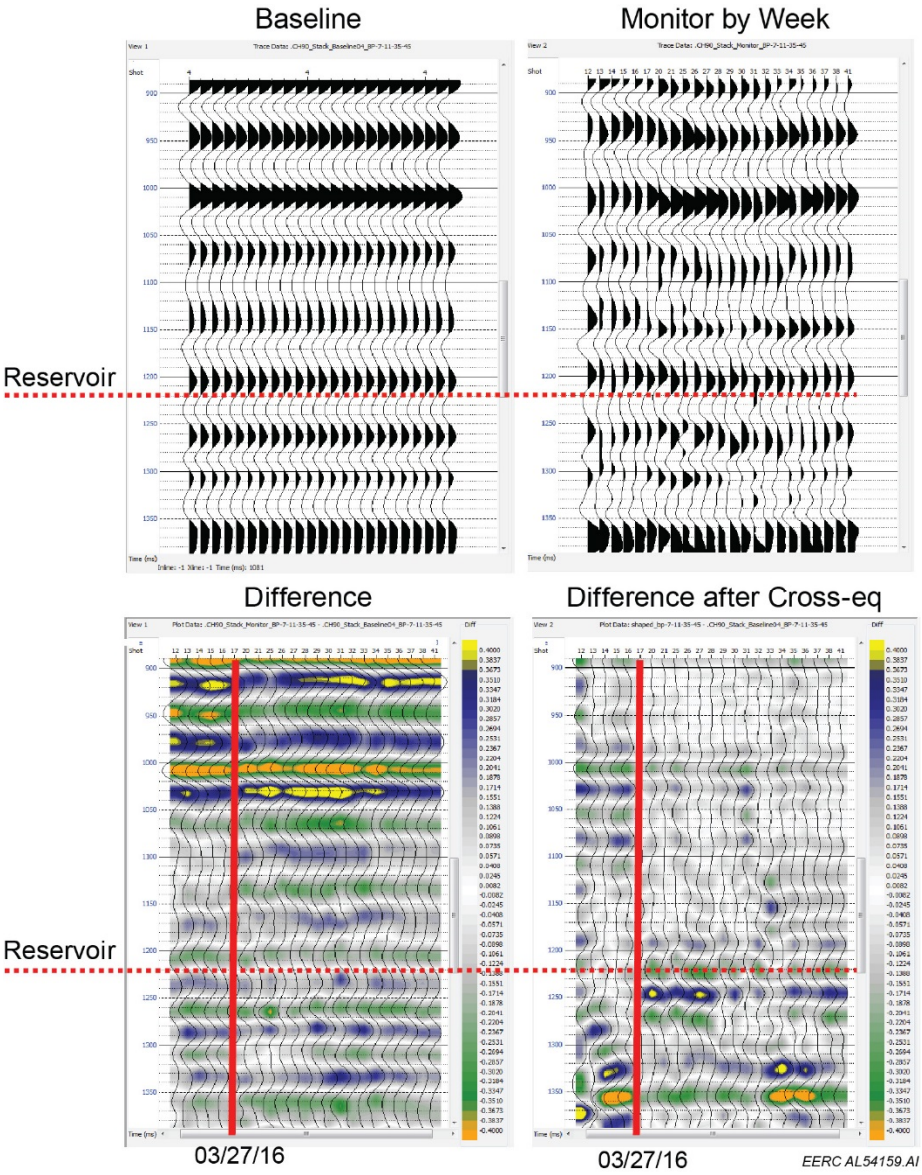

Figure 32. Time-lapse difference results for Channel 90 before and after cross equalization. A lasting change on the cross-equalized difference display is interpreted to be due to CO_2. The change occurs at Week 17, around March 27, 2016, as indicated by the red vertical line.

Channel 91 (Figure 33)

- Channel 91 is offset 3377 feet from the source with the monitor point ~630 feet south and cross-dip of CO_2 Injector 35-06; a visible CO_2 effect is possible based on the simulation result but, if present, would likely appear on later weeks. Baseline 3 is the reference (November 29, 2015).

- Prior to cross equalization, differences at reservoir level are ambiguous. After cross equalization, no reservoir changes are indicated. There appears to be no indication of the presence of CO_2, but the data appear to be impacted by acquisition noise.

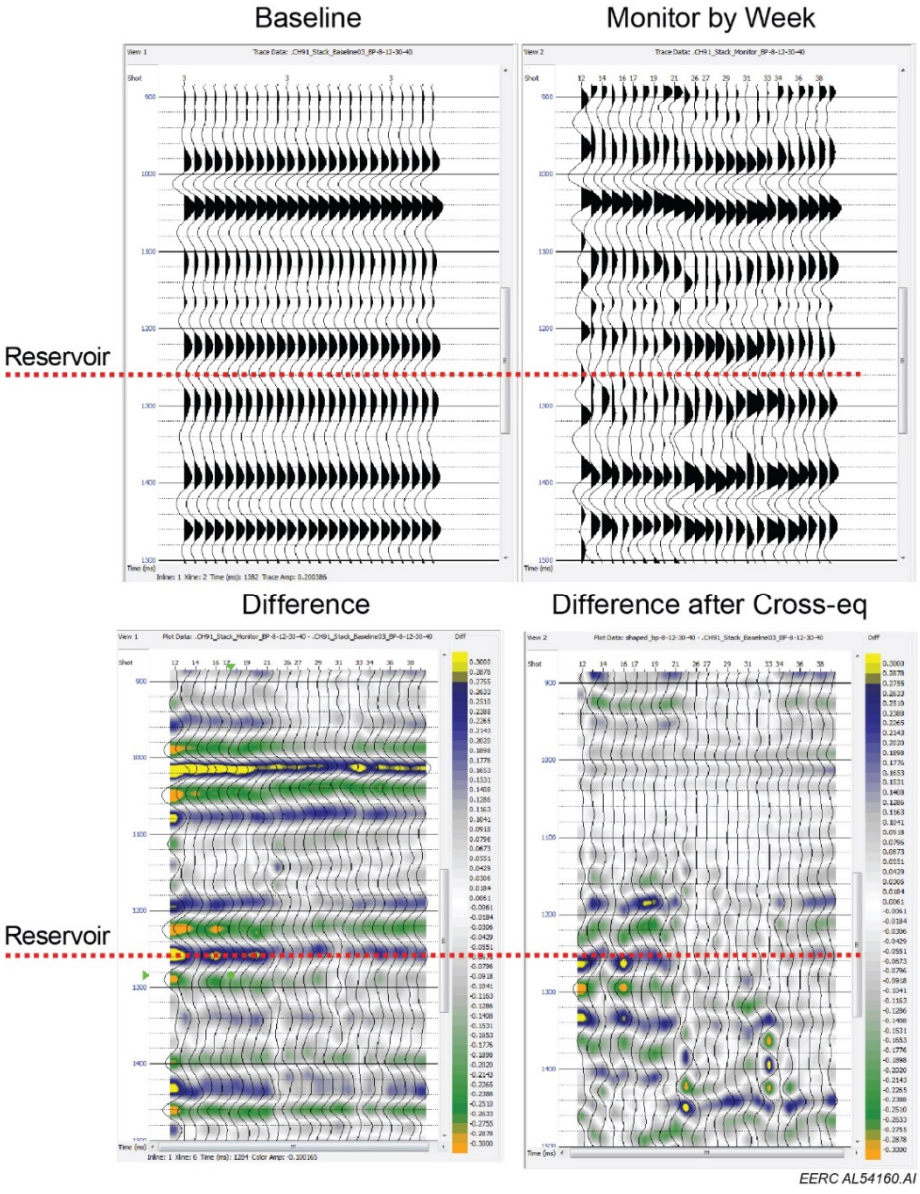

Figure 33. Time-lapse difference results for Channel 91 before and after cross equalization.

Channel 92 (Figure 34)

- Channel 92 is offset 3620 feet from the source with a monitor point ~1000 feet south of CO_2 Injector 35-06 and ~1200 feet ENE of CO_2 Injector 35-12. A visible CO_2 effect is possible but not expected based on the simulation result. Baseline 2 (November 15, 2015) was the reference.

- Differences are visible at Week 21 (May 14, 2017) on trace data, difference data, and after cross equalization. The type of difference matches expectations of what a CO_2 effect would look like, but the location and timing do not correspond with the simulation output, and CO_2 has seemingly bypassed Channel 91.

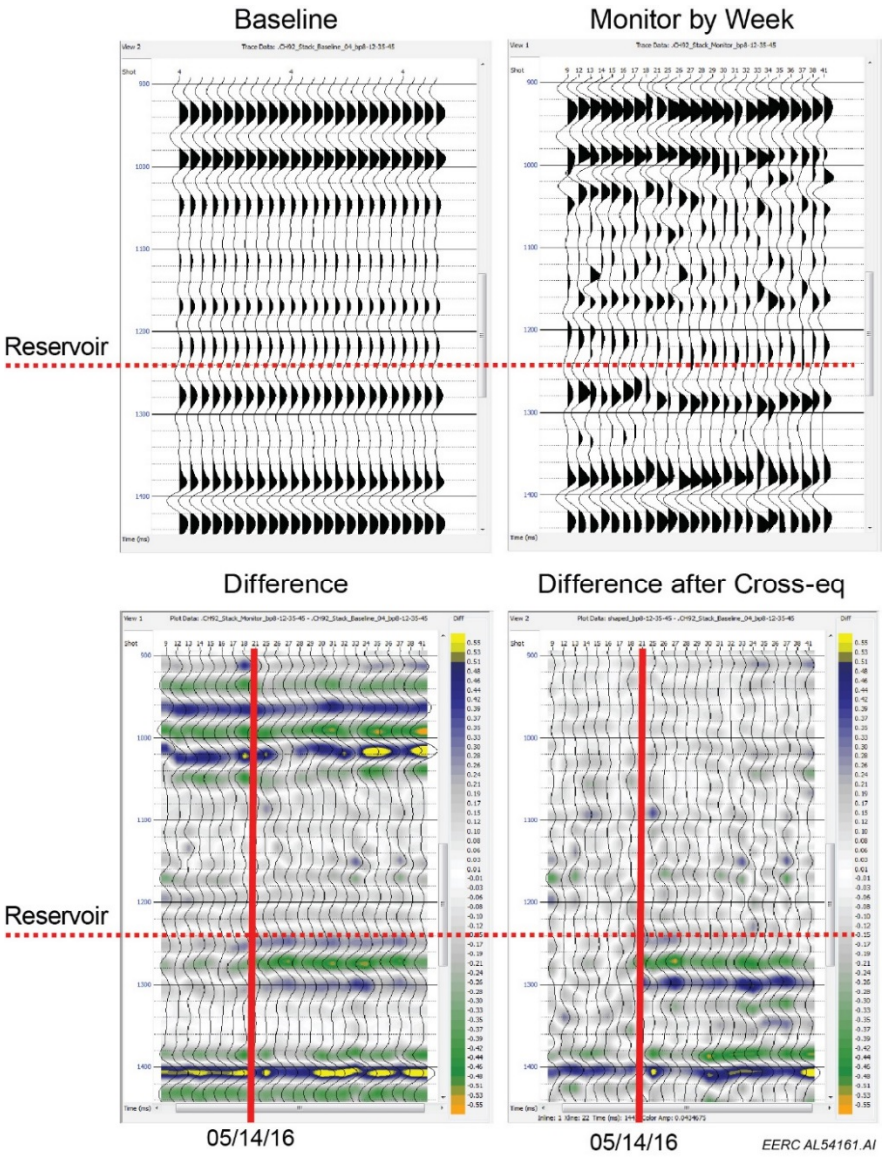

Figure 34. Time-lapse difference results for Channel 92 before and after cross equalization. An apparent CO_2 effect starts about May 14, 2016, as indicated by the vertical red line.

DISCUSSION

Twenty additional time-lapse difference displays are included in Appendix E, and this discussion incorporates those results as well. In summary, of the 26 channels chosen for analysis:

- Six channels show CO_2 where change is expected (90, 52, 57, 58, 79, 81).
- Three channels show change but are not validated by the simulation result (92, 49, 86).
- Five channels show no change where no change is expected (31,16,10,11,87).
- Twelve channels have ambiguous results (88, 89, 91, 17, 18, 48, 51, 53, 56, 59, 9, 85).

That equates to 14 positive interpreted results (the first three categories) and 12 ambiguous results. This is a very encouraging tally for a proof-of-concept study that was impacted by a variety of noise sources. As the ambiguous readings are largely due to the effect of noise on the data, a future effort that better mitigates noise during acquisition would very likely show a greater percentage of positive interpreted results.

The time-lapse results that were straightforward to interpret showed change (or no change) at or below the reservoir and were corroborated by the reservoir simulation. Most of the sensors with results containing ambiguous differences that made interpretation difficult either have low signal to noise or they are located at far offsets from the source. Both low signal to noise and far offset data impact the effectiveness of cross-equalization design. The cross-equalization process performs poorly on data with low source-to-noise ratio, and on far offsets the design window becomes squeezed by the later arrival times of first breaks and guided waves, limiting the statistics on which to design phase and amplitude corrections.

Low signal to noise affects the time-lapse difference results in other ways. If noise dominates coherent events in the design window used for time-lapse calibration, then phase and time corrections, and near-surface effects, may not be properly sampled and corrected, resulting in ambiguous differences on the time-lapse difference displays. Also, if noise dominates the reservoir reflection, a common occurrence given the low-amplitude nature of the reservoir reflection, but is not properly accounted for in the statistical design window, then noise anomalies may be introduced at the reservoir level and obscure time-lapse changes due to CO_2. Several acquisition lessons learned may be applied to a future implementation of the SASSA method that will reduce the level of noise (Appendix F).

Identification of time-lapse changes was straightforward on Channels 92 and 86, but validating the interpretation was not. Results do not match what is expected based on reservoir simulations and nearby production data. However, the monitor locations associated with Channels 92 and 86 are near the 2-D line, which also shows change in the reservoir in the area near these channels (Figure 35). The two results, time-lapse differences on the channel data and the same on the 2-D line data, appear to validate each other. Confidence is high that these changes are real and that they are caused by CO_2. That they are not validated by the reservoir simulations is probably due to the uncertainty associated with the underlying geologic model and the fact that there are multiple saturation results that can result from the same set of injection and production data. The difficulty is in reconciling the fact that the nearby production well, 35-11, did not have

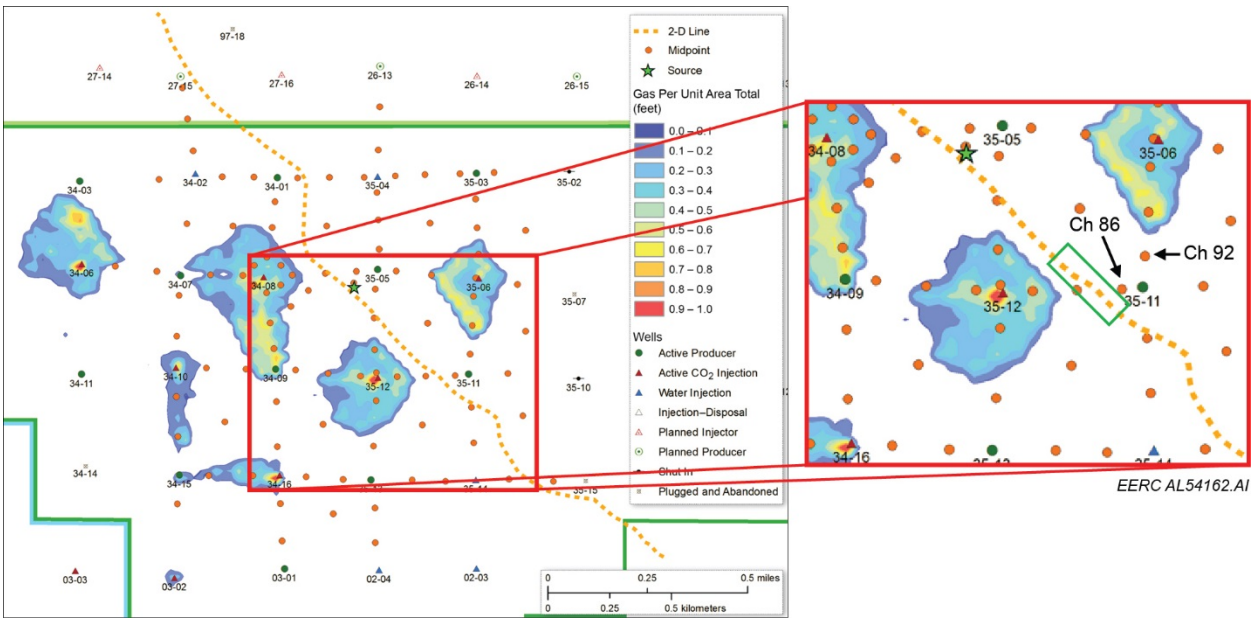

Figure 35. Map of gas saturation per unit area total generated from dynamic reservoir simulations. The orange dots depict the monitor locations. The light orange dashed line corresponds to the 2-D line. The green outline highlights the area of interpreted change in the receiver from the 2-D time-lapse data. Monitor points corresponding to Channel 86 and 92 from the main array are labeled because they also have interpreted change in the reservoir and are located near the 2-D line trace.

CO_2 breakthrough in October 2016, and the two monitor locations are only 265 feet away (Channel 92) and 178 feet away (Channel 86) and are registering a CO_2 effect as early as May 2016. Pressure changes can cause a time-lapse change, and this has been observed in other parts of the field (Salako, and others, 2017), but the change over the project acquisition period was less than 10%, and the pressure profile does not match the time of the observed change.

Previous studies done at Bell Creek have shown that CO_2 migration is heavily influenced by reservoir heterogeneities. Results from a chemical tracer study done in Development Phase 5 suggest the presence of permeability barriers and high-permeability streaks or fractures that complicate flow patterns (Fanchi and Dauben, 1982). Salako and others (2017) used 4-D seismic analysis to image and identify such permeability barriers in Development Phases 1–3 that impede the migration of CO_2. Similar reservoir heterogeneities could be influencing flow patterns in Phase 4 and explain the disconnect between time-lapse seismic and production data. A seismic attribute display created using spectral decomposition provides an enlightening image of the reservoir in Phase 4, by showing in strong relief the heterogeneities in the reservoir and around Well 35-11 (Figure 36). On the image, Well 35-11 appears to be in a lithology associated with a purple color, whereas the monitor points for Channels 92 and 86 may be in a different lithology 265 feet to the north and 178 feet to the west, respectively. Whatever the case, it is clear that the reservoir in the Phase 4 study area is much more heterogeneous than in the nearby Phase 2 to the southwest. 4-D seismic data collected in the fall of 2017 may confirm the presence of permeability barriers and high-permeability streaks or fractures in this area.

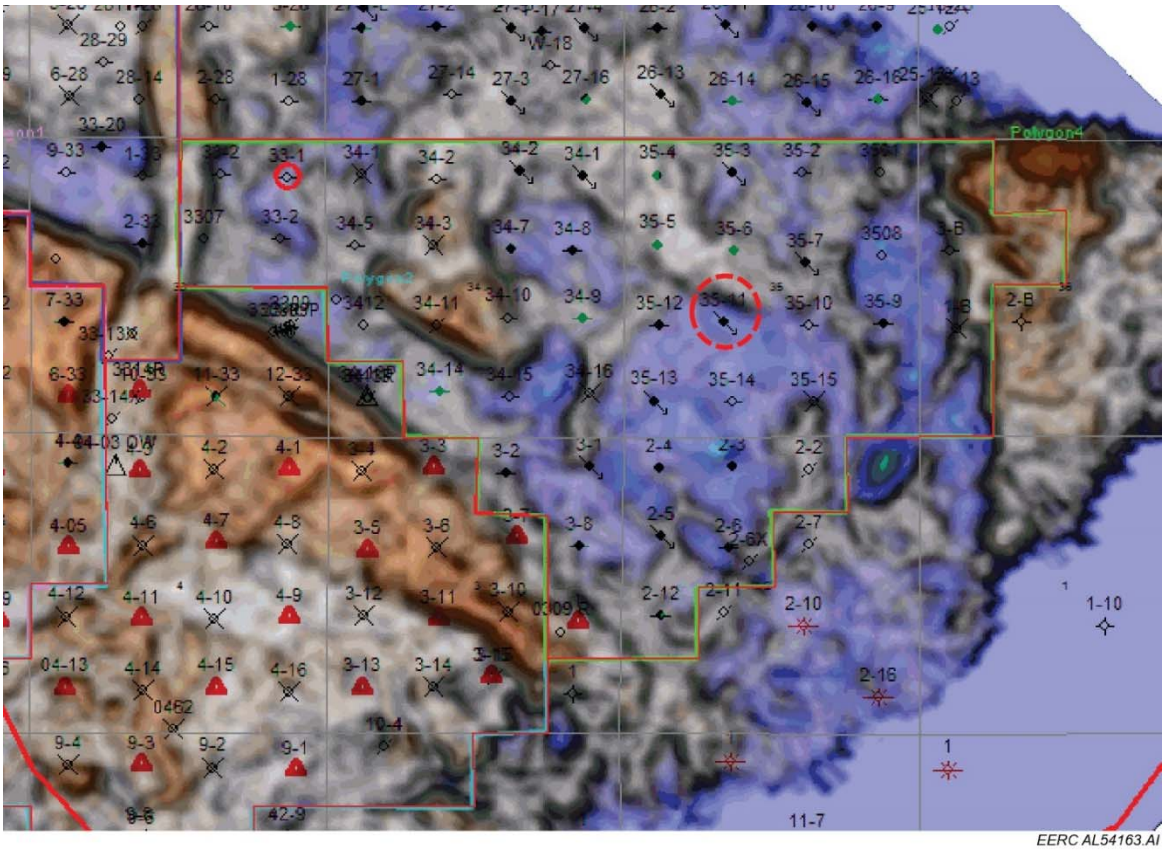

Figure 36. Map of the reservoir from a spectral decomposition analysis. Shadowing highlights lateral discontinuities or edges; color fill can be used to infer lithology or thickness changes within the reservoir. Phase 4 complexity appears greater than Phase 2 to the southwest. The red dashed circle outlines Well 35-11 (modified from a presentation by Thang Pham of Denbury on January 7, 2015).

Lessons Learned

1. The GISCO seismic source as deployed was robust and stable. It can be fired more times each week than was done initially. Additional shots can increase the signal-to-noise ratio when stacked. A disadvantage is that it requires active operation by a technical person and cannot be operated automatically.

2. The best time to shoot is in the early morning to avoid wind noise and noise from human activity. Automated shooting with a source that does not require personal interaction would be an improvement, as acquisition could easily be done at the quietest hours.

3. Noise from a variety of sources was not always able to be removed in processing and creates interpretation ambiguity in the time-lapse processed data.

4. Several "baseline" data sets are better than a single baseline data set, and the baseline least affected by noise should be used in the interpretation as the reference. The amount of variability

exhibited on baseline data sets was unexpected. The same baseline acquisition may be noisy on one node's data, but quiet on another's, so different baselines may be the time-lapse reference on different nodes for a given monitor acquisition date.

5. Seasonal changes in near-surface conditions are pervasive and highly variable over the year of data collection; their impact on data at reservoir depth was not excessive and appeared to be corrected with cross-equalization methods.

6. A "time-zero node" placed just outside the source shed provided a means to recover shots when global positioning system (GPS) time stamps were lost or unrecoverable from the source signature recorder. It also provided a way to calculate static shifts to correct traces for errant triggering early in the project.

7. An inexpensive third-party accelerometer attached to the source weight provided a useful backup to the accelerometer that came with the source, and a more interpretable waveform.

8. The addition of a weather station to the source structure that includes a wind speed indicator and an additional Internet camera to view outdoor conditions prior to shooting would be helpful to avoid proceeding with acquisition during noisy conditions.

9. Assessment of cultural noise at each receiver station is needed to judge background noise levels at individual receiver locations and may spur receiver relocation. The noise assessment also informs the processing for the individual receiver gather data.

10. Surface geology at the source location is important. If possible, avoiding source placement on swelling clays could avoid a problem with the sinking of the strike plate over time.

11. Siting the source at a location with good drainage is a necessity. In spite of being located on a topographical rise, the source location became waterlogged in the spring.

12. Additional design considerations for the strike plate will be considered to improve or increase the surface area of the base to mitigate sinking over time. The footing was pounded 6 inches or more into the ground, requiring additional plates to be added and the source tires to be dug into the ground to lower the source platform to ensure the source weight would not fall too far and be stranded (unable to be lifted).

13. A more robust means of isolating the source electronics from high-voltage transients in addition to high current surges is needed. This could be as simple as plugging the battery chargers into the UPS (uninterruptible power supply) system instead of the wall.

14. Spare parts on hand for mission vital equipment is imperative; this includes a spare control electronics card.

15. The PVC (polyvinyl chloride) pipe and caps protected the nodes from theft, wildlife, and livestock very well. They may be dug in deeper to minimize wind noise. Wind was a big factor in the acquisition noise on data.

16. Nodes in their PVC protectors were difficult to locate in the snow. A marker made from sticks or other material would prevent lost time searching.

17. Satellite Internet is slow with a long latency and requires a very tight antenna alignment that is not reliable when winter winds blow against the satellite dish or when rain is falling. Two service calls were needed during the year for the source system.

18. If there is an internal component failure with a node it cannot be determined until data harvest, resulting in missed data collection. Several weeks of data failed to record at one location because of a node that failed to properly deploy.

19. To prevent the source from firing in a runaway condition, multiple fail-safes are needed to stop the source from shooting. These include the hardware limit switch and a single-shot Web relay signal. The hardware limit switch will fail over time, and a replacement will be needed.

20. The Web camera has proven to be vital for safe remote shooting. A second camera should be mounted outside the source shed to provide a view of the weather conditions.

21. The source signature recorder performed well, but the GPS time stamp file was corrupted during the overvoltage incident in early September. As a result, five previously acquired data sets were not harvested. A change in procedure was implemented to download and save the time stamp file after each acquisition, so that loss was not possible.

Future Work

There are several possibilities for future work to further analyze the SASSA data and SASSA trace-based analysis method. Only vertical component data were processed and analyzed for periods when the source was being actively fired, but three-component data were acquired both actively when the source was being fired as well as passively when the nodes were recording but the source was not actively being fired. A recently awarded project proposes to integrate this active and passive three-component SASSA data into a multidimensional processing workflow for improved noise analysis and attenuation. The SASSA data will be assessed to determine their suitability for the application of interferometric and compressive sensing algorithms, which could improve the spatial resolution of the SASSA technique. Seismic noise from cultural and meteorological sources (passive seismic data) will be analyzed to estimate a representative noise model of active oil fields. The noise model is a product that can be used to define improved data-processing workflows. The ultimate product of this proposed study is an integrated data acquisition-processing system for low-cost, time-lapse seismic CO_2 injection monitoring.

A new time-lapse analysis method originally proposed by Levin (2010) was tested on 4-D seismic previously collected at Bell Creek and the 2-D line collected as part of the SASSA project. Results of this testing show that this method is complementary to conventional time-lapse analysis (Livers and others, 2017). The method uses spectral ratios and shaping filters computed on windows above and including the reservoir to cancel out signal common to both windows such as monochromatic noise. The method may be especially valuable in situations where varying coherent noise and the complications due to seasonal near-surface changes and changes in coupling

impact the interpretation of conventional methods. The advantages of the method could be especially helpful to mitigating ambiguity on the main SASSA array data. Promising results from the testing done in this study warrant future application of the method to the main array data.

Another way to test the SASSA trace-based analysis method is to apply the SASSA method to existing time-lapse seismic from other sites with geologic injection of CO_2. Time-lapse seismic data have been acquired at CO_2 injection sites, including Bell Creek. Several time-lapse seismic data sets were acquired at Bell Creek as part of time-lapse 2-D, 3-D, and vertical seismic profile (VSP) surveys that can be parsed and used to simulate arrays with a stationary source. The advantage of using these data sets is that the location of CO_2 imaged by conventional time-lapse analysis of these data have been verified with repeat surveys and other complementary monitoring methods such as repeat pulse neutron logging campaigns and the seismic data were acquired using stronger sources that produced data with a wider bandwidth.

Other current DOE projects being conducted at Bell Creek will produce additional time-lapse data sets and may lead to new geologic interpretation of the SASSA study area. A 3-D baseline survey was collected over the SASSA project area in 2012 as part of the PCOR Partnership Program, and a repeat survey was collected in 2017 as part of the K-wave project being conducted by the EERC. The time-lapse analysis of the 4-D data is expected to reveal the CO_2 locations and plume geometry in Phase 4, which may confirm the existence of time-lapse changes interpreted in the SASSA 2-D and main array data. There is also analysis of time-lapse InSAR data from Bell Creek being done through the PCOR Partnership. Time-lapse InSAR data indicate uplift in Phase 4, and this in-depth analysis may provide additional insight into the geomechanics of Phase 4. This new information will be used to update reservoir simulations, which can be used to improve SASSA interpretations.

There is also potential to redeploy the SASSA array in the Bell Creek Field and collect another year's worth of time-lapse data at a new location. With the knowledge gained from the feasibility test lessons learned, new acquisition techniques would be applied, including shooting the source during time periods when noise due to weather and human activity is minimized and using a different, stronger source such as an orbital vibrator to improve the signal-to-noise ratio of the overall data and boost the bandwidth. Applying the lessons learned and leveraging previous experience in the field, significant improvements to general data quality and operational efficiency would be likely.

Potential Benefits of a Commercialized SASSA System

While not currently at the commercial readiness stage, the current project has been a successful feasibility study that resulted in many lessons learned that would be applied to any future implementation of the SASSA technology. Also, during the term of the project, new and affordable, remotely operable source options have come on the market that feature significantly higher energy output and programmable, hands-free operations. A system much closer to commercial viability is possible and would offer several benefits for monitoring CO_2 injection for either EOR or carbon capture, utilization, and storage (CCUS) applications. These benefits are detailed as follows.

Remote Source Operation

The proof-of-concept project has shown that remote operation via the Internet or other communication means is easily accomplished and obviates the need for local staff for monitoring operations, thereby reducing the cost of monitoring.

Low Impact

A relatively low number of sensors needs to be installed compared to traditional surface seismic surveys. The feasibility study used only 96 sensors, but the SASSA system does not have a limit. The unobtrusive installation of sensors at ground level or just below the surface, combined with the infrequent access needed to service them, means that landowners, facility operators, and other local stakeholders are not impacted in any significant way by an installed, operating SASSA system.

Simple Processing Workflow

Once optimized for the specific monitoring site characteristics, the basic nature of the processing workflow can be applied easily and results provided quickly. Once scripts are created, processing subsequent data is routine and quick, as SASSA data volumes tend to be manageable in size. This rapid turnaround would provide actionable data over periods of weeks instead of months or years.

Increased Temporal Resolution

Monitoring data sets were acquired on a weekly and semiweekly basis for the proof-of-concept study. Finer time increments are possible, but balanced by diminishing returns. When the processed data are displayed chronologically on interpretation panels, the ability to monitor subsurface changes over time in detail is demonstrated. The incremental results can help determine when and where the CO_2 saturation front has progressed, provide actionable information to the field operator, help to improve the accuracy of reservoir simulations, and inform the timing of acquisition of more expensive conventional 3-D repeat surveys.

Ease of Use

While significant geophysical expertise was employed on the proof-of-concept study, the system was user-friendly enough that when operations became routine, nonexperts could be trained to handle the field aspects of the monitoring, leaving the processing and interpretation to more qualified staff.

Dual Purpose

The system and method is adaptable and can be used to monitor multiwell injection patterns in fields undergoing CO_2 EOR and the progress of the CO_2 saturation front away from a single well or multiple wells at a CCUS site.

Addresses NETL Goals

As a CO_2 injection monitoring system, a commercialized SASSA system would directly address the goal of NETL's Office of Research and Development (ORD) to develop and validate technologies to measure and account for 99% of injected CO_2 in the injection zones. By tracking the progress of the subsurface CO_2 saturation front, the system helps to address the goals of ensuring containment effectiveness and developing best practices for site operations.

CONCLUSION

Autonomous equipment and innovative processing techniques were used to apply the seismic method to monitor individual, strategically chosen reservoir reflection points for detectable signal character changes that could be attributed to the passing of a CO_2 saturation front. A sparse array of 96 receivers and a single stationary 850-lb weight drop source referred to as the scalable automated semipermanent seismic array was designed to monitor four overlapping "five-spot" EOR injector—producer patterns. The array was successfully deployed in the Bell Creek oil field from October 2015 to October 2016. Forty-one sets of data were successfully acquired, including five sets of pre-CO_2 injection or baseline data.

Significant effort was applied to developing a processing flow for application in the common receiver domain to preserve amplitudes on individual channel data. Simple processing and time-lapse analysis was applied to 39 sets of data for the 96 receiver locations in the array. Advanced processing was applied to a subset of 26 receivers. As noted in the discussion section, interpretation results from this subset are very encouraging, with 14 positive interpreted results and 12 channels that had ambiguous results. Results were not always black and white, but confidence is high that the data show changes due to CO_2. Ambiguity in identifying changes due to CO_2 exists mostly because of acquisition noise levels. Several types of seismic noise had an impact on the interpretability of the data, and extra effort should be made to mitigate their impacts on a future implementation based on the documented lessons learned.

Validation methods from reservoir simulations and a time-lapse 2-D line acquired through the middle of the study area helped the interpretation. Simulated CO_2 saturation plumes and the 2-D line do not appear to overlap, but indications on both SASSA data and the 2-D line suggest that changes thought to be due to CO_2 were encountered.

The ultimate aim of the project was to evaluate whether deployment of SASSA technology can provide a cost-effective monitoring solution for future CO_2 injection projects. Current results and expected improvements from future application of the many lessons learned from this pilot study suggest that SASSA is a viable monitoring technology for certain geologic settings. Future iterations and technology advances will likely produce significant improvements and efficiencies.

REFERENCES

Barajas-Olalde, C., Livers, A.J., Burnison, S.A., Hamling, J.A., and Gorecki, C.D., 2017, Estimating time-lapse near-surface velocity models using ground roll from coarsely sampled 2-D land crooked surveys: Presented at the23rd European Meeting of Environmental and Engineering Geophysics.

Bosshart, N.W., Jin, L., Dotzenrod, N.W., Burnison, S.A., Ge, J., He, J., Burton-Kelly, M.E., Ayash, S.C., Gorecki, C.D., Hamling, J.A., Steadman, E.N., and Harju, J.A., 2015, Bell Creek test site – simulation report: Plains CO_2 Reduction (PCOR) Partnership Phase III Task 9 Deliverable D66 (Update 4) for U.S. Department of Energy National Energy Technology Laboratory Cooperative Agreement No. DE-FC26-05NT42592, EERC Publication EERC-10-09, Grand Forks, North Dakota, Energy & Environmental Research Center, August.

Burnison, S.A., Bosshart, N.W., Salako, O., Reed, S., Hamling, J.A., and Gorecki, C.D., 2017b, 4-D seismic monitoring of injected CO2 enhances geological interpretation, reservoir simulation, and production operations: Energy Procedia, v. 114, p. 2748–2759.

Burnison, S.A., Beddoe, C.J., Glazewski, K.A., Salako, O., Hamling, J.A., Ayash, S.C., and Gorecki, C.D., 2015, Technical design of a scalable, automated, semipermanent seismic array (SASSA) method for detecting CO_2 extent during geologic CO_2 injection: Deliverable D2 Interim Report on Completion of Technical Design (Oct 1, 2013 – Oct 31, 2015) for U.S. Department of Energy National Energy Technology Laboratory Cooperative Agreement No. DE-FE0012665, Grand Forks, North Dakota, Energy & Environmental Research Center, October.

Burnison, S.A., Burton-Kelly, M.E., Zhang, X., Gorecki, C.D., Steadman, E.N., and Harju, J.A., 2014, Bell Creek test site – 3-D seismic and characterization report: Plains CO_2 Reduction (PCOR) Partnership Phase III Task 4 Deliverable D96 for U.S. Department of Energy National Energy Technology Laboratory Cooperative Agreement No. DE-FC26-05NT42592, EERC Publication 2015-EERC-04-04, Grand Forks, North Dakota, Energy & Environmental Research Center, March.

Burnison, S.A., Livers, A.J., Hamling, J.A., Salako, O., and Gorecki, C.D., 2017a, Design and implementation of a scalable, automated, semipermanent seismic array for detecting CO_2 extent during geologic CO_2 injection: Energy Procedia, v. 114, p. 3879–3888.

Fanchi, J.R., Dauben, D.L., and Carroll, H.B., 1982, An evaluation of the Bell Creek Field micellar-polymer pilot: Department of Energy Report under Contract No. DE-AC19-80BC10033.

Jin, L., Bosshart, N.W., Oster, B.S., Hawthorne, S.B., Peterson, K.J., Burton-Kelly, M.E., Feole, I.K., Jiang, T., Pekot, L.J., Peck, W.D., Ayash, S.C., and Gorecki, C.D., 2016, Bell Creek test site – simulation report: Plains CO_2 Reduction (PCOR) Partnership Phase III draft Task 9 Deliverable D66 (Update 5) executive summary for U.S. Department of Energy National

Energy Technology Laboratory Cooperative Agreement No. DE-FC26-05NT42592, Grand Forks, North Dakota, Energy & Environmental Research Center, August.

Levin, S.A., 2010, Systems and methods for monitoring time-dependent subsurface changes: U.S. Patent 7,843,766 B2.

Livers, A.J., Burnison, S.A., Barajas-Olalde, C., Salako, O., and Gorecki, C.D., 2017, Scalable, automated, semipermanent seismic array method for detecting CO_2 extent during geological CO_2 injection—application of Levin's 4-D Quick Look to time-lapse seismic data sets: Prepared for U.S. Department of Energy National Energy Technology Laboratory Cooperative Agreement No. DE-FE0012665, Grand Forks, North Dakota, Energy & Environmental Research Center, August 2017.

Pham, T., 2015, Muddy sand reservoir characterization, Bell Creek Field, MT: Denbury presentation.

Salako, O., Livers, A.J., Burnison, S.A., Hamling, J.A., Wildgust, N., Gorecki, C.D., Glazewski, K.A., and Heebink, L.V., 2017, Analysis of expanded seismic campaign: Plains CO_2 Reduction (PCOR) Partnership Phase III Task 9 Deliverable D104 for U.S. Department of Energy National Energy Technology Laboratory Cooperative Agreement No. DE-FC26-05NT42592, Grand Forks, North Dakota, Energy & Environmental Research Center, March.

APPENDIX A

MAIN ARRAY DATA ACQUISITION DETAILS

MAIN ARRAY DATA ACQUISITION DETAILS

This appendix includes maps and tables that contain additional information about the array design and data acquisition (Figures A-1–A-2 and Tables A-1–A-2).

To get ground-truth measurements of coordinates and elevations for the final semipermanent array, on the third semipermanent seismic array (SASSA) trip (December 7–11, 2015), manual global positioning system location measurements were taken at each node location.

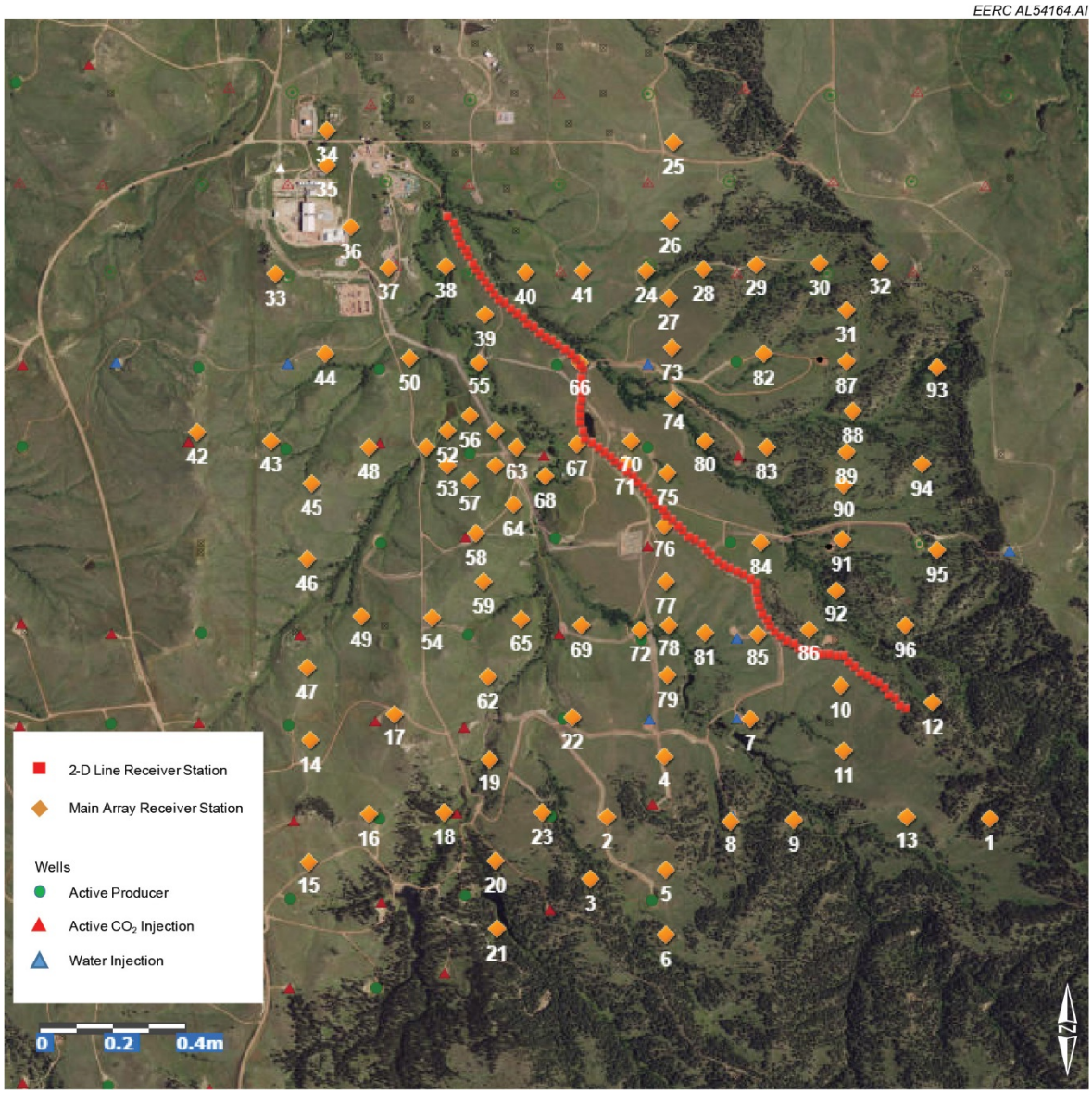

Figure A-1. Overhead view of SASSA study area with topography, showing channel locations and numbers, and the orientation of the 2-D line. Source location is beneath the label for Channel 70.

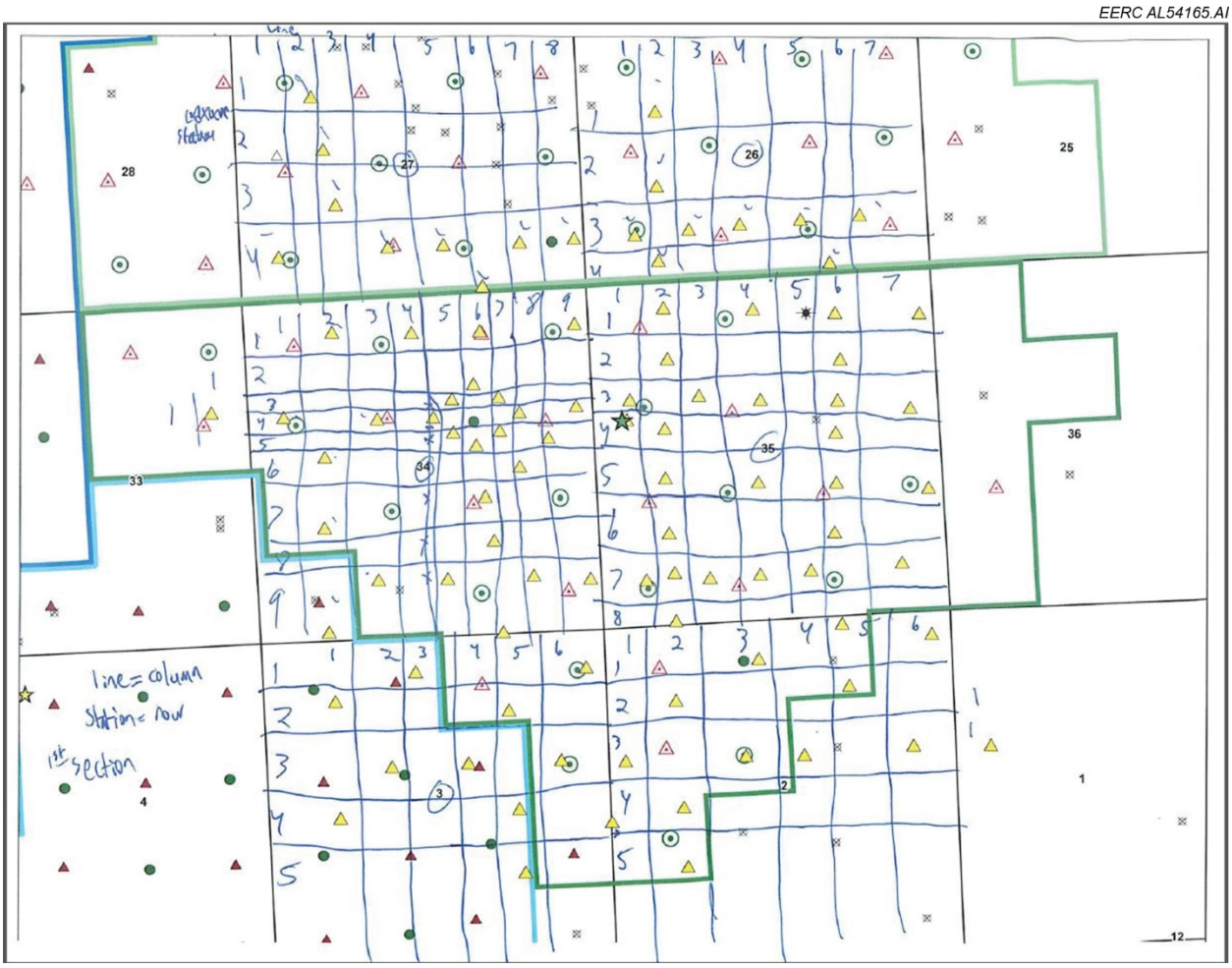

Figure A-2. Original “Line and Station” node location grid. FairfieldNodal acquisition job setup requires a line and station location for each node. Columns indicate lines, rows are station. The values are preceded by the section number (e.g., the most northwest section is 27). The northwesternmost node has line and station (272, 271). The southernmost node in Section 3 has line and station (25, 25). Arbitrary node spacing required a nonuniform gridding system for different sections.

Table A-1. Main Array Channel and Location Crosswalk

Channel	Xft_1927 MT Stateplane FIPS 2503	Yft_1927 MT State Plane FIPS 2503	Lidar Elevation, ft amsl	Piper Reference Pick Time, ms	Interpreted Reservoir Time, ms	Offset, ft
1	3147105.82	427642.89	3967.07	1545.75	1395.75	7470.88
2	3141500.72	427353.31	3845.00	1478.00	1328.00	5192.88
3	3141293.53	426436.31	3846.60	1516.00	1366.00	6112.31
4	3142278.07	428296.95	3771.93	1436.00	1286.00	4325.46
5	3142403.26	426640.01	3894.61	1518.00	1368.00	5979.51
6	3142449.46	425687.09	3896.49	1545.75	1395.75	6928.71
7	3143517.70	428901.65	3765.19	1410.00	1260.00	4180.75
8	3143305.21	427404.35	3832.10	1488.00	1338.00	5459.75
9	3144245.61	427472.81	3826.80	1492.00	1342.00	5783.35
10	3144810.30	429459.46	3822.51	1454.00	1304.00	4548.72
11	3144908.24	428524.01	3798.20	1474.00	1324.00	5291.95
12	3146173.74	429306.19	3883.08	1506.00	1356.00	5712.31
13	3145898.60	427612.45	3839.36	1534.50	1384.50	6630.33
14	3137062.88	428235.82	3796.36	1518.75	1368.75	6163.87
15	3137152.99	426464.35	3872.96	1620.00	1470.00	7457.65
16	3137980.98	427204.90	3860.74	1534.00	1384.00	6379.30
17	3138274.27	428698.06	3823.06	1488.00	1338.00	5001.44
18	3139095.53	427289.41	3718.37	1470.00	1320.00	5767.72
19	3139705.17	428109.90	3732.11	1448.00	1298.00	4774.02
20	3139883.18	426625.05	3788.52	1514.25	1364.25	6129.76
21	3139971.68	425630.04	3802.24	1586.25	1436.25	7076.31
22	3140893.75	428789.53	3725.31	1396.00	1246.00	3800.38
23	3140523.26	427370.57	3813.36	1476.00	1326.00	5261.25
24	3141628.59	435371.13	3718.50	1386.00	1236.00	2829.53
25	3141928.02	437267.59	3775.94	1480.00	1330.00	4743.74
26	3141947.21	436117.21	3774.98	1416.00	1266.00	3602.98
27	3141978.84	434991.26	3720.90	1370.25	1220.25	2497.72
28	3142457.17	435444.31	3764.12	1400.00	1250.00	3062.01
29	3143237.12	435562.91	3821.08	1408.00	1258.00	3496.72
30	3144156.30	435618.65	3854.88	1430.00	1280.00	4081.86
31	3144601.10	434972.02	3908.59	1436.00	1286.00	3961.62
32	3145045.88	435695.31	4038.23	1505.25	1355.25	4765.59
33	3136175.44	435022.51	3763.81	1532.25	1382.25	5844.28
34	3136816.53	437171.96	3610.17	1566.00	1416.00	6560.88
35	3136850.49	436664.45	3617.22	1532.25	1382.25	6188.10
36	3137262.06	435771.19	3647.42	1503.00	1353.00	5300.99
37	3137830.40	435201.21	3648.22	1442.00	1292.00	4504.42
38	3138687.25	435277.61	3634.31	1418.00	1268.00	3898.71
39	3139292.01	434603.17	3647.46	1396.00	1246.00	2995.22
40	3139858.12	435255.14	3654.99	1412.00	1262.00	3151.86

Continued . . .

Table A-1. Main Array Channel and Location Crosswalk (continued)

Channel	Xft_1927 MT Stateplane FIPS 2503	Yft_1927 MT State Plane FIPS 2503	Lidar Elevation, ft amsl	Piper Reference Pick Time, ms	Interpreted Reservoir Time, ms	Offset, ft
41	3140686.15	435330.65	3686.77	1384.00	1234.00	2892.54
42	3135149.26	432654.15	3878.96	1561.50	1411.50	6320.78
43	3136259.23	432589.18	3762.71	1478.00	1328.00	5210.06
44	3136986.84	433896.24	3707.82	1464.00	1314.00	4681.20
45	3136883.11	431989.96	3753.26	1464.75	1314.75	4619.60
46	3136883.41	430895.15	3718.70	1448.00	1298.00	4873.83
47	3136960.21	429303.09	3772.74	1496.00	1346.00	5554.04
48	3137696.10	432575.72	3709.91	1406.00	1256.00	3773.13
49	3137712.43	430102.15	3734.39	1437.75	1287.75	4481.69
50	3138210.46	433895.44	3646.58	1413.00	1263.00	3526.98
51	3138539.17	432614.84	3652.56	1392.75	1242.75	2930.75
52	3138826.89	432876.56	3652.65	1332.00	1182.00	2662.81
53	3138850.04	432378.19	3676.72	1323.00	1173.00	2624.45
54	3138767.46	430121.91	3760.98	1404.00	1254.00	3629.82
55	3139250.46	433902.84	3641.40	1318.00	1168.00	2600.61
56	3139153.39	433106.95	3655.48	1307.25	1157.25	2382.67
57	3139206.74	432178.16	3696.45	1284.75	1134.75	2292.09
58	3139329.98	431404.75	3736.05	1323.00	1173.00	2424.57
59	3139478.36	430706.98	3742.99	1329.75	1179.75	2710.24
60	3139535.73	432918.68	3663.87	1240.00	1090.00	1968.95
61	3139561.36	432407.06	3685.57	1257.75	1107.75	1912.81
62	3139627.89	429316.11	3715.10	1400.00	1250.00	3717.92
63	3139858.74	432688.80	3668.83	1214.00	1064.00	1616.68
64	3139863.63	431849.84	3710.00	1248.00	1098.00	1749.95
65	3140078.84	430175.33	3726.40	1345.50	1195.50	2748.34
66	3140733.83	433974.93	3675.19	1226.25	1076.25	1606.93
67	3140735.38	432783.42	3674.78			771.16
68	3140307.12	432296.05	3658.54	1185.75	1035.75	1188.59
69	3140956.41	430130.04	3723.89	1300.50	1150.50	2469.86
70	3141547.19	432881.19	3698.73			344.07
71	3141460.93	432546.57	3726.23			8.19
72	3141814.96	430117.20	3702.02	1354.50	1204.50	2453.40
73	3142054.07	434269.37	3713.05	1262.25	1112.25	1819.85
74	3142130.04	433534.14	3684.77	1176.75	1026.75	1188.73
75	3142086.51	432434.46	3716.92			627.41
76	3142094.61	431671.75	3762.55			1075.05
77	3142153.79	430842.48	3740.07	1262.25	1112.25	1836.05
78	3142247.07	430223.23	3703.94	1352.25	1202.25	2449.68
79	3142270.55	429486.32	3733.21	1374.00	1224.00	3163.00

Continued . . .

Table A-1. Main Array Channel and Location Crosswalk (continued)

Channel	Xft_1927 MT Stateplane FIPS 2503	Yft_1927 MT State Plane FIPS 2503	Lidar Elevation, ft amsl	Piper Reference Pick Time, ms	Interpreted Reservoir Time, ms	Offset, ft
80	3142613.29	432940.10	3698.16	1208.25	1058.25	1210.12
81	3142788.66	430134.49	3739.12	1356.75	1206.75	2749.01
82	3143423.39	434252.59	3760.26	1381.50	1231.50	2594.48
83	3143541.99	432895.92	3768.23	1350.00	1200.00	2102.19
84	3143520.57	431491.34	3757.61	1338.75	1188.75	2306.73
85	3143563.97	430161.55	3784.53	1394.00	1244.00	3174.03
86	3144312.36	430269.91	3825.46	1406.00	1256.00	3642.12
87	3144649.23	434212.12	3852.53	1426.00	1276.00	3590.09
88	3144765.11	433497.37	3797.58	1400.00	1250.00	3430.52
89	3144724.48	432884.70	3835.02	1406.00	1256.00	3272.93
90	3144692.12	432402.73	3808.96	1392.00	1242.00	3226.20
91	3144712.25	431603.56	3791.77	1408.00	1258.00	3377.32
92	3144676.77	430866.42	3783.71	1388.00	1238.00	3620.83
93	3145976.48	434208.39	3887.25	1469.25	1319.25	4804.12
94	3145839.00	432777.89	3891.51	1450.00	1300.00	4376.03
95	3146128.25	431533.54	3894.99	1464.00	1314.00	4767.90
96	3145723.64	430395.56	3826.25	1450.00	1300.00	4767.16

Table A-2. Remote Data Acquisition Summarized Observer's Log

Date	Day	Data Week	Shots	Notes
6-Oct-15	Tuesday	1	100	Baseline – initial shooting, temporary install
30-Oct-15	Friday		50	Setup error – nodes not on
9-Nov-15	Monday		50	Setup error – nodes not on
15-Nov-15	Sunday	2	50	Baseline No. 2
23-Nov-15	Monday		50	Setup error – nodes not on
29-Nov-15	Sunday	3	51	Baseline No. 3
6-Dec-15	Sunday		51	Setup error - nodes not on
13-Dec-15	Sunday	4	50	Baseline No. 4
20-Dec-15	Sunday		50	Baseline – triggering starts to fail – 19 records
27-Dec-16	Sunday		36	Failed attempt – triggering failure
28-Dec-15	Monday	5	50	Changed trigger signal threshold – 50 good shots
3-Jan-16	Sunday	6	59	Some trigger issues – 50 good shots
10-Jan-16	Sunday	7	54	Good shots
17-Jan-16	Sunday	8	50	Some trigger issues – unknown quantity
24-Jan-16	Sunday	9	51	Some trigger issues – unknown quantity
31-Jan-16	Sunday		0	No firing done. Waiting to raise footing.
7-Feb-16	Sunday	10	71	36 shots with correct time zero.
14-Feb-16	Sunday	11	76	23 shots have proper time zeros
21-Feb-16	Sunday	12	52	Adjusted "Timebreak" threshold
28-Feb-16	Sunday	13	52	Successful
6-Mar-16	Sunday	14	50	Successful – complete after 15 min
13-Mar-16	Sunday	15	50	Successful
20-Mar-16	Sunday	16	50	Successful
27-Mar-16	Sunday	17	51	Successful
3-Apr-16	Sunday	18	50	Successful
10-Apr-16	Sunday	19	51	Successful. 46 good shots
17-Apr-16	Sunday		0	Connection problems. Acquired ~ 20 shots
24-Apr-16	Sunday		0	No internet connection
1-May-16	Sunday		0	Wet ground in shed – omitted firing
7-May-16	Sunday	20	67	Many false triggers
14-May-16	Saturday	21	68	Some false triggers
21-May-16	Sunday	22	60	10 false triggers
28-May-16	Saturday	23	52	Successful
4-Jun-16	Saturday		55	Only 13 shots successfully triggered
5-Jun-16	Sunday		4	Source not triggering

Continued . . .

Table A-2. Remote Data Acquisition Summarized Observer's Log (continued)

Date	Day	Data Week	Shots	Notes
6-Jun-16	Monday	24	56	Successful – trigger changed from switch to accelerometer
12-Jun-16	Sunday	25	60	Successful
18-Jun-16	Saturday	26	61	Successful
26-Jun-16	Sunday	27	60	Successful
28-Jun-16	Tuesday		29	From EERC – shooting for EERC film crew
1-Jul-16	Friday		6	From EERC – looking at sample rate
3-Jul-16	Sunday	28	60	Successful
10-Jul-16	Sunday	29	54	Successful
16-Jul-16	Sunday	30	55	Successful
23-Jul-16	Saturday	31	54	Successful
30-Jul-16	Saturday		54	Lost – data file corrupted
7-Aug-16	Sunday		50	Lost – data file corrupted
13-Aug-16	Saturday		52	Lost – data file corrupted
21-Aug-16	Sunday		50	Lost – data file corrupted
27-Aug-16	Saturday		52	Lost – data file corrupted
2-Sep-16	Saturday			No Internet; discovered electrical damage
23-Sep-16	Friday	32	51	From source shed – successful
28-Sep-16	Wednesday	33	50	Successful
1-Oct-16	Saturday	34	51	Limit switch failure
5-Oct-16	Wednesday	35	100	Successful
7-Oct-16	Friday	36	101	Web relay failed
12-Oct-16	Wednesday	37	100	Web relay reprogrammed
15-Oct-16	Saturday	38	100	Web relay failed
18-Oct-16	Tuesday	39	82	Web relay failed, computer restart
22-Oct-16	Saturday	40	100	Successful
25-Oct-16	Tuesday	41	100	From Gillette – successful

Table A-2 is a listing of all data acquisitions for the SASSA project. The data set week number indicates successfully recorded data sets and corresponds to the labels on interpretation displays.

APPENDIX B

DYNAMIC RESERVOIR SIMULATIONS

DYNAMIC RESERVOIR SIMULATIONS

SIMULATION MODEL DEVELOPMENT FOR THE BELL CREEK PHASE 4/SASSA AREA

Based on the Version 3 geologic model created as part of the Plains CO_2 Reduction (PCOR) partnership's Bell Creek activities, a simulation model was developed for the Bell Creek Phase 4/semipermanent seismic array (SASSA) area as shown Figure B-1. The simulation model has 189×199×23 cells, resulting in 865,053 grid cells to perform dynamic calculation. There were 37 active wells in the Phase 4 model including 18 production wells, 10 WAG injection wells, and 9 water injection wells. The detailed well distribution is shown in Figure B-2.

Pressure-volume-temperature (PVT) data for crude oil samples from the Bell Creek field were used to define PVT relationships under reservoir conditions. A cubic equation of state (PR-EOS) model was developed to perform phase equilibrium and property calculations in simulation. The EOS model contained seven pseudo-components, which include CO_2, N_2 to C_2H, C_3H to NC_4, IC_5 to C7, C8 to C13, C14 to C24, and C25 to C36. The model was tuned to match laboratory results from a set of fluid experiments before being integrated into the simulation model for dynamic calculation. The fluid experiments included constant composition expansion (CCE), differential liberation (DL) analysis, separator, swelling test, and fluid compositional analysis.

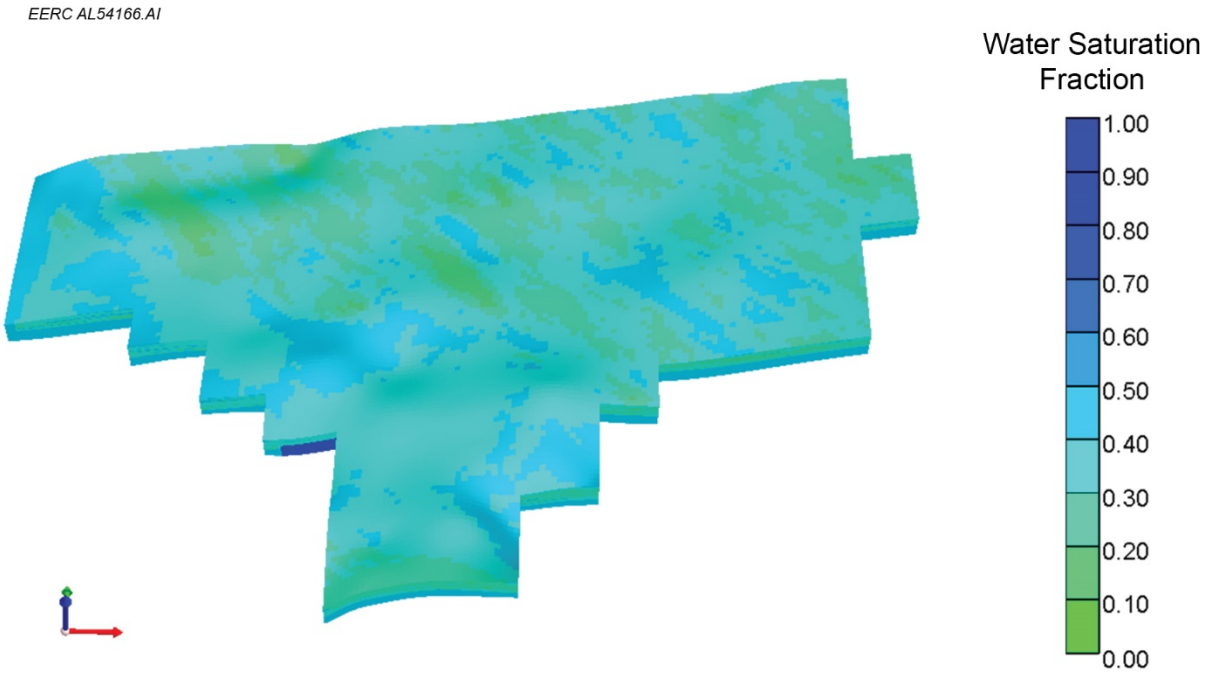

Figure B-1. Schematic of the Bell Creek Phase 4 model.

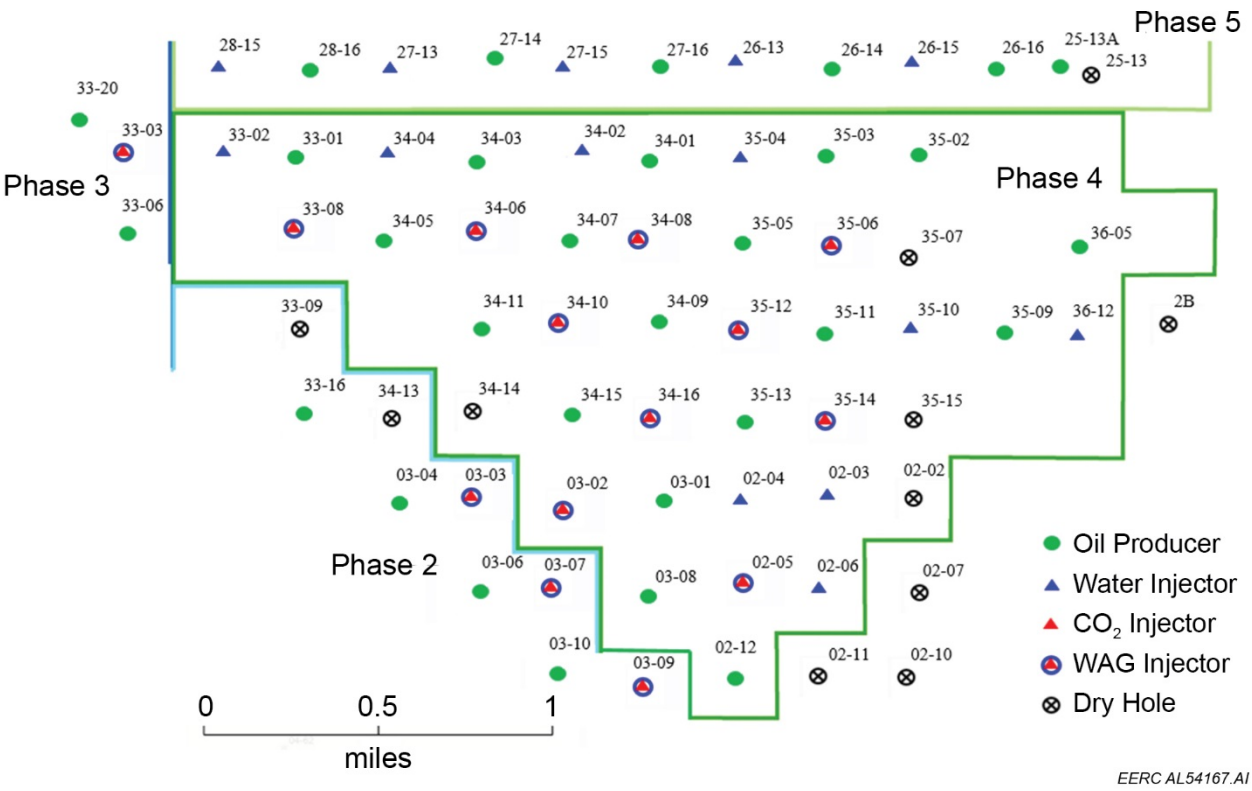

Figure B-2. Well distribution in the Bell Creek Phase 4 and surrounding area.

Fluid flow simulations were performed using CMG's GEM – a general compositional reservoir simulator which is able to predict the composition change of fluids and CO_2 plume distribution in a large-scale CO_2 flooding. History match of available production/injection data was conducted to ensure the simulation model can mimic the reservoir behavior and make reasonable predictions under various operational conditions. After satisfactory history match results were achieved, the distribution of CO_2 and pressure plumes were observed, and different predictive simulation cases were run to evaluate the future performance of CO_2 flooding in the reservoir.

Production Analysis and History Match

The Phase 4 area is located in the east-central region of the field. There is no evident edge water (aquifer support) connecting to the pay zone. However, local water invasion is identified from production performance, especially for wells in the southwestern and middle areas of the phase. Figure B-3 shows high initial water cut in wells along the southwestern boundary of the phase, indicating that there is considerable water invasion, or that initial water saturation is high in this part of the reservoir. Figure B-4 illustrates the early (almost instant) water breakthrough but relatively stable water cut in wells in the middle of Phase 4, which indicates the existence of movable water in this region before waterflooding.

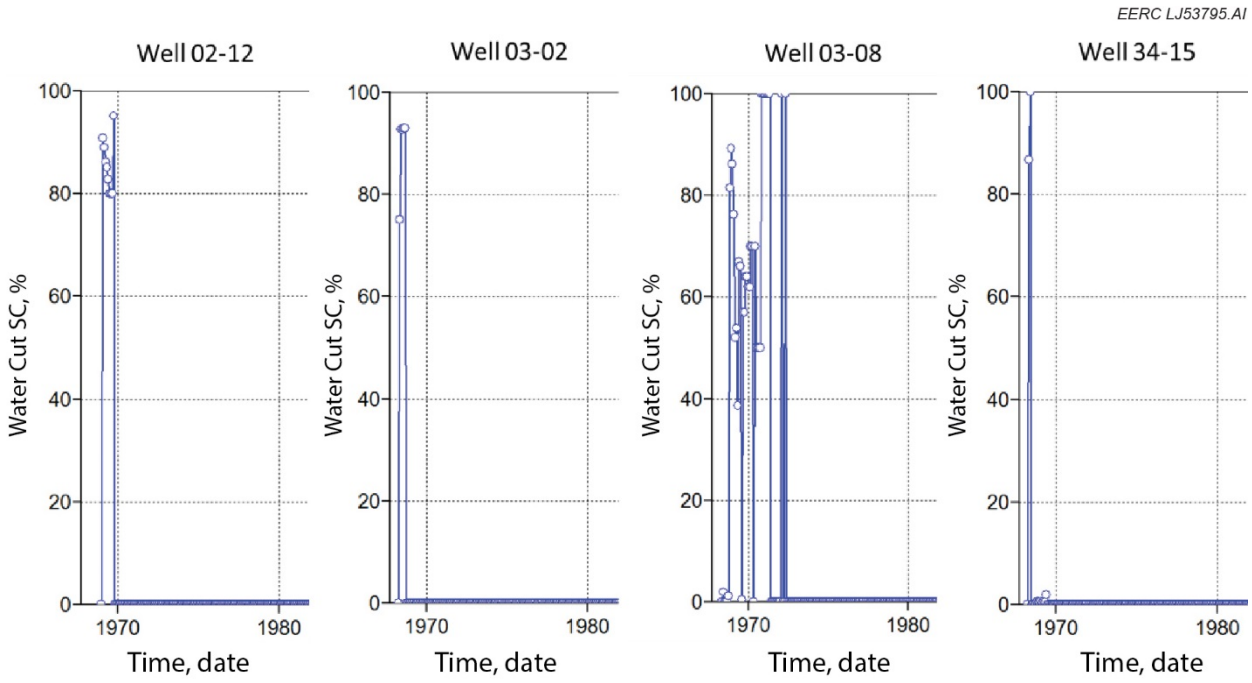

Figure B-3. High initial water cut in the wells along the southwestern boundary of Phase 4 (SC: standard conditions).

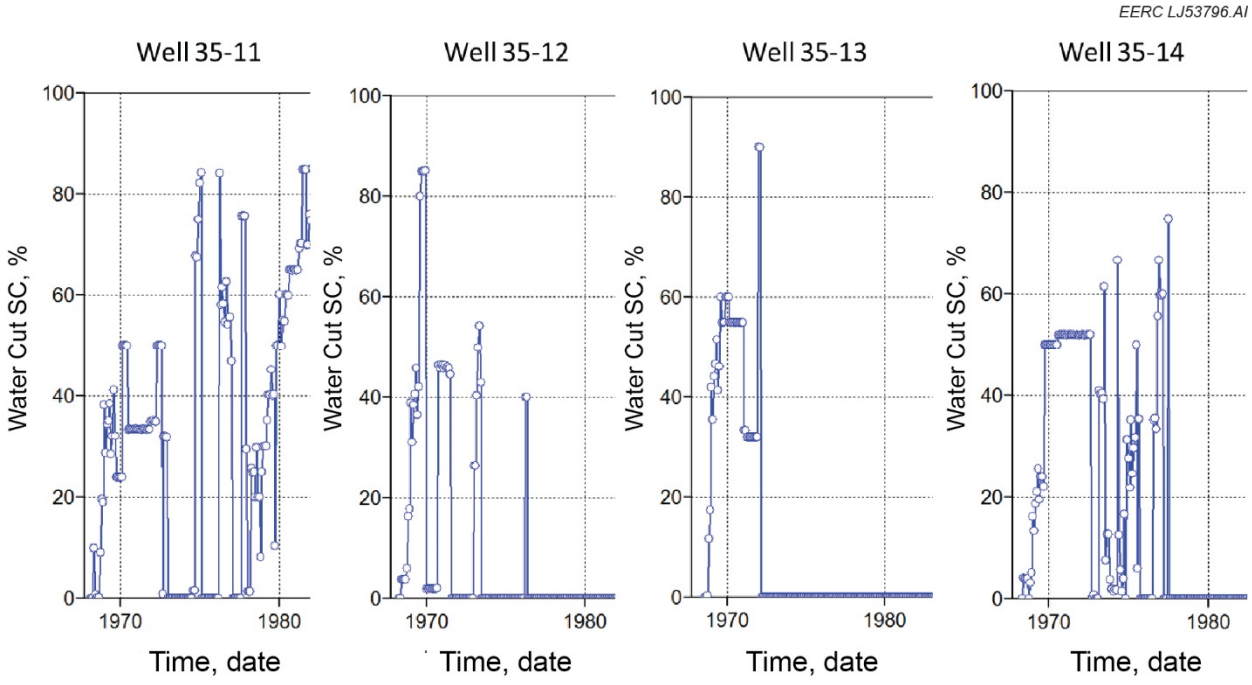

Figure B-4. Early water breakthrough to wells in the middle of Phase 4.

Production performance is also used to analyze fluid flow between phases as it is an important factor for waterflooding and CO_2 flooding design and operations. Figure B-2 shows that Phase 4 connects to Phases 2, 3, and 5; however, there is no clear geological boundary between Phases 4 and 5. Figure B-3 and Figure B-5 show the water cut behavior of wells located on both sides of the Phases 2–4 boundary. The wells in Phase 4 have high initial water cut while the nearby wells in Phase 2 have water breakthrough after years of production, clearly indicating that there is no fluid flow across the boundary. The northwestern corner of Phase 4 connects to the eastern side of Phase 3. The boundary between the two phases may also be impermeable based on the difference of well performance shown in Figure 6.

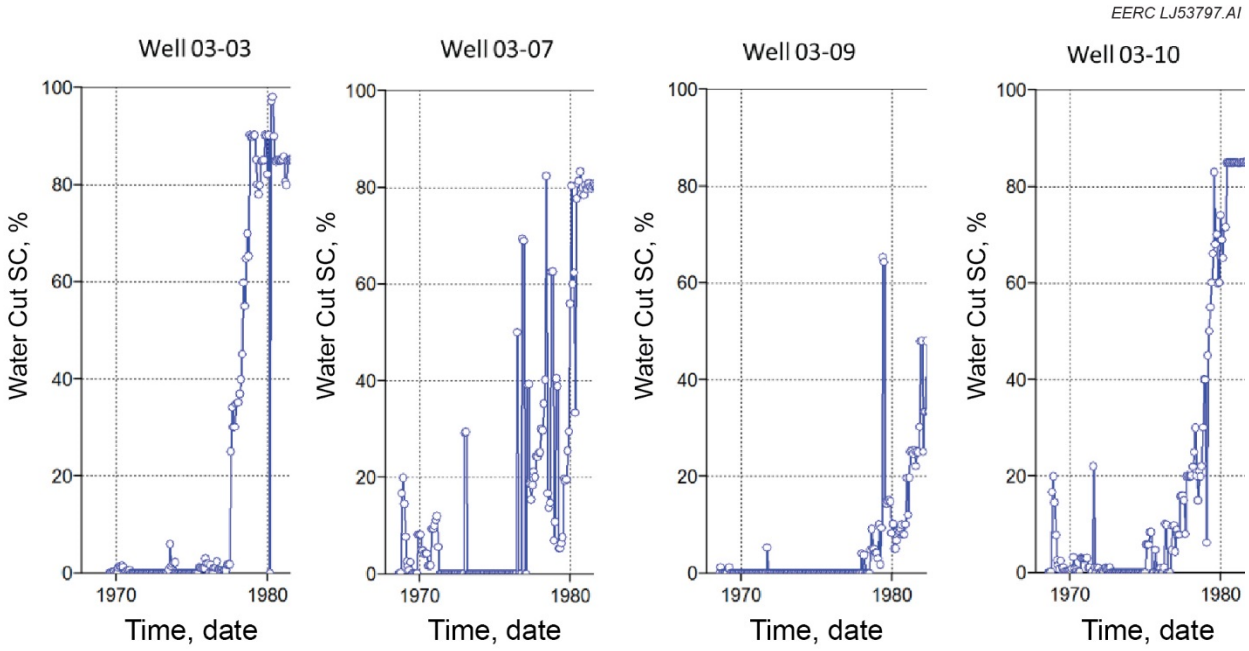

Figure B-5. Low initial water cut in the wells along the eastern boundary of Phase 2, indicating good boundary sealability between Phases 2 and 4.

After analyzing the boundary conditions of the Phase 4 area, a systematic history matching process was conducted to reproduce the production data in this phase (Bosshart and others, 2015; Jin and others, 2016). Similar to the previously reported studies, liquid production and injection rates were used as primary constraints. Oil, water, and gas production rates were used in comparison to the simulated results. In the primary production stage, local water saturation (especially for the southwestern and middle portions of the phase) was adjusted to match the water cut performance. In the waterflooding stage, areas of overestimated petrophysical properties and out-of-boundary flow were adjusted to match the oil and water production rates. In the CO_2 flooding stage, relative permeability curves and endpoint saturations were tuned because the interaction between CO_2 and formation fluids having the ability to change the shape of relative permeability curves. Reasonably good matching results were achieved for oil, water and gas production data as shown in Figure B-7 to Figure B-10.

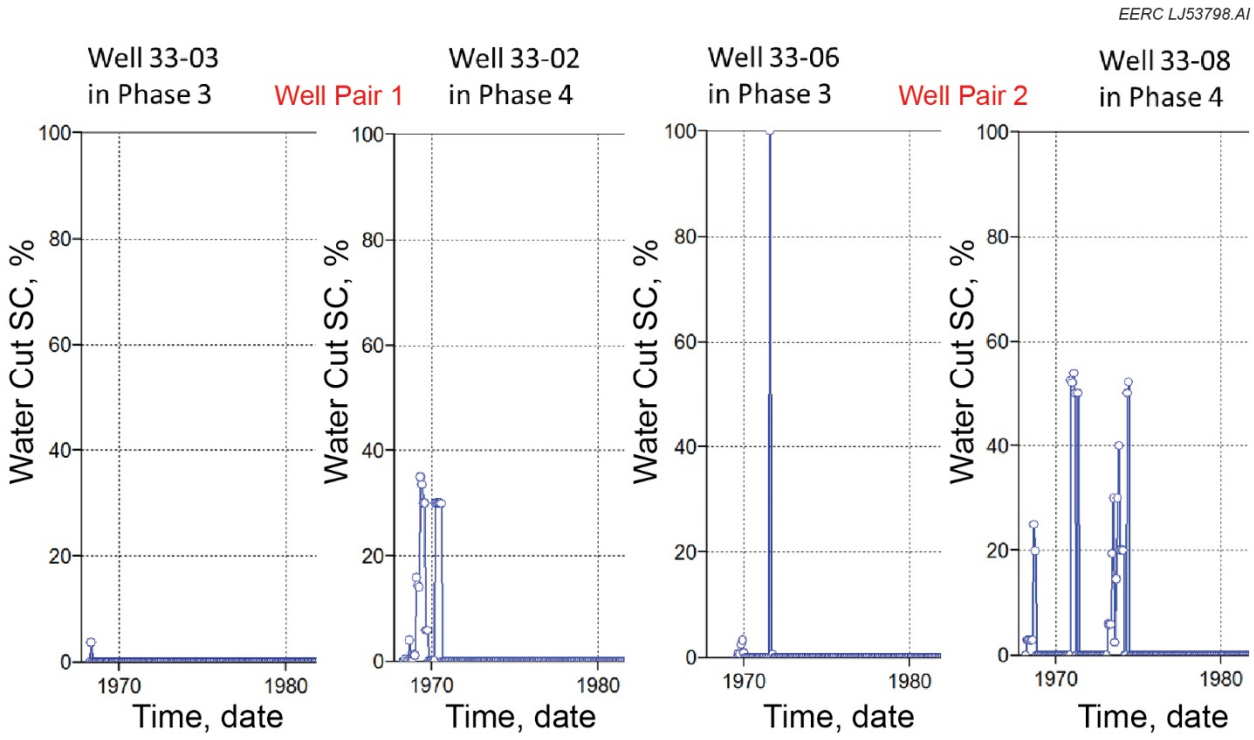

Figure B-6. Comparison of water cut in wells along the boundary between Phases 3 and 4.

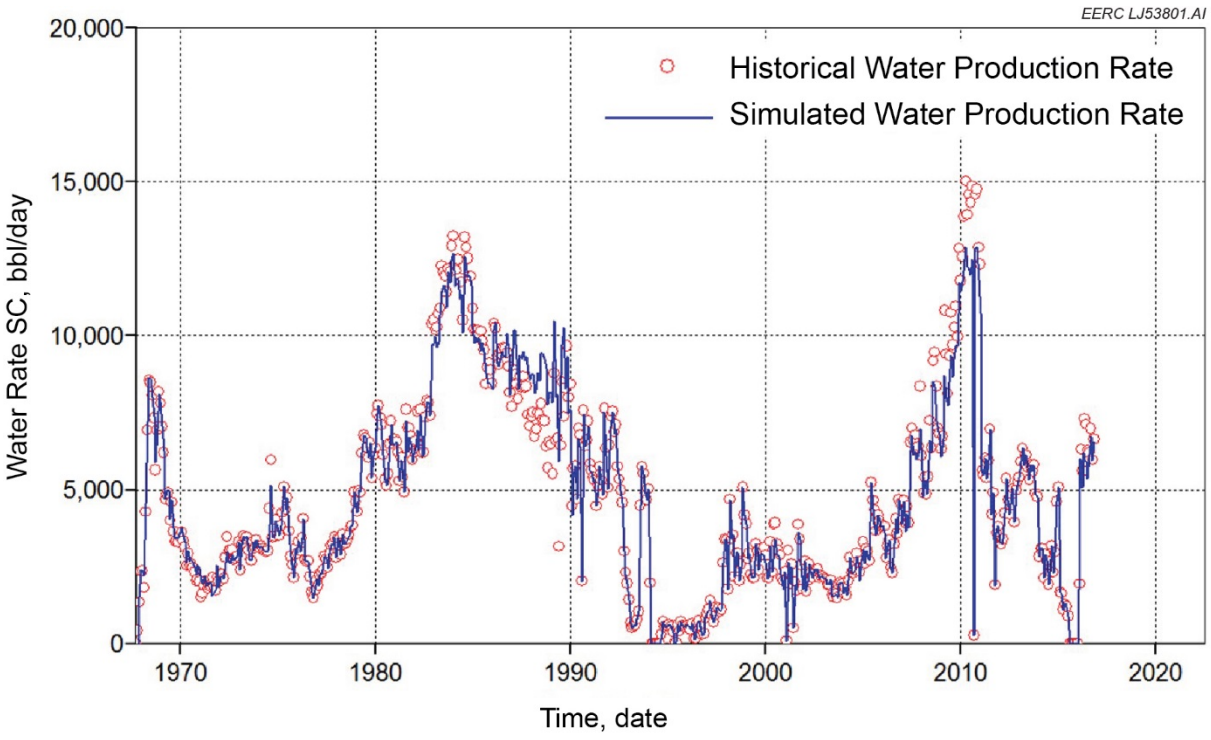

Figure B-7. History matched liquid production rate of the Bell Creek Phase 4 model.

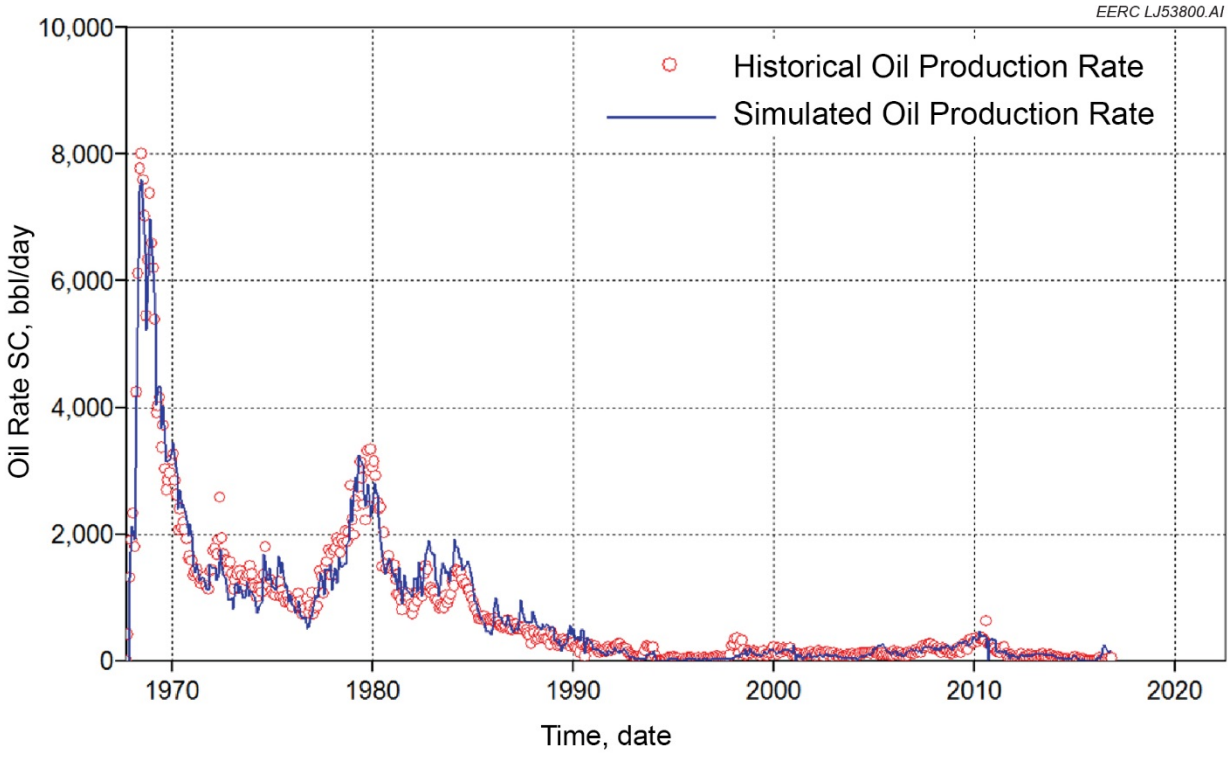

Figure B-8. Bell Creek Phase 4 oil production rate history match results.

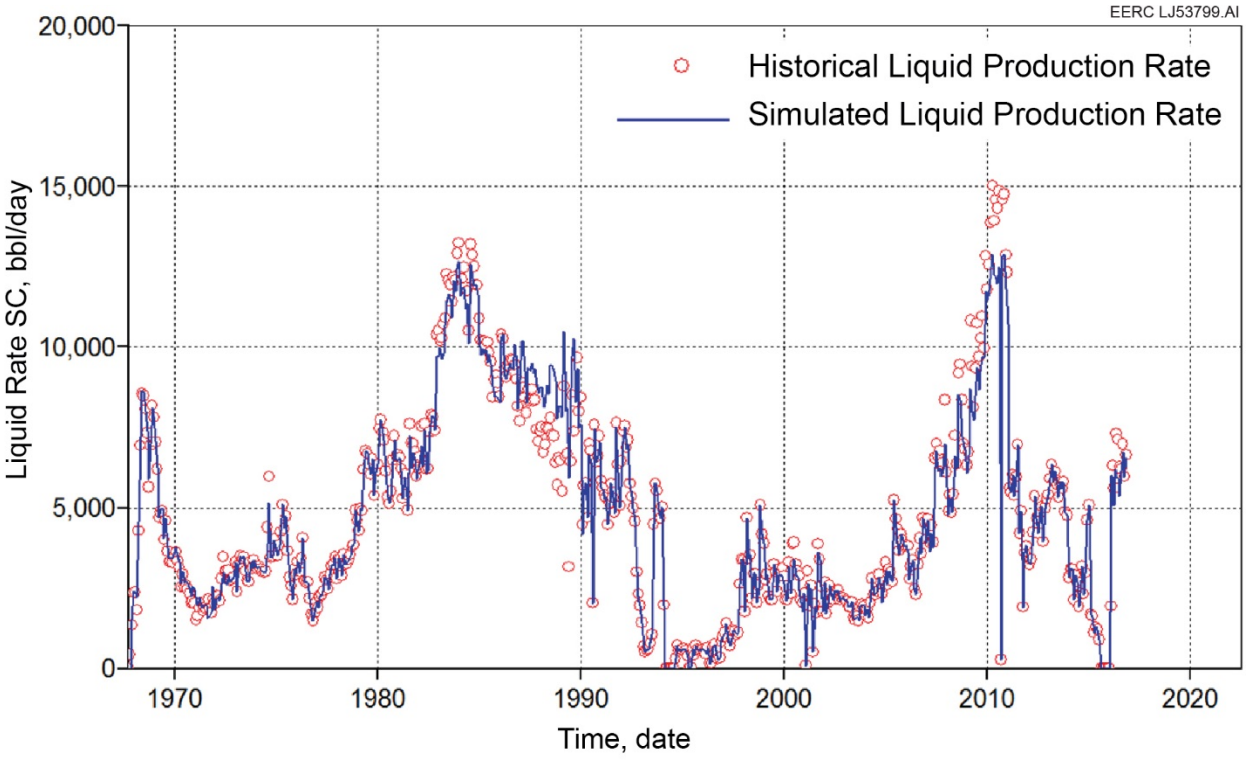

Figure B-9. Bell Creek Phase 4 water production rate history match results.

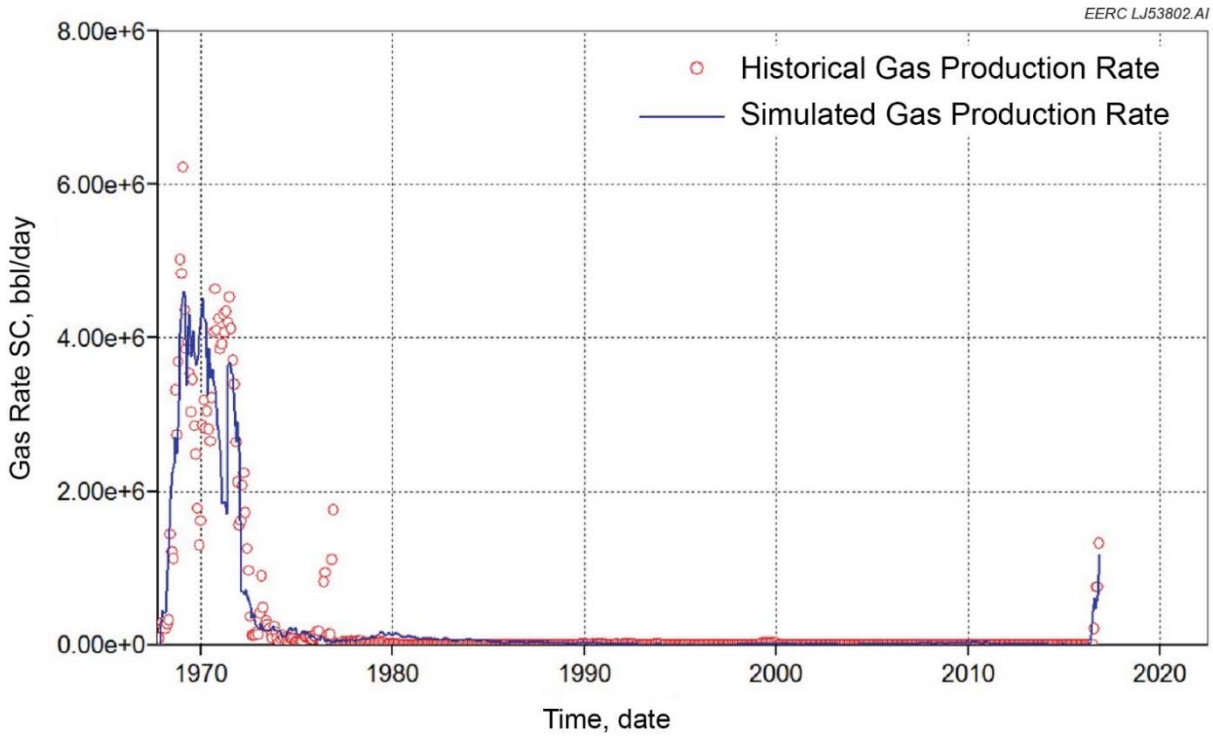

Figure B-10. Bell Creek Phase 4 gas production rate history match results.

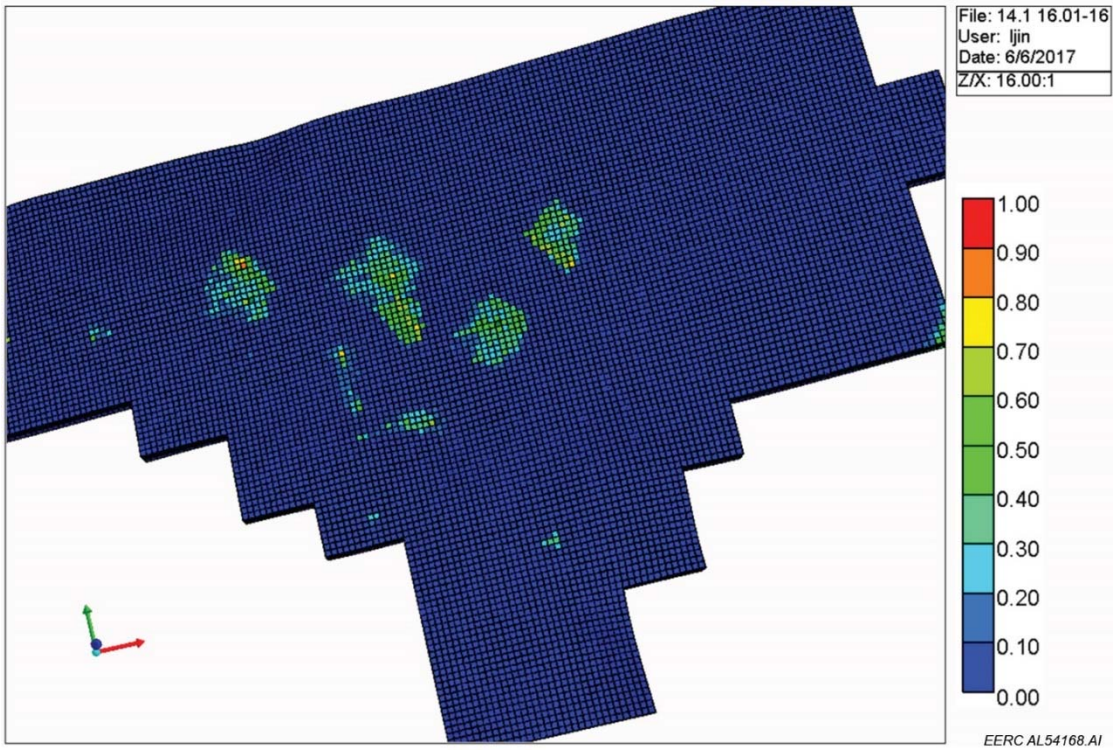

Figure B-11. Reservoir simulation of gas saturation per unit area in the reservoir at semipermanent seismic array project end, computed after history matching.

APPENDIX C

2-D LINE DATA PROCESSING

2-D LINE DATA PROCESSING

This section includes an expanded discussion of the 2-D line data processing flow development and a more detailed description of the final processing flow that was applied to the data.

As part of the processing flow development, an in-depth analysis of near-surface changes and QC of the data was done. Although minimum time-lapse near-surface variations were expected because of the chronological acquisition of the baseline and monitor surveys, an intensive analysis was conducted to confirm our approach. The success of this approach was independently confirmed by the results of a nonlinear tomography method using refracted waves (Figure C-1) and a surface wave method using ground roll (Figure C-2). The successful application of the surface wave method to the 2-D survey data also confirmed the effectivity of the seismic source Gisco ESS 850 to put low-frequency energy into the ground and the ability of the 3C FairfieldNodal Zland nodes to record low frequencies with high fidelity (Barajas-Olalde and others, 2017).

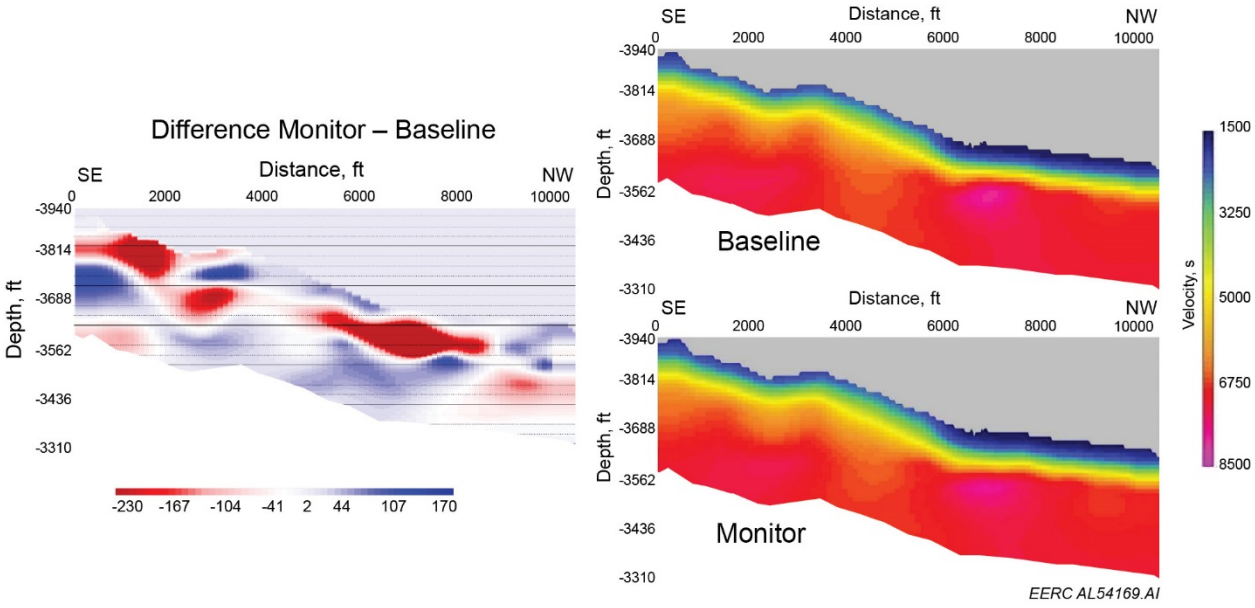

Figure C-1. Difference monitor minus baseline near-surface velocity models estimated from the nonlinear tomography using refracted waves.

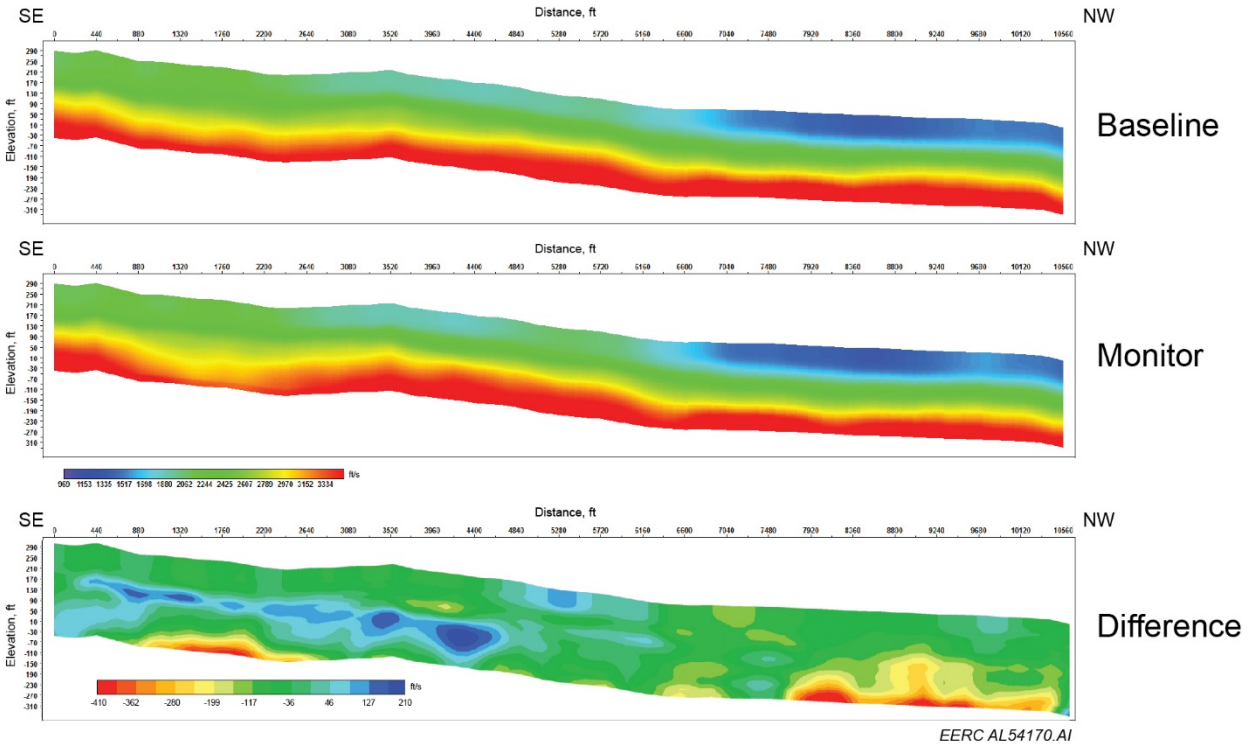

Figure C-2. Estimated near-surface shear-wave velocity models and their difference obtained from a surface wave method and ground roll noise.

The QC of the seismic records revealed different noise conditions of the baseline and monitor surveys. The monitor survey appeared to have a lower signal-to-noise ratio than the baseline survey in most of the shot gathers. Attempts were made to improve the signal-to-noise ratio of the monitor survey. Noise attenuation was conducted in cascade in the common shot gather domain followed by the common receiver domain. However, it was noticed that the signature of the target thin reservoir was affected by the noise attenuation in cascade. Because of time constraints, a conservative noise attenuation workflow was used for the processing of the monitor and baseline surveys. This workflow included only monochromatic noise, three passes of ground roll attenuation, and two passes of random noise attenuation in the shot gather domain. The remnant of ground roll noise was muted using an inside mute function. This mute function combined with an outside mute function was used to remove guided waves in the near offsets. The inside mute function was also defined to try to keep shallow reflectors as much as possible; however, some remnant guided waves were still observed in some gathers (see Figure C-3), and they were carried over up to the final stack.

The baseline and monitor surveys were processed following the conventions of time-lapse surveys. A similar workflow was applied to the two surveys with the exception of the statics corrections and noise attenuation steps due to differences in signal to noise and noise characteristics. Seismic data processing was performed by using GeoThrust 2-D also called ThrustLine, a GeoTomo software package based on seismic data analysis in shot-receiver coordinates. This type of coordinates overcomes the common midpoint assumption breakdown

when data are acquired on areas with irregular topography, complex near surface, and complex subsurface (GeoTomo, 2016). A summary of the data processing workflow is as follows:

1. Upload data
   - Data format: SEG-Y
   - Input data
     - Record length: 4000 ms
     - Sampling interval: 2 ms

2. Apply Geometry
   - Assign x, y, and z values to each record trace associated with each shot to allow sorting. Same coordinates used in baseline and monitor surveys
   - Define a line traverse to map field coordinates along a crooked line. Transform field coordinates into GeoThrust shot-receiver coordinates

3. Near-surface model estimation
   - Pick first-arrival times to estimate layer velocity and thickness to build an initial near-surface model
   - Estimate final near-surface model using nonlinear traveltime tomography

4. Determine replacement velocity, static corrections, and pick floating datum
   - Use near-surface model to pick floating datum and intermediate datum and compute replacement velocity
   - Use near-surface model, datum, and replacement velocity to compute static corrections

5. Trace edits
   - Traces with anomalous amplitudes are identified and removed

6. Time resampling
   - Max. trace length: 3000 ms; sample rate: 4 ms

7. Geometrical spreading correction
   - A time-variant, approximate correction for the geometrical decay of energy as the wavefront propagates away from the source
   - Power of Time: 1.8, power of offset: 0.5

8. Monochromatic noise attenuation
   - Application of the HANA (high amplitude noise attenuation) algorithm to attenuate noise that presents itself as a single frequency

9. Surface consistent scaling
   - A time-invariant trace amplitude correction incorporating source, receiver, offset, and CIP factors

10. Ground roll attenuation and muting
    - Cascade application of radial trace filtering to target and remove ground roll followed by a mute to remove additional ground roll that was not attenuated

11. Surface consistent deconvolution
    - A deconvolution operator to flatten the spectrum of the data. White noise prevents zero division. Incorporates source, receiver, offset, and CIP factors

12. First break mute
    - removal of direct arrivals and refracted waves

13. Bandpass filter (Ormsby filter: 5, 8, 56, 65 Hz)
    - The frequency content of the data was limited to the frequency range of frequencies used in the time and frequency domain filter

14. Apply tomostatics corrections
    - Correcting for elevation differences and time-shifting data to the seismic reference datum.

15. Apply residual statics corrections
    - Application of small static shifts that increase event coherence among trace gathers are computed

16. Random noise attenuation
    - Using the Cadzow algorithm which uses eigenvalue filtering to attenuate random noise

17. Second pass of surface consistent scaling
    - Applied as before

18. Velocity picking
    - Evaluate velocity model generated by picking velocities using constant velocity stacks and common image point semblance displays (Figure C-3)

19. Pre-stack time migration
    - The processed gathers, with the migration velocities applied, are migrated using the Kirchoff algorithm. This imaging process repositions amplitudes from their apparent reflected location to their actual geometric location in space (Figure C-4)

20. Time resampling
    - Max. trace length: 2200 ms; sample rate: 4 ms

21. Muting
    - Mute out of migration swings on common image point gathers

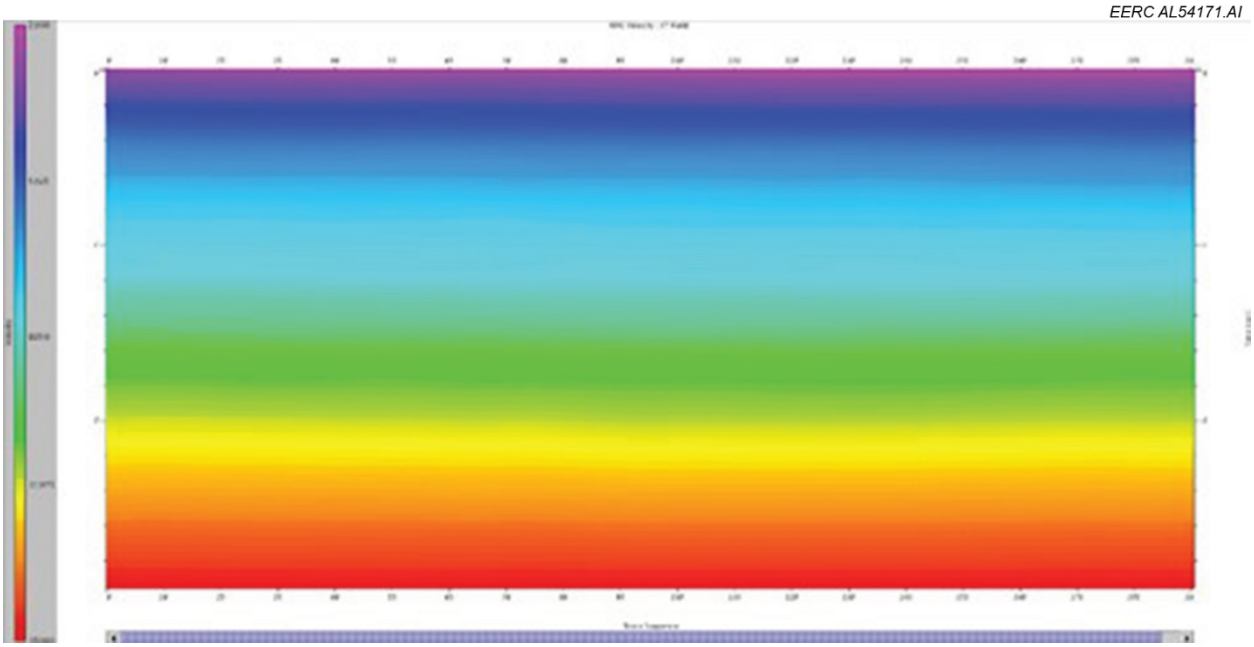

Figure C-3. Estimated RMS velocity field from baseline and monitor surveys. This velocity field is one of the inputs for prestack time migration.

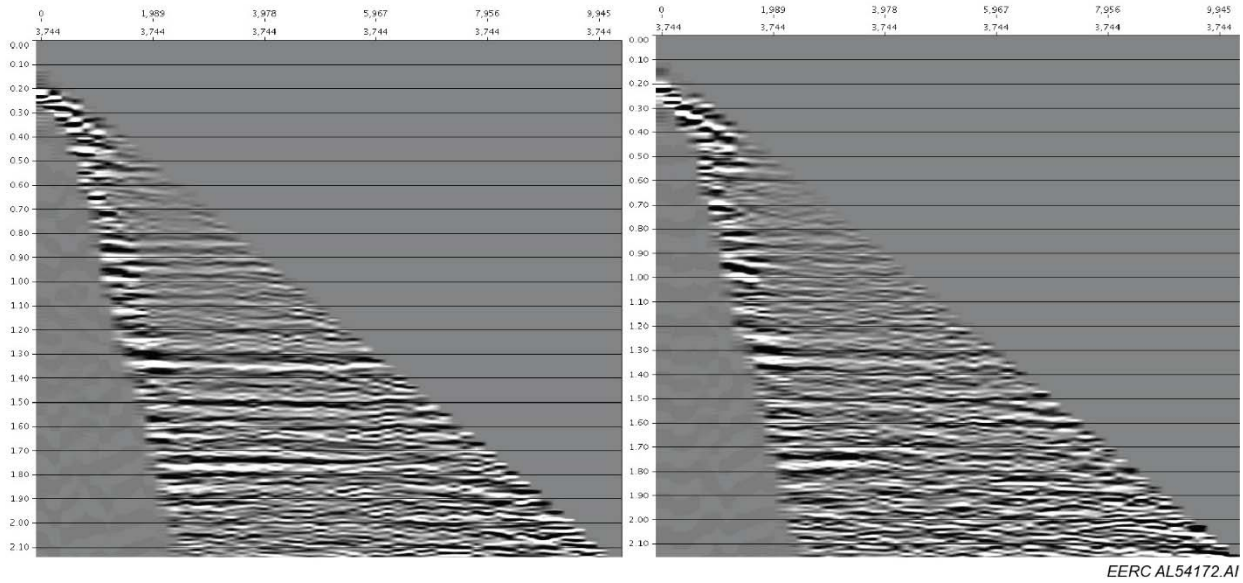

Figure C-4. Example of post processed Kirchhoff prestack time-migrated CIP gather (Gather 94). Left: baseline survey; right: monitor survey.

22. Stack
    - The traces in each migrated CIP gather are summed together to create a single CIP trace

23. Bandpass filter (Ormsby filter: 8, 12, 25, 35 Hz)
    - The frequency content of the data was limited to the frequency range of frequencies used in the time and frequency domain filter

24. Output SEGY files

APPENDIX D

MAIN ARRAY DATA PROCESSING DETAIL SIMPLE PROCESSING FLOW

MAIN ARRAY DATA PROCESSING DETAIL
SIMPLE PROCESSING FLOW

The simple processing sequence applied to the semipermanent seismic array (SASSA) array data using RadExPro seismic processing software is detailed below, with a brief explanation of each step.

1. Upload raw field data into RadExPro
   - Data format: SEG-D
   - Input data
     - Record length: 4000 ms
     - Sampling interval: 2 ms

2. Apply geometry to headers
   - Assign x, y, and z values to each record trace associated with each shot to allow sorting

3. Save data from the vertical geophone to a separate file
   - Raw field records contain data from the vertical geophone and the two orthogonal horizontal geophones for each channel. Only the vertical component data were used in this project.

4. Sort vertical component data into common receiver gathers
   - Raw field records contain data from each of the 96 channels and for processing data from each channel was separated out into different files.

5. Bandpass filter (Ormsby filter: 2, 5, 75, 90 Hz)
   - The frequency content of the data was limited to the frequency range of frequencies used in the time and frequency domain filter.

6. Geometrical spreading corrections
   - A time-variant, approximate correction for the geometrical decay of energy as the wavefront propagates away from the source.
   - Linear gain correction: 1/s

7. Trace edits
   - Traces with anomalous amplitudes were identified and removed.

8. Attenuation of strong noise (e.g., burst noise)
   - Burst noise removal algorithm was applied using the following parameters
     - Window size for average value calculation: 5
     - Rejection percentage: 50
     - Amplitude threshold percentage for exclusion: 5
     - Amplitude threshold multiplier for application: 3

9. Time and frequency domain filtering
   - Attenuates burst noise and random noise that are localized in the time and frequency domain by calculating the median values over a specified window and replacing sample values with a specified threshold value specified as a multiple of the median value. The following parameters were used:
     – Time domain options:
       1. Start time (ms): 0
       2. End time (ms): 4000
       3. Time window (ms): 100
       4. % of tapering: 15
     – Frequency domain options:
       1. Min frequency (Hz): 2
       2. Max frequency (Hz): 90
       3. Trace aperture: 25
       4. Threshold: multiplier: 5

10. Vertical stack of common receiver gathers
    - The traces in each CRG are summed together to create a single trace

11. Bandpass filter (Ormsby filter: 4, 8, 56, 64 Hz)
    - The frequency content of the data was limited to the specified frequency range

12. Create monitor stack section
    - Generated a separate file that contained one stacked trace for every week of data for a particular channel

13. Create baseline stack sections
    - Generated a stack by repeating each baseline trace according to number of traces in monitor stacks.

14. Output SEGY files of monitor and baselines

ADVANCED PROCESSING FLOW

The advanced processing sequence applied to the SASSA array data using VISTA seismic processing software is detailed below, with a brief explanation of each step.

1. Upload data into VISTA processing software
   - Data format: SEG-Y
   - Geometry and trace edits were applied to data prior to uploading
   - Input data
     – Record length: 4000 ms
     – Sampling interval: 2 ms

2. Header conditioning for VISTA seismic data processing software
   - This step ensures that the SASSA data can be used as common receiver gathers.

3. Geometrical spreading correction
   - A time-variant, approximate correction for the geometrical decay of energy as the wavefront propagates away from the source.
   - Exponential gain constant: 1

4. Bandpass filter (Ormsby filter: 2, 7, 55, 60 Hz)
   - The frequency content of the data was limited to the specified frequency range

5. Attenuation of monochromatic noise
   - Data are transformed into the frequency domain, and a filter is applied to remove noise corresponding to a specific narrow frequency range.
   - Adjustable notch filter. Frequency range and percentage of amplitude reduction are adjustable. Although the industrial installations are the known source of this noise, there were spatial and temporal amplitude variations of this noise that required adjusting the filter parameters for each sensor.

6. Attenuation of strong noise (e.g., burst noise) that can dominate the stack
   - THOR module. This is a friendly amplitude-variation-with-offset filter that removes and replaces strong noise using threshold median in the frequency domain.

7. Attenuation of white noise
   - 4D-DEC module: This is a filter based on principal component decomposition in the time domain that preserves amplitudes and statics.
   - Several passes in cascade depending on the signal-to-noise ratio.

8. Vertical stack of common receiver gathers
   - The traces in each CRG are summed together to create a single trace

9. Time resampling
   - Data was limited to a specific time window contain the signal of interest.
   - Time window: 0–2000 ms.

10. Trace selection of baseline and monitor
    - Traces corresponding to weeks that had anomalous amplitudes due to noise were removed from the data set.

11. Mute of first breaks and guided waves

12. Create monitor stack section
    - Generated a separate file that contained one stacked trace for every week of data for a particular channel.

13. Create baseline stack sections
    - Generated a stack by repeating each baseline trace according to number of traces in monitor stacks.

14. Create difference monitor minus baseline stack

15. Output SEGY files of monitor, baselines and difference stacks

APPENDIX E

INTERPRETATION RESULTS

INTERPRETATION RESULTS

This appendix contains results for 20 channels that had advanced processing applied but were not included in the main body of the report. The following results are grouped into smaller subsets based on the spatial location of the monitor points in order to easily reference each channel's corresponding monitor location on accompanying gas saturation maps.

Group 1

Figure E-1. Highlights the midpoints corresponding to the four channels in Group 1.

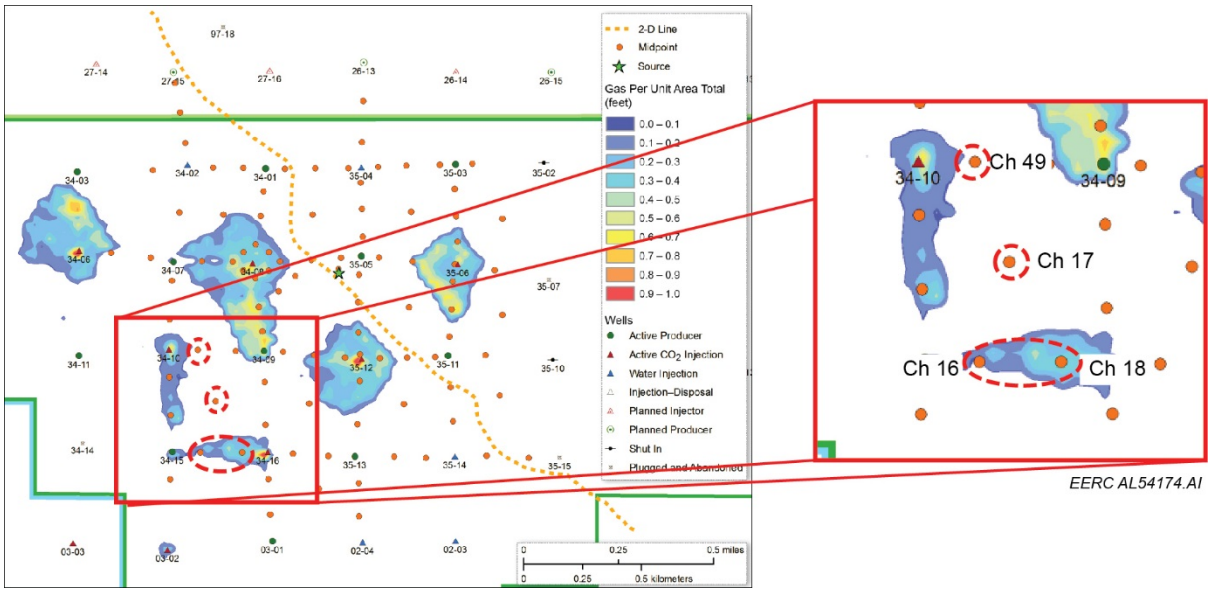

Figure E-1. Map of gas saturation per unit area total generated from one possible dynamic reservoir simulation realization. The dashed red areas highlight the monitor locations corresponding to the channels in Group 1. The orange dots depict the monitor locations. The light orange dashed line corresponds to the 2-D line.

Channel 16 (Figure E-2)

- Channel 16 is offset 6379 feet from the source with the monitor point located ~944 feet west of a CO_2 injection well that started injecting in August 2016. No CO_2 effect in expected at this location. Baseline 4 (December 13, 2015) is used as the reference.

- Prior to cross equalization, there are small differences below the reservoir that become distinguishable at Week 17 and appear to get larger over time. After cross equalization, differences are corrected on almost every trace. Differences that remain appear to be due to noise. The presence of CO_2 is not indicated, as expected.

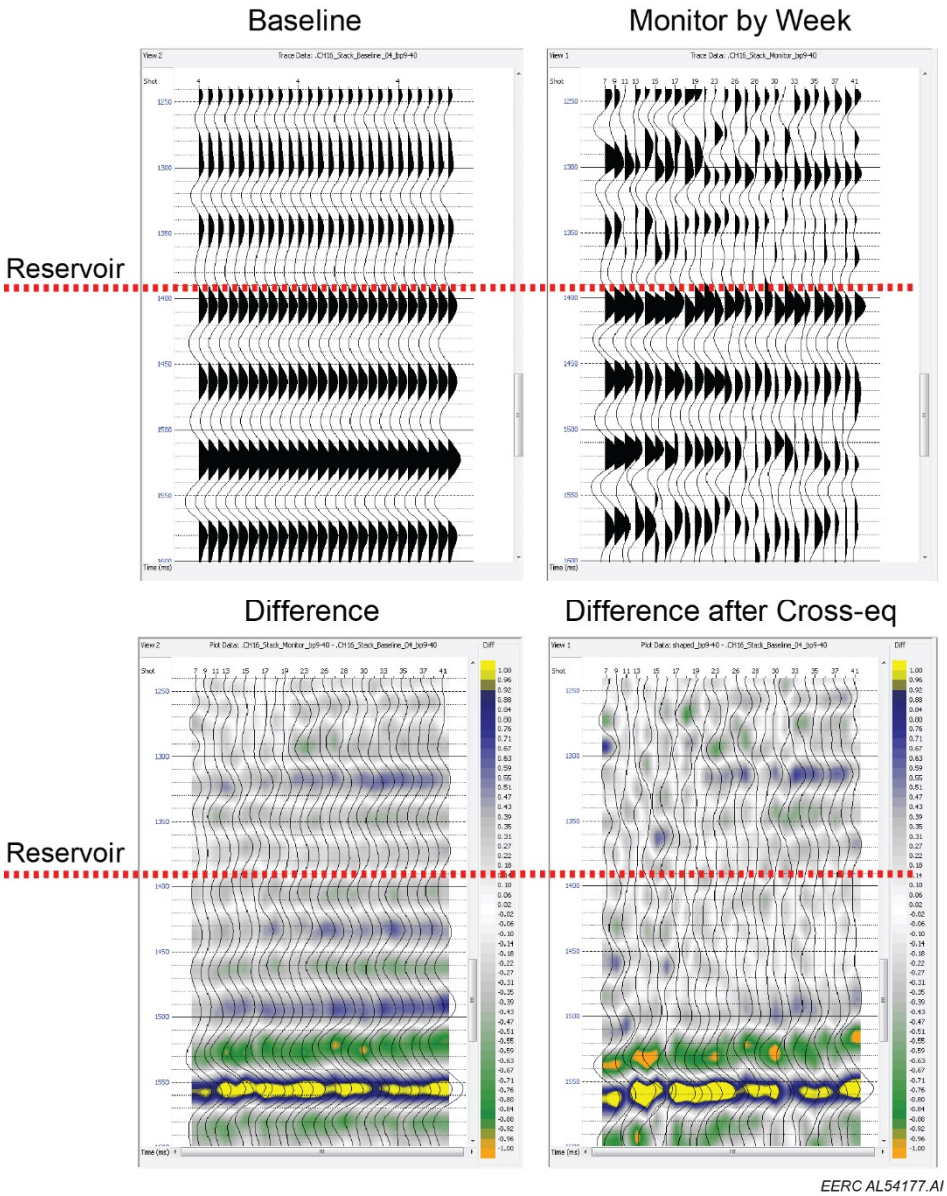

Figure E-2. Time-lapse difference results for Channel 16 before and after cross equalization. The dotted red line indicates the interpreted reservoir location. No CO_2 is indicated at this location.

Channel 17 (Figure E-3)

- Channel 17 is offset 5001 feet from the source with the monitor point located ~1007 feet northwest and 970 feet southeast of a CO_2 injection well that started injecting in August and February 2016. A CO_2 effect is possible but not expected at this location. Baseline 4 (December 12, 2015) is used as the reference.

- Prior to cross equalization, there are differences across all weeks on several reflection events. After cross equalization, differences at the reservoir level are ambiguous.

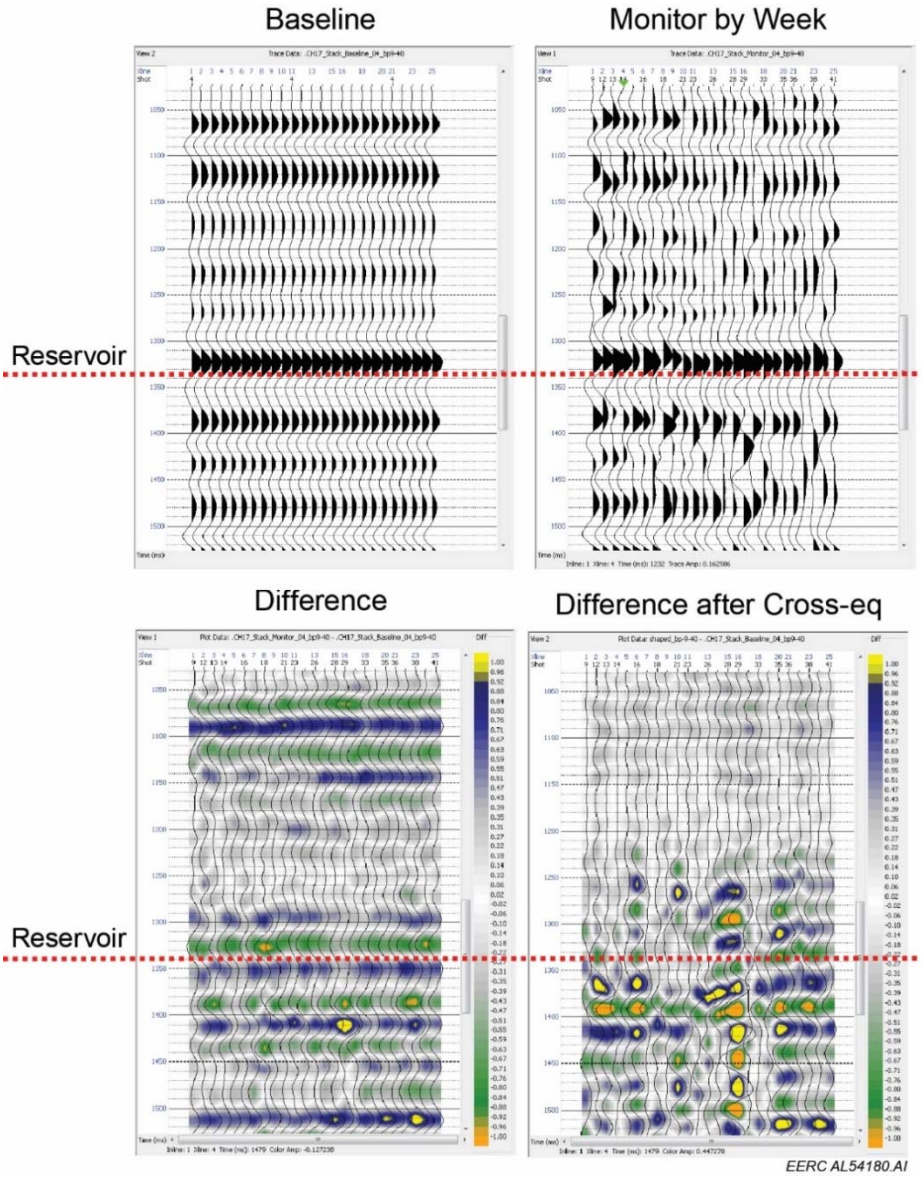

Figure E-3. Time-lapse difference results for Channel 17 before and after cross equalization. No CO_2 is expected, and results are ambiguous because of noise.

Channel 18 (Figure E-4)

- Channel 18 is offset 5767 feet from the source with the monitor point located ~340 feet west of a CO_2 injection well that started injecting in August 2016. A CO_2 effect is expected at this location. Baseline 4 (December 13, 2015) is used as the reference.

- Prior to cross equalization, there are differences across all weeks on several reflection events. After cross equalization, differences at the reservoir appear to begin on Week 25 (June 12, 2016) but initially have a noisy character. This change occurs before the start of injection. A more subtle change is visible on Week 33 (September 28, 2016) when reflections on the monitor data itself appear to stabilize. Ultimately, the interpretation is ambiguous.

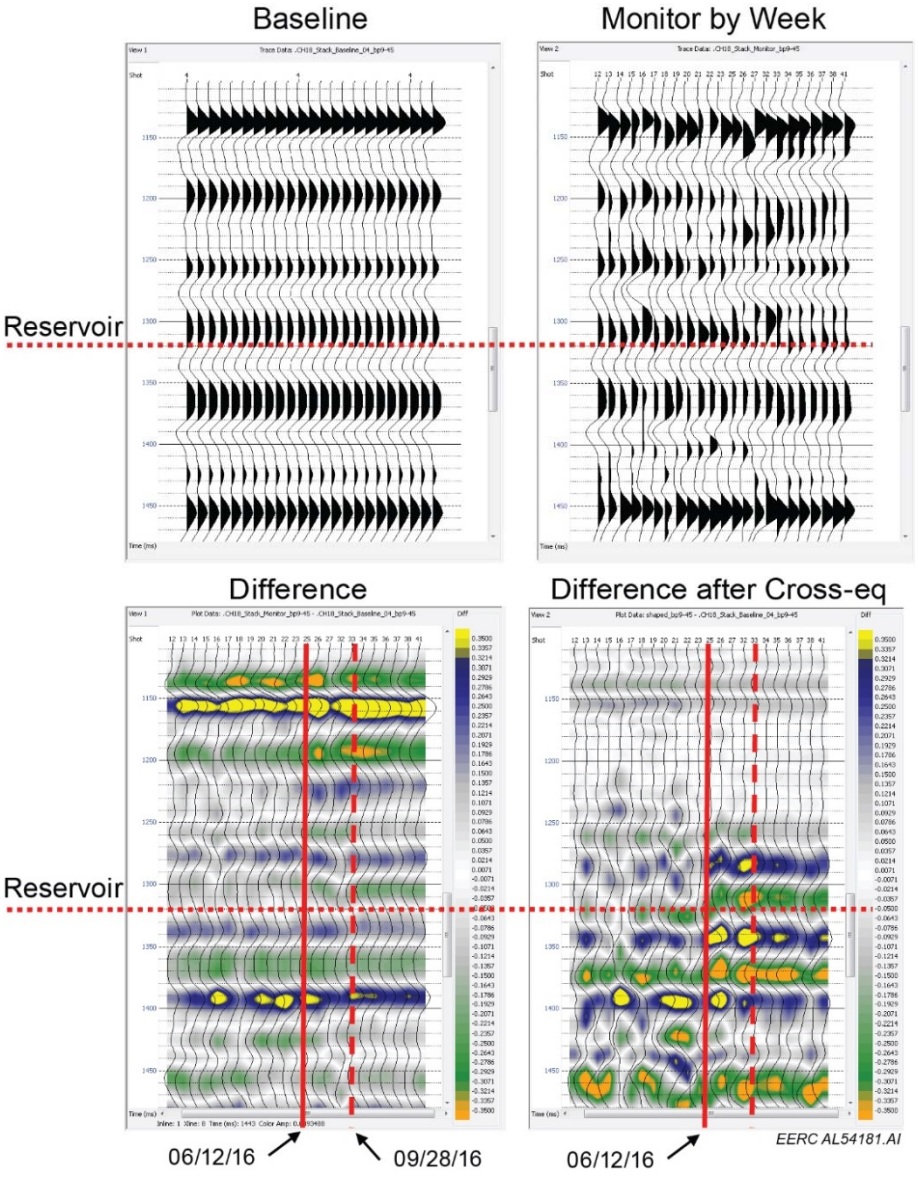

Figure E-4. Time-lapse difference results for Channel 18 before and after cross equalization. A CO_2 effect is expected at this location, but the interpretation is ultimately ambiguous.

Channel 49 (Figure E-5)

- Channel 49 is offset 4481 feet from the source with the monitor point located ~415 feet west of a CO_2 injection well that started injecting in February 2016. A CO_2 effect is expected at this location as early as the end of February (Weeks 12–13). Baseline 2 (November 15, 2015) is used as the reference.

- Prior to cross equalization, difference change starts at Week 13 (February 28, 2016) and increases in magnitude at Week 21 (May 21, 2016). After cross equalization, differences at the reservoir still begin on Week 13. This change may indicate the presence of CO_2 as expected.

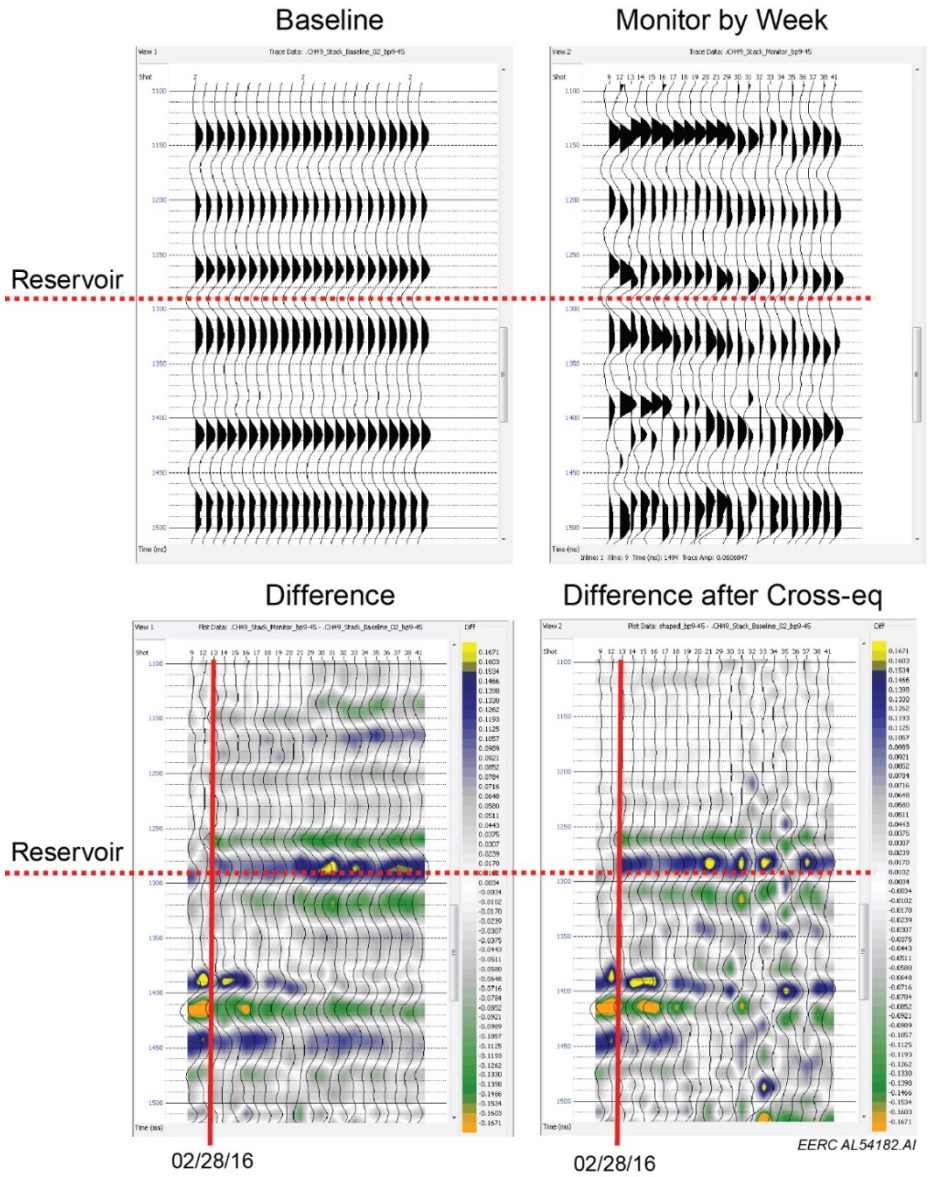

Figure E-5. Time-lapse difference results for Channel 49 before and after cross equalization. CO_2 appears to be present at this location starting about Week 13, February 28, 2016, as indicated by the vertical red line.

Group 2

Figure E-6 highlights the midpoints corresponding to the eight channels in Group 2.

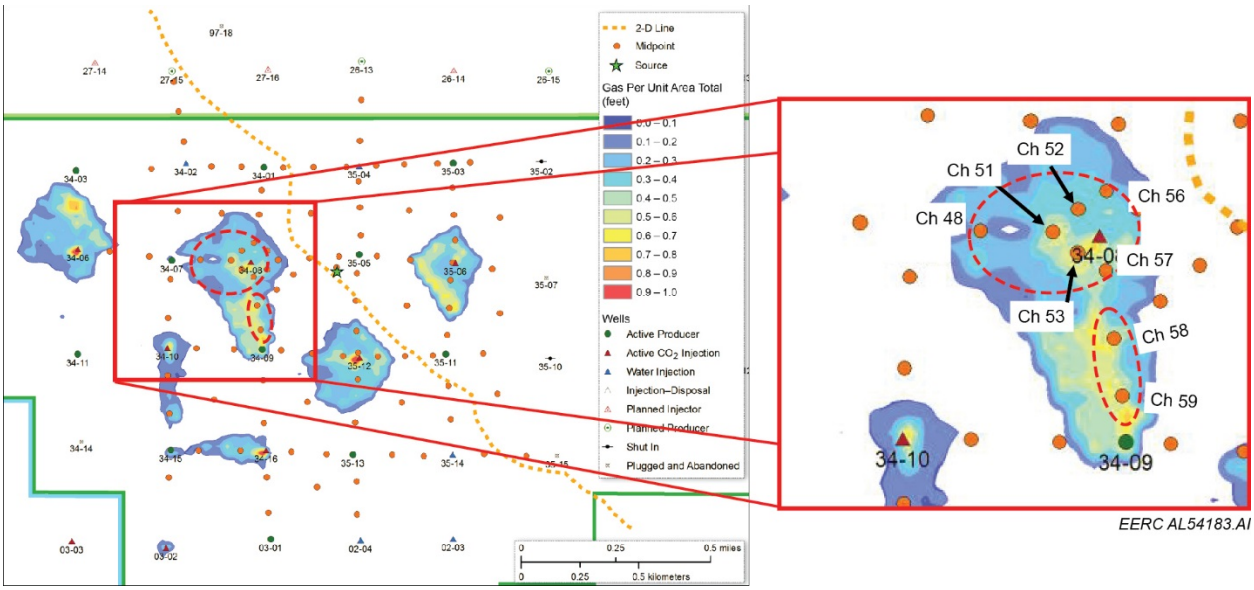

Figure E-6. Map of gas saturation per unit area total generated from dynamic reservoir simulations. The dashed red areas highlight the monitor locations corresponding to the channels in Group 2. The orange dots depict the monitor locations. The light orange dashed line corresponds to the 2-D line.

Channel 48 (Figure E-7)

- Channel 48 is offset 3773 feet from the source with the monitor point located ~1080 feet west of a CO_2 injection well that started injecting in January 2016. A CO_2 effect is possible at this location. Baseline 4 (December 13, 2015) is used as the reference.

- Prior to cross equalization, there are very small differences at the reservoir that are discontinuous. After cross equalization, these differences are enhanced, but remain discontinuous. These changes are ambiguous.

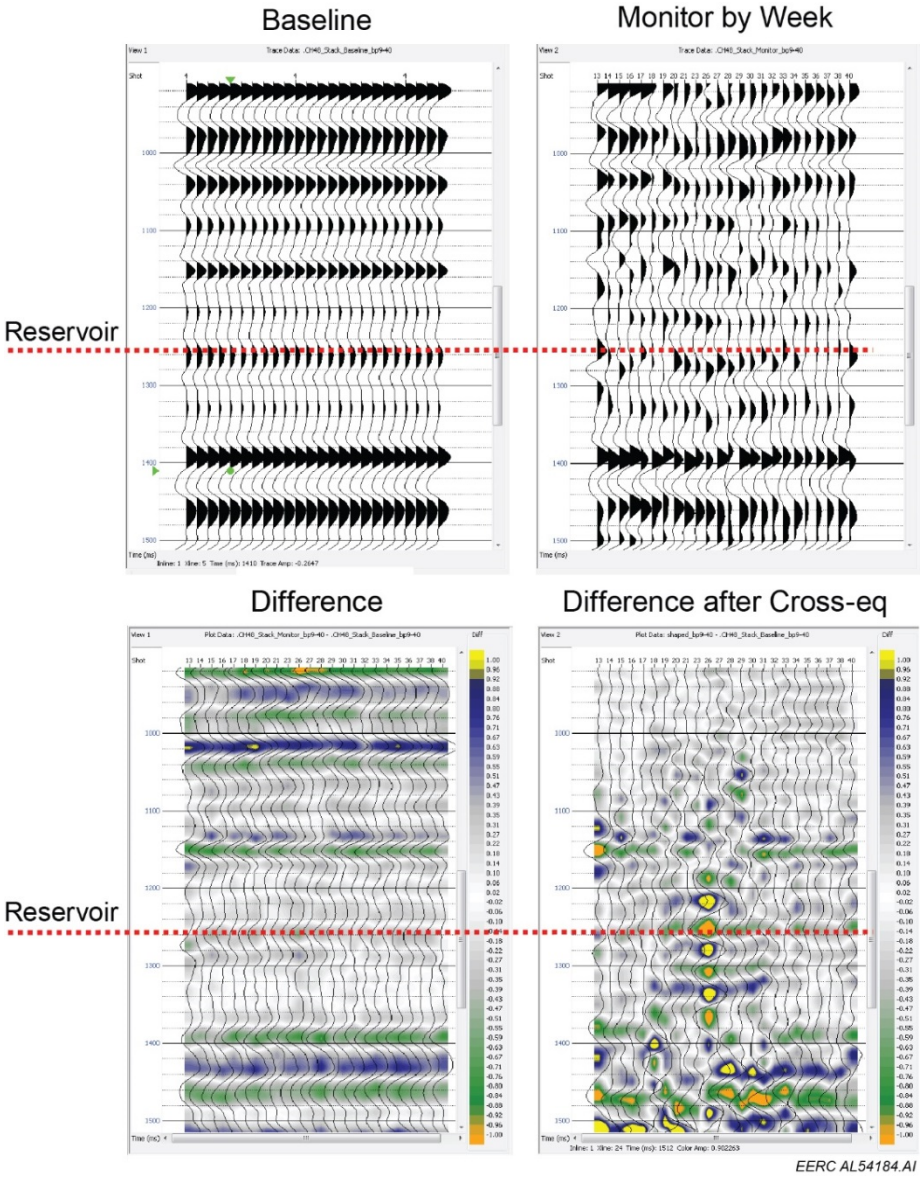

Figure E-7. Time-lapse difference results for Channel 48 before and after cross equalization. Changes visible at the reservoir level are discontinuous and ambiguous.

Channel 51 (Figure E-8)

- Channel 51 is offset 2930 feet from the source with the monitor point located ~280 feet west of a CO_2 injection well that started injecting in January 2016, and a CO_2 effect is expected at this location. Baseline 4 (December 13, 2015) is used as the reference.

- Prior to cross equalization, there are differences across all weeks on several reflection events. After cross equalization, there is change at the reservoir starting at Week 13 (February 28, 2016), but it is very discontinuous. These changes are ambiguous.

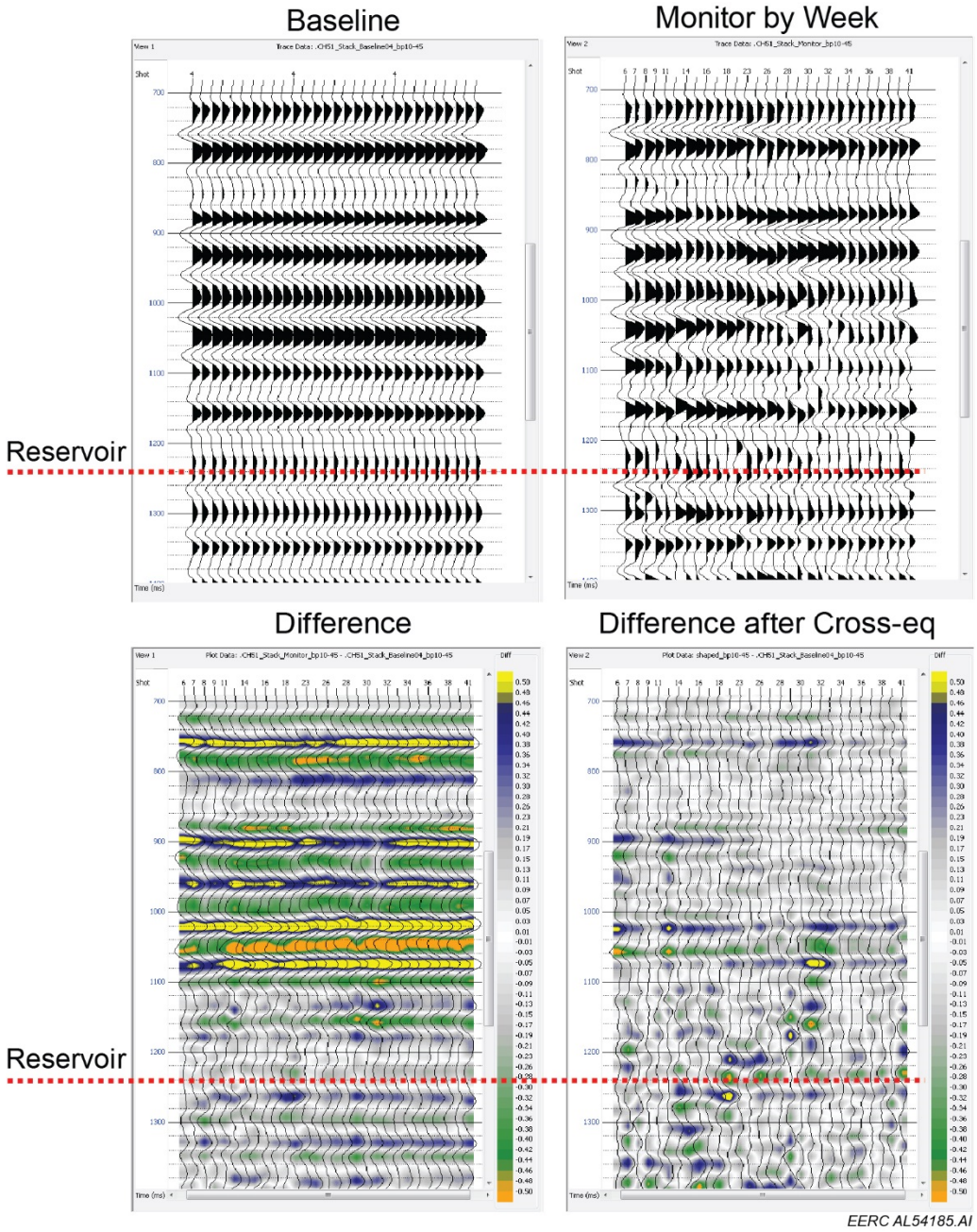

Figure E-8. Time-lapse difference results for Channel 51 before and after cross equalization.

Channel 52 (Figure E-9)

- Channel 52 is offset 2662 feet from the source with the monitor point located ~200 feet west of a CO_2 injection well that started injecting in January 2016, and a CO_2 effect is expected at this location. Baseline 3 (November 29, 2015) is used as the reference.

- After cross equalization, there is change at the reservoir starting at Week 9 (January 24, 2016) that is discontinuous, but becomes more continuous starting at Week 19 (April 10, 2016). This change is interpreted to be due to CO_2.

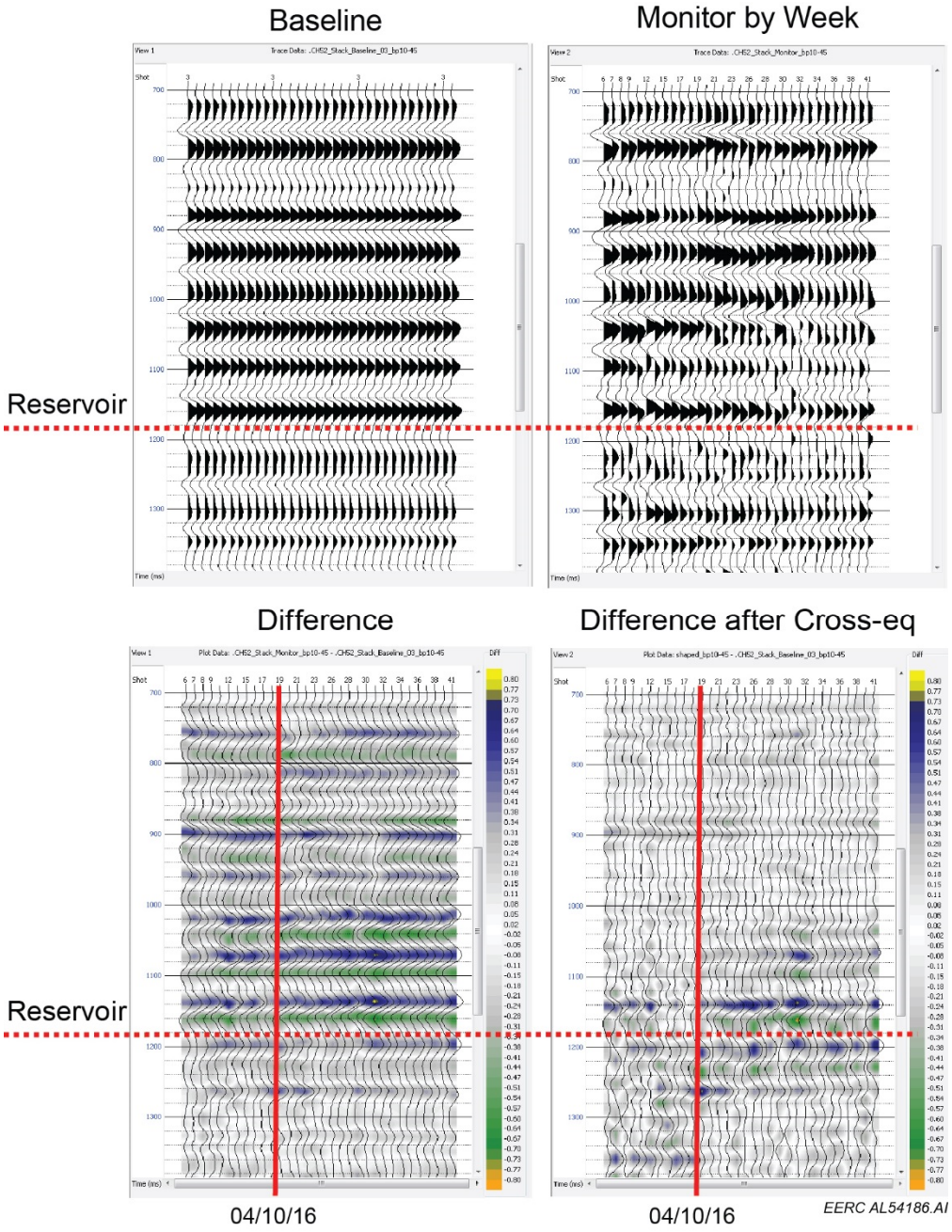

Figure E-9. Time-lapse difference results for Channel 52 before and after cross equalization.

Channel 53 (Figure E-10)

- Offset 2624 feet from the source with the monitor point located ~162 feet west of a CO_2 injection well that started injecting in January 2016, a CO_2 effect is expected at this location. Baseline 3 (November 29, 2015) is used as the reference.

- Prior to cross equalization, there are differences across all weeks on several reflection events. After cross equalization, there is no change at the reservoir level, but continuous change remains above the reservoir even though the magnitude of change has been decreased.

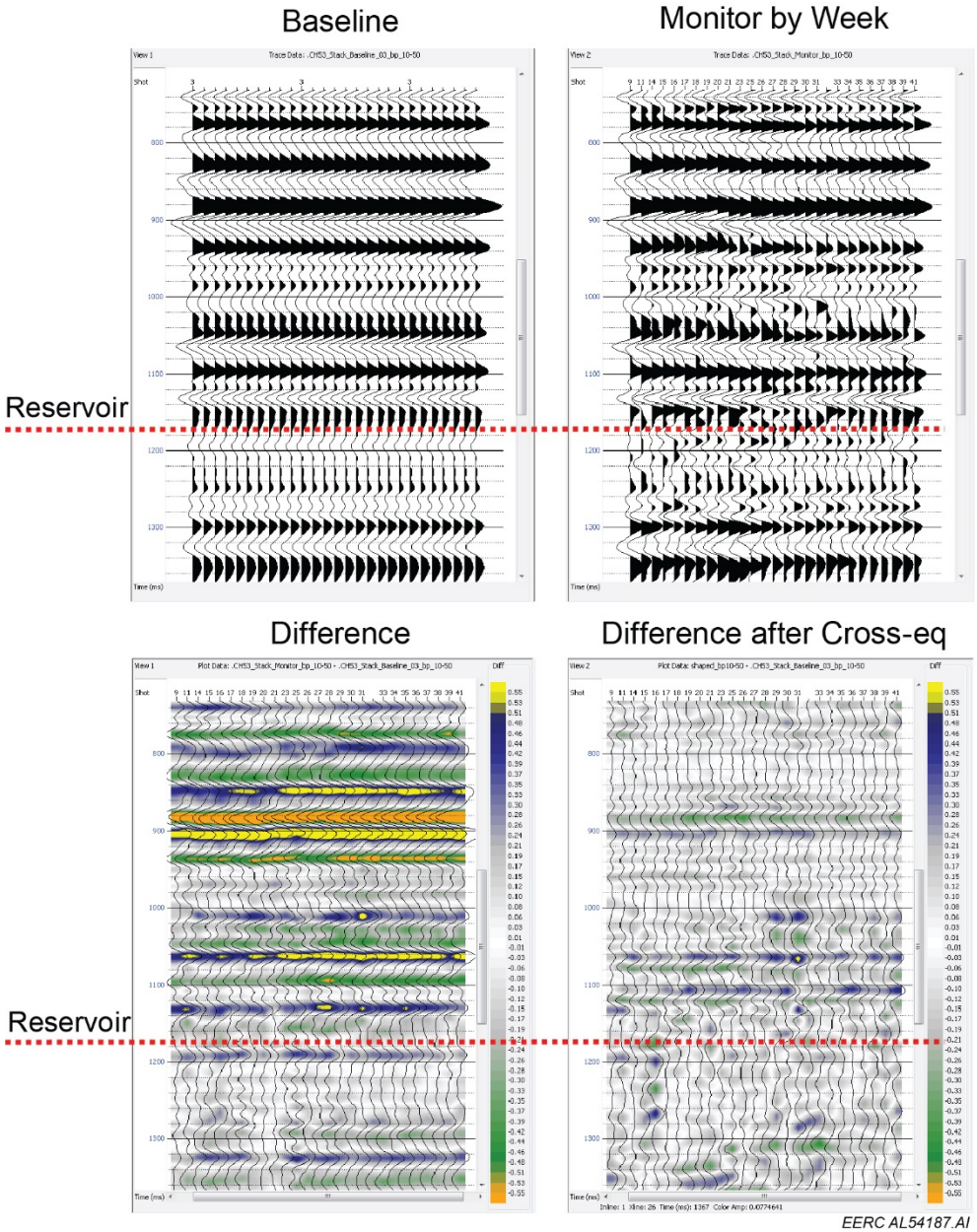

Figure E-10. Time-lapse difference results for Channel 53 before and after cross equalization.

Channel 56 (Figure E-11)

- Offset 2382 feet from the source with the monitor point located ~280 feet north of a CO_2 injection well that started injecting in January 2016, a CO_2 effect is expected at this location. Baseline 3 (November 29, 2015) is used as the reference.

- Prior to cross equalization, little to no change is observed at the reservoir. After cross equalization, change at the reservoir level starts at Week 12 (February 2, 2016) but is very discontinuous and several weeks show no change.

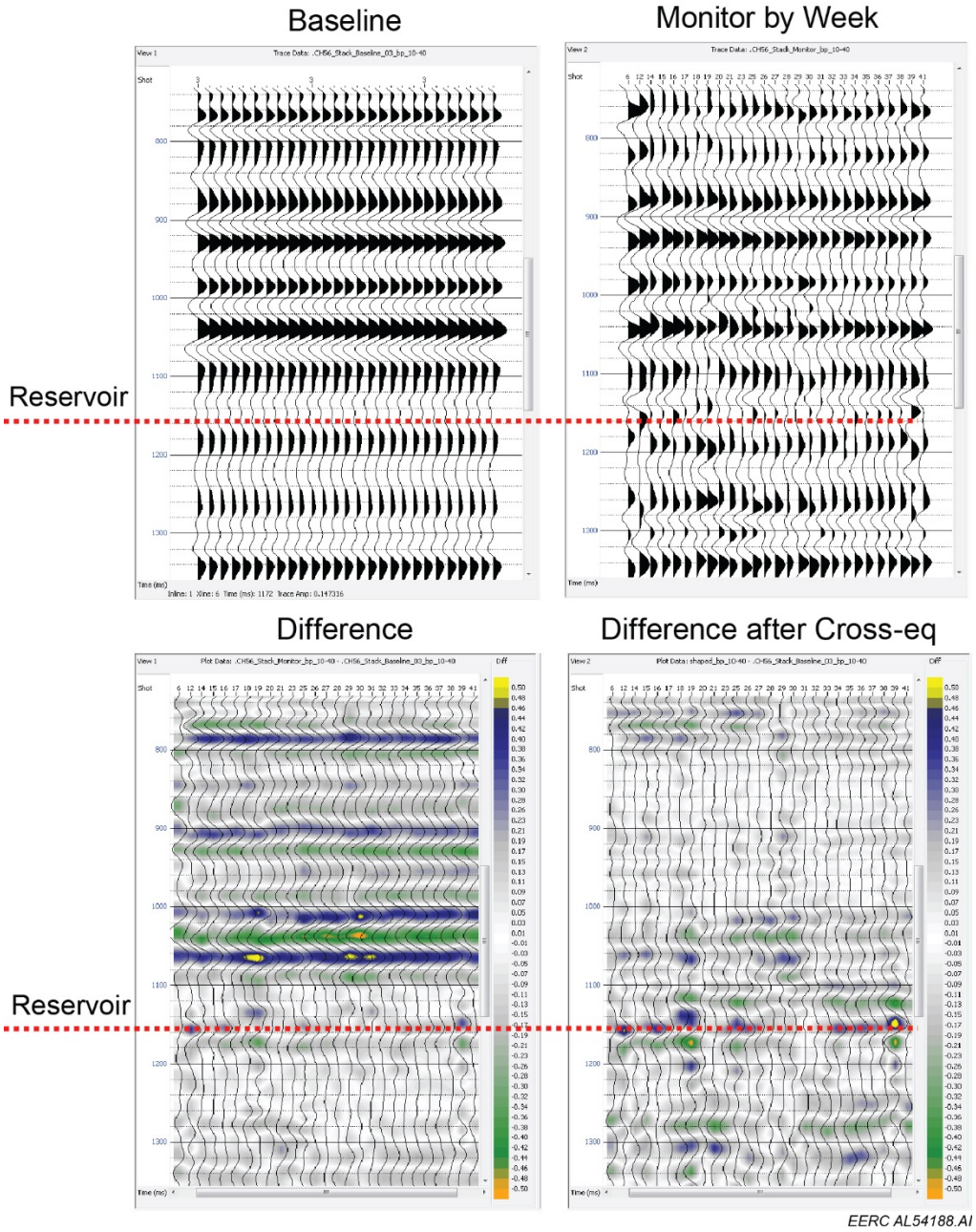

Figure E-11. Time-lapse difference results for Channel 56 before and after cross equalization.

Channel 57 (Figure E-12)

- Offset 2292 feet from the source with the monitor point located ~198 feet south of a CO_2 injection well that started injecting in January 2016, a CO_2 effect is expected at this location. Baseline 2 (November 15, 2015) is used as the reference.

- Change starts at Week 6 (January 3, 2016) and increases and becomes more continuous at Week 20 (May 7, 2016). After cross equalization, change at the reservoir level remains, but is more discontinuous. This is interpreted as a change due to CO_2.

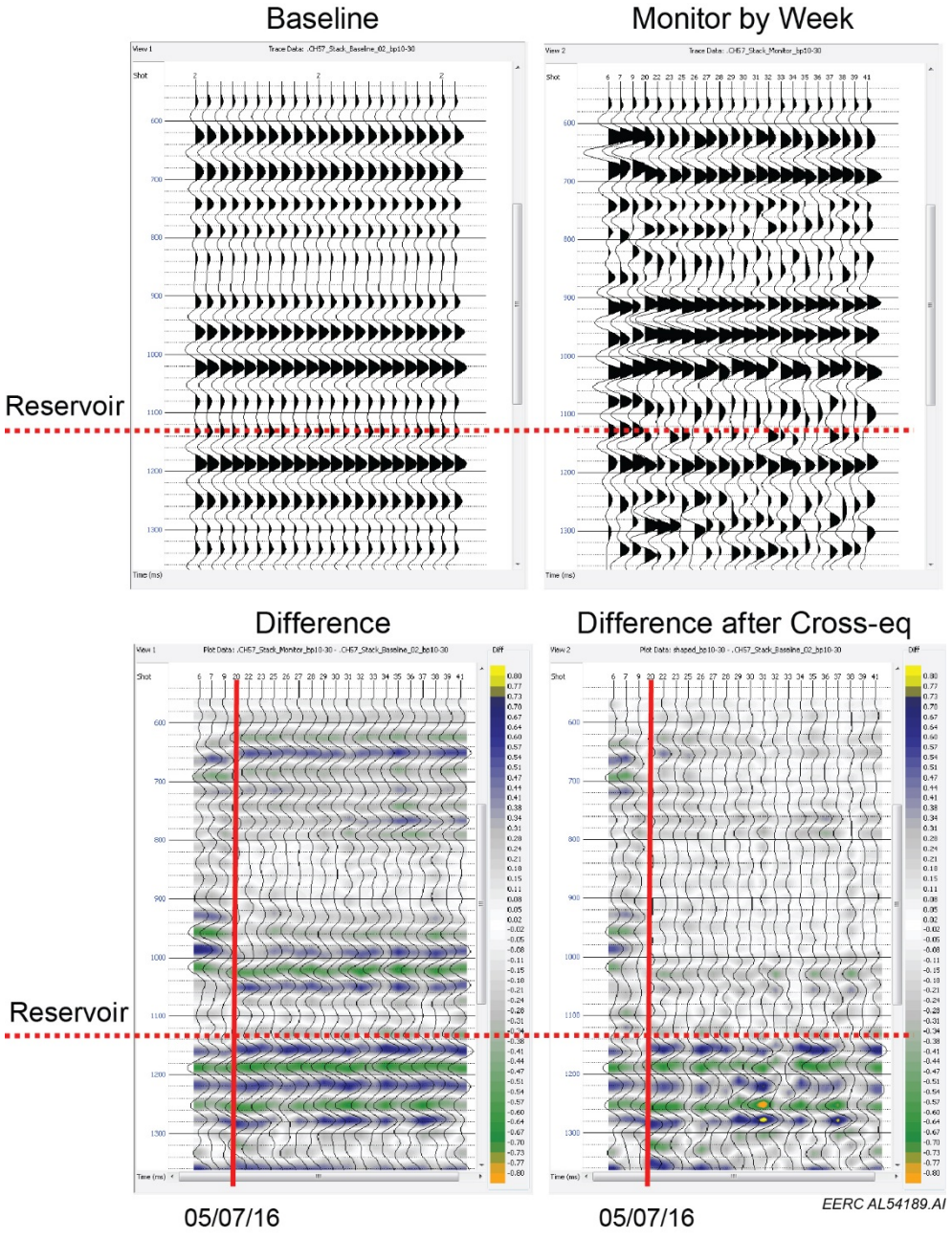

Figure E-12. Time-lapse difference results for Channel 57 before and after cross equalization.

Channel 58 (Figure E-13)

- Offset 2424 feet from the source with the monitor point located ~608 feet south of a CO_2 injection well that started injecting in January 2016, a CO_2 effect is expected at this location. Baseline 2 (November 15, 2015) is used as the reference.

- Prior to cross equalization, there is change across all weeks that becomes more continuous at Week 23 (May 26, 2016). Cross equalization results are ambiguous and impacted by noise. The change on the difference display is interpreted as due to CO_2.

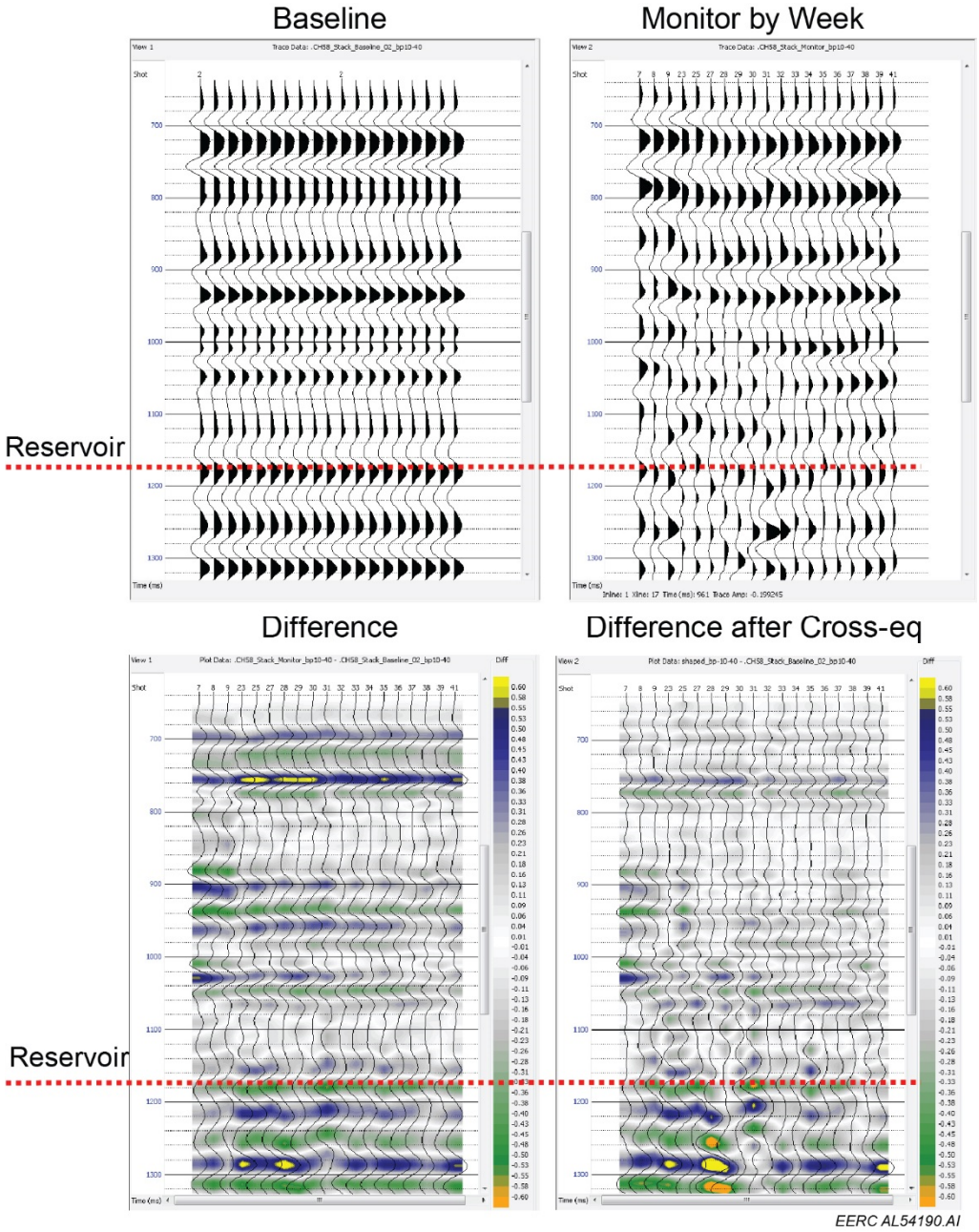

Figure E-13. Time-lapse difference results for Channel 58 before and after cross equalization.

Channel 59 (Figure E-14)

- Offset 2710 feet from the source with the monitor point located ~960 feet south of a CO_2 injection well that started injecting in January 2016, a CO_2 effect is expected at this location. Baseline 2 (November 15, 2015) is used as the reference.

- Prior to cross equalization, change at the reservoir level is ambiguous. After cross equalization, ambiguity remains, although changes at Week 32 are intriguing.

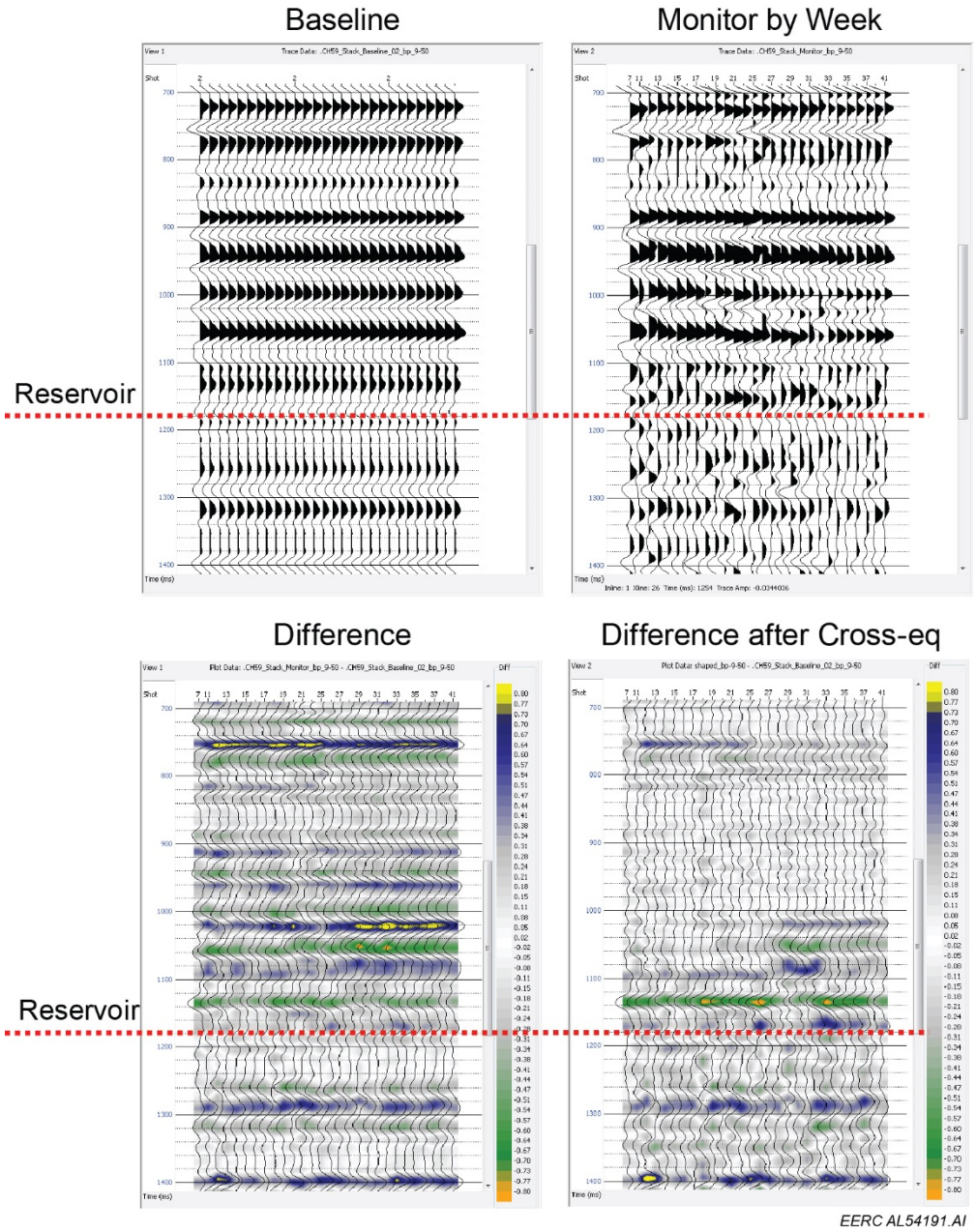

Figure E-14. Time-lapse difference results for Channel 59 before and after cross equalization.

Group 3

Figure E-15 highlights the midpoints corresponding to the eight channels in Group 3.

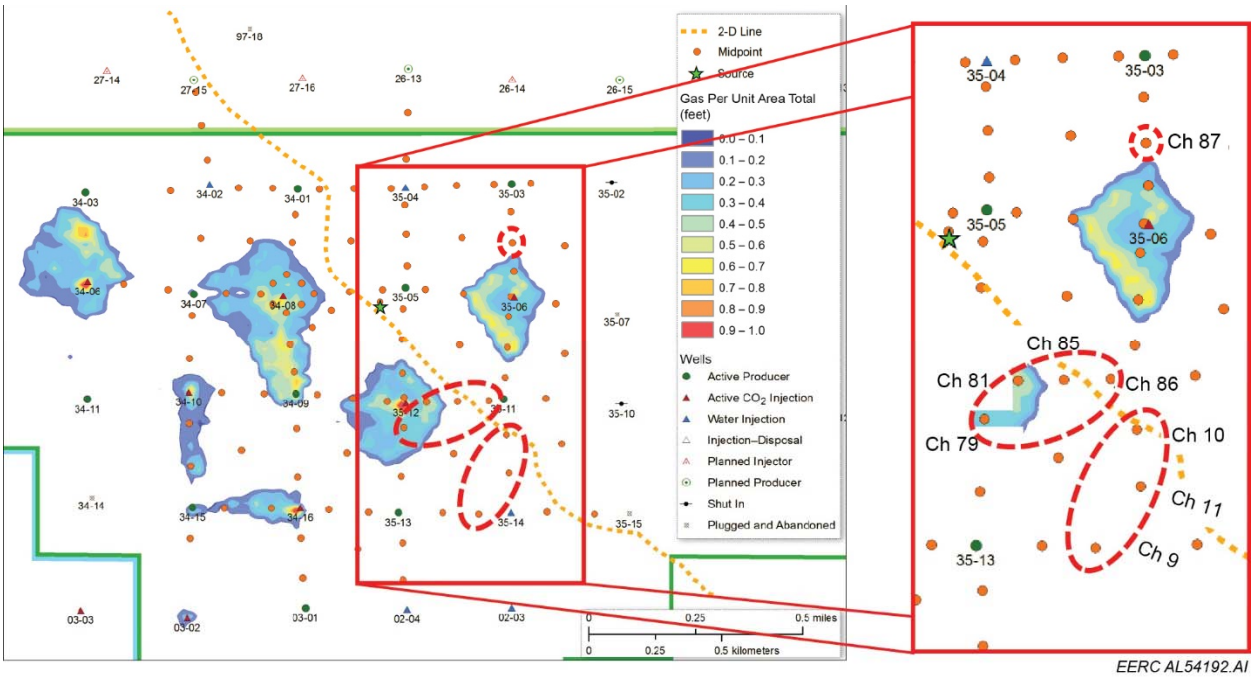

Figure E-15. Map of gas saturation per unit area total generated from dynamic reservoir simulations. The dashed red areas highlight the monitor locations corresponding to the channels in Group 3. The orange dots depict the monitor locations. The light orange dashed line corresponds to the 2-D line.

Channel 9 (Figure E-16)

- Offset 5783 feet from the source with the monitor point located ~400 feet west of a water injection well that started injecting in November 2015, a pressure effect may be present at this location. Baseline 3 (November 29, 2015) is used as the reference.

- There are differences across all weeks on several reflection events. After cross equalization, change is ambiguous, but waveform stability starts at Week 32.

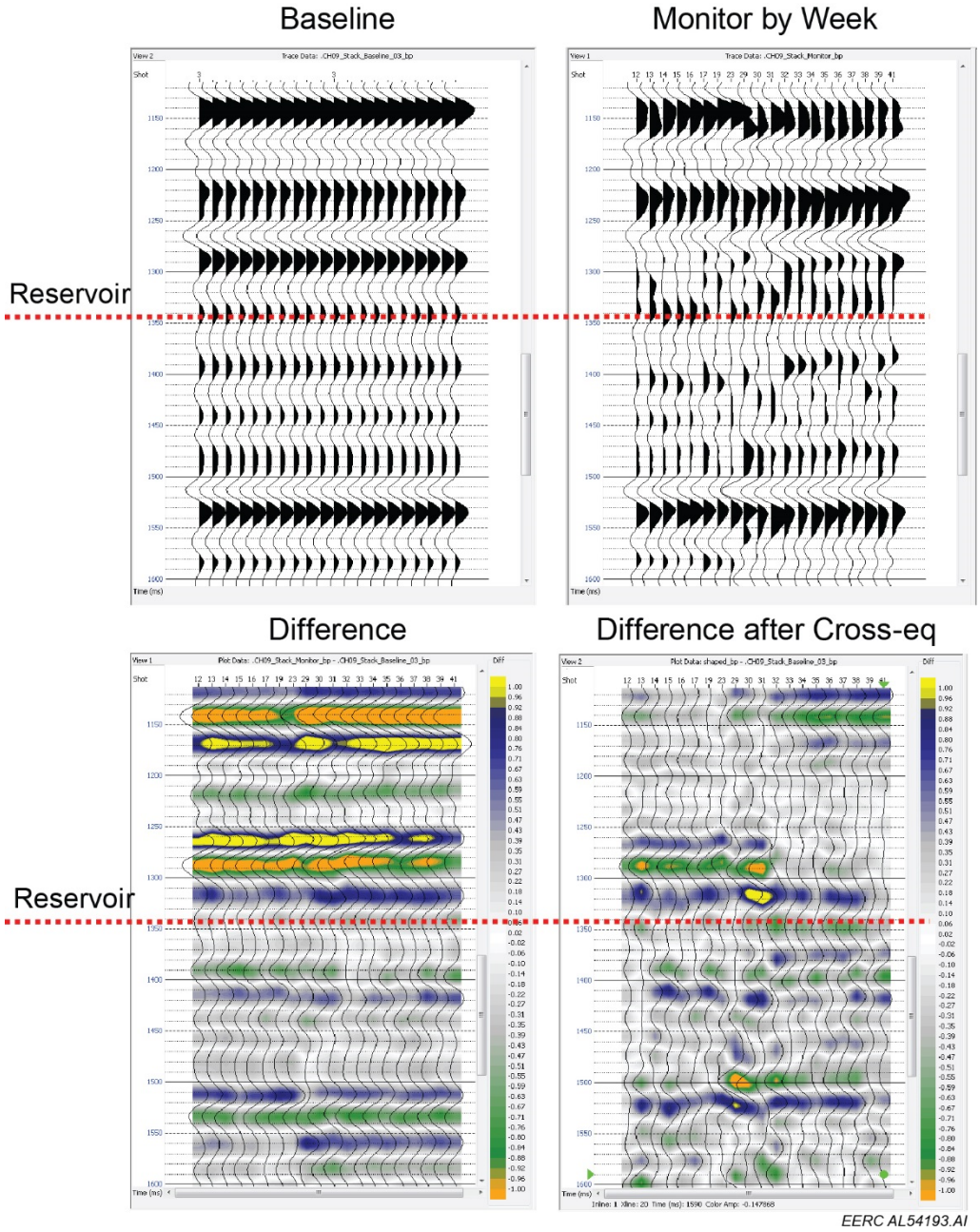

Figure E-16. Time-lapse difference results for Channel 9 before and after cross equalization.

Channel 10 (Figure E-17)

- Offset 4548 feet from the source with the monitor point located ~980 feet north of a water injection well that started injecting in November 2015, a pressure effect may be present at this location. Baseline 3 (November 29, 2015) is used as the reference.

- Prior to cross equalization, there are differences across all weeks on several reflection events. After cross equalization, changes are corrected above and at the reservoir.

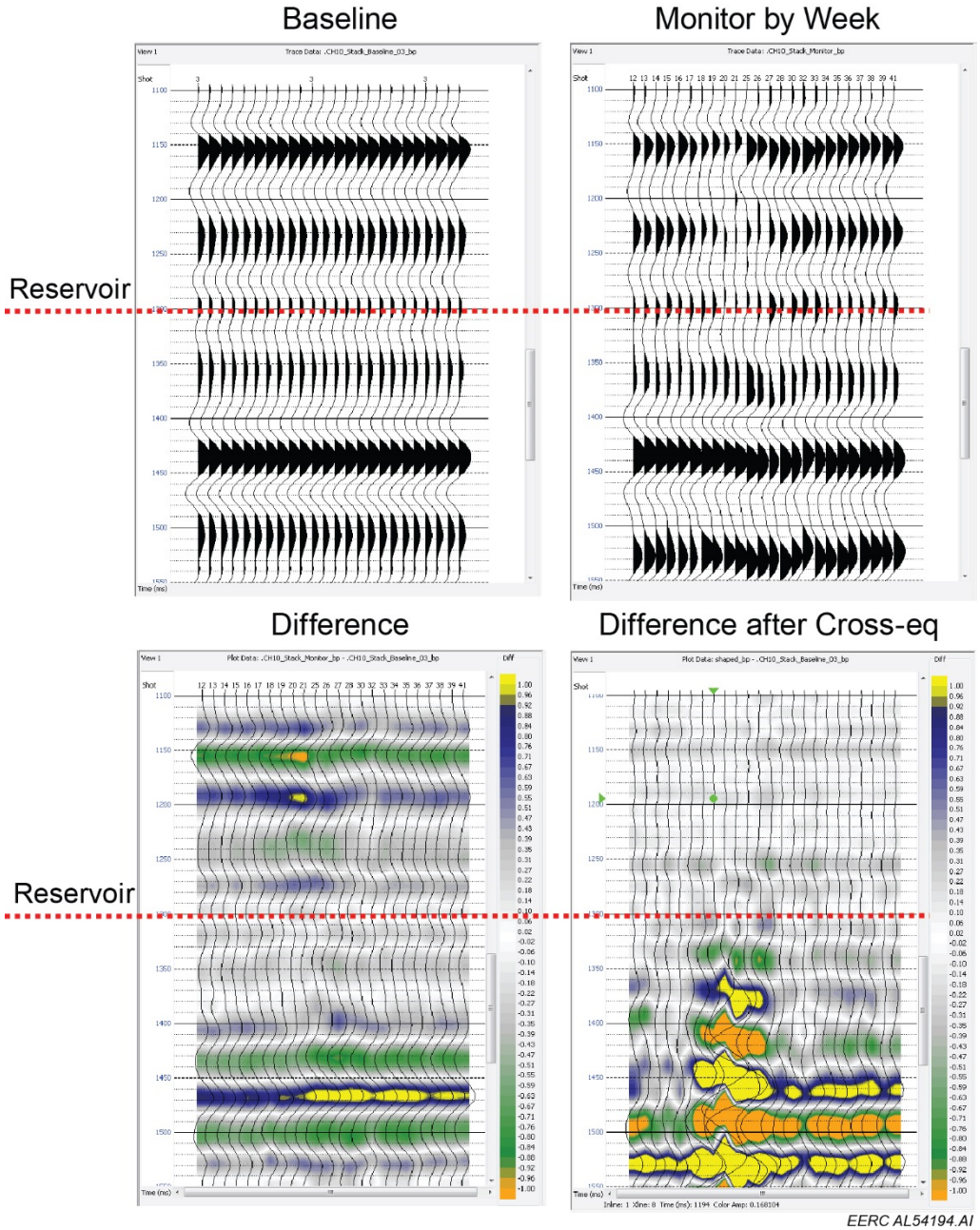

Figure E-17. Time-lapse difference results for Channel 10 before and after cross equalization.

Channel 11 (Figure E-18)

- Offset 5291 feet from the source with the monitor point located ~490 feet north of a water injection well that started injecting in November 2015, a pressure effect may be present at this location. Baseline 2 (November 15, 2015) is used as the reference.

- Prior to cross equalization, there are differences across all weeks on several reflection events. After cross equalization, changes are corrected above and at the reservoir.

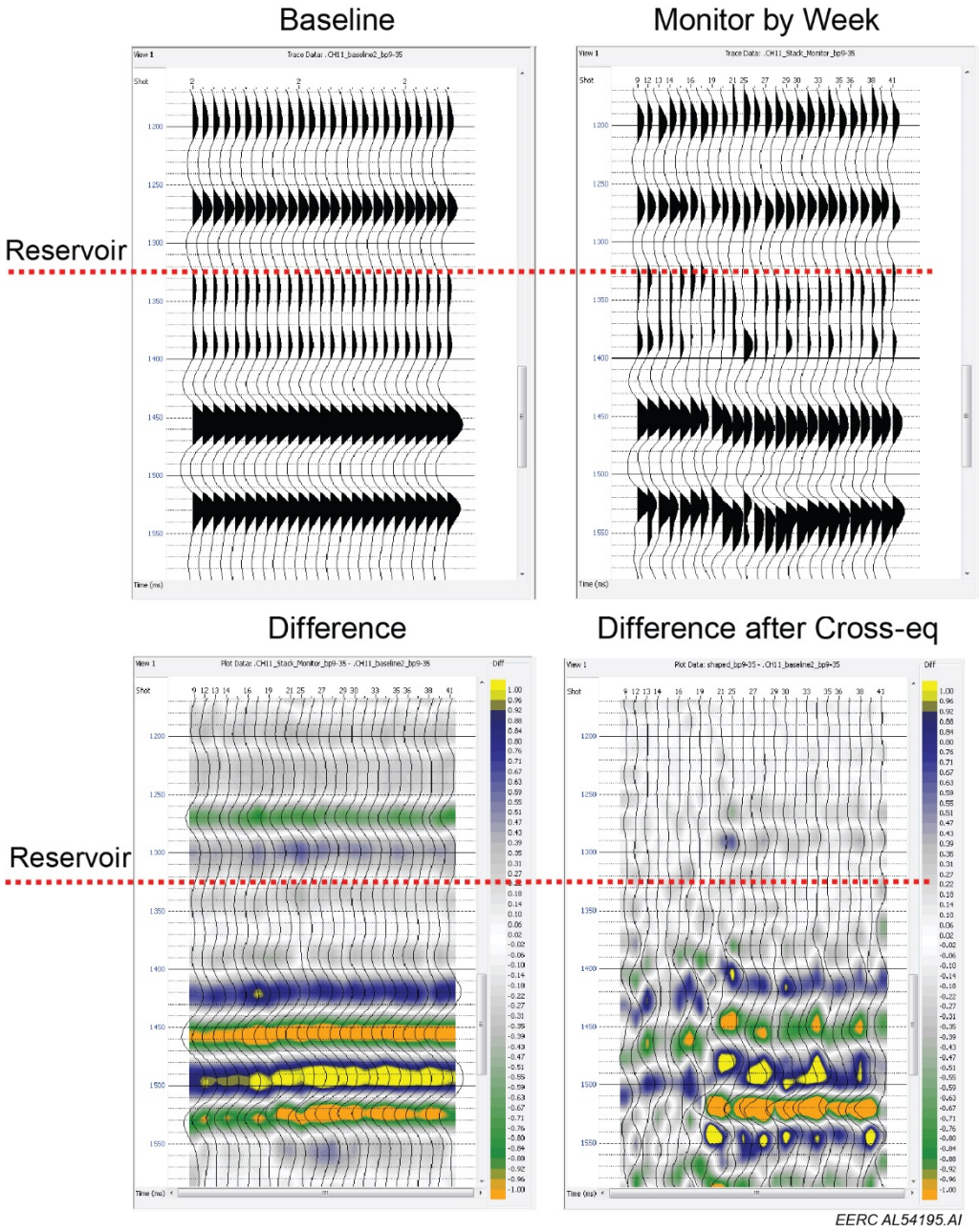

Figure E-18. Time-lapse difference results for Channel 11 before and after cross equalization.

Channel 79 (Figure E-19)

- Offset 3162 feet from the source with the monitor point located ~310 feet south of a CO_2 injection well that started injecting in January 2016. a CO_2 effect is expected at this location. Baseline 3 (November 29, 2015) is used as the reference.

- Prior to cross equalization, there are differences across all weeks on several reflection events. After cross equalization, the change at the reservoir level is still present, but more discontinuous. This change is interpreted to be due to CO_2.

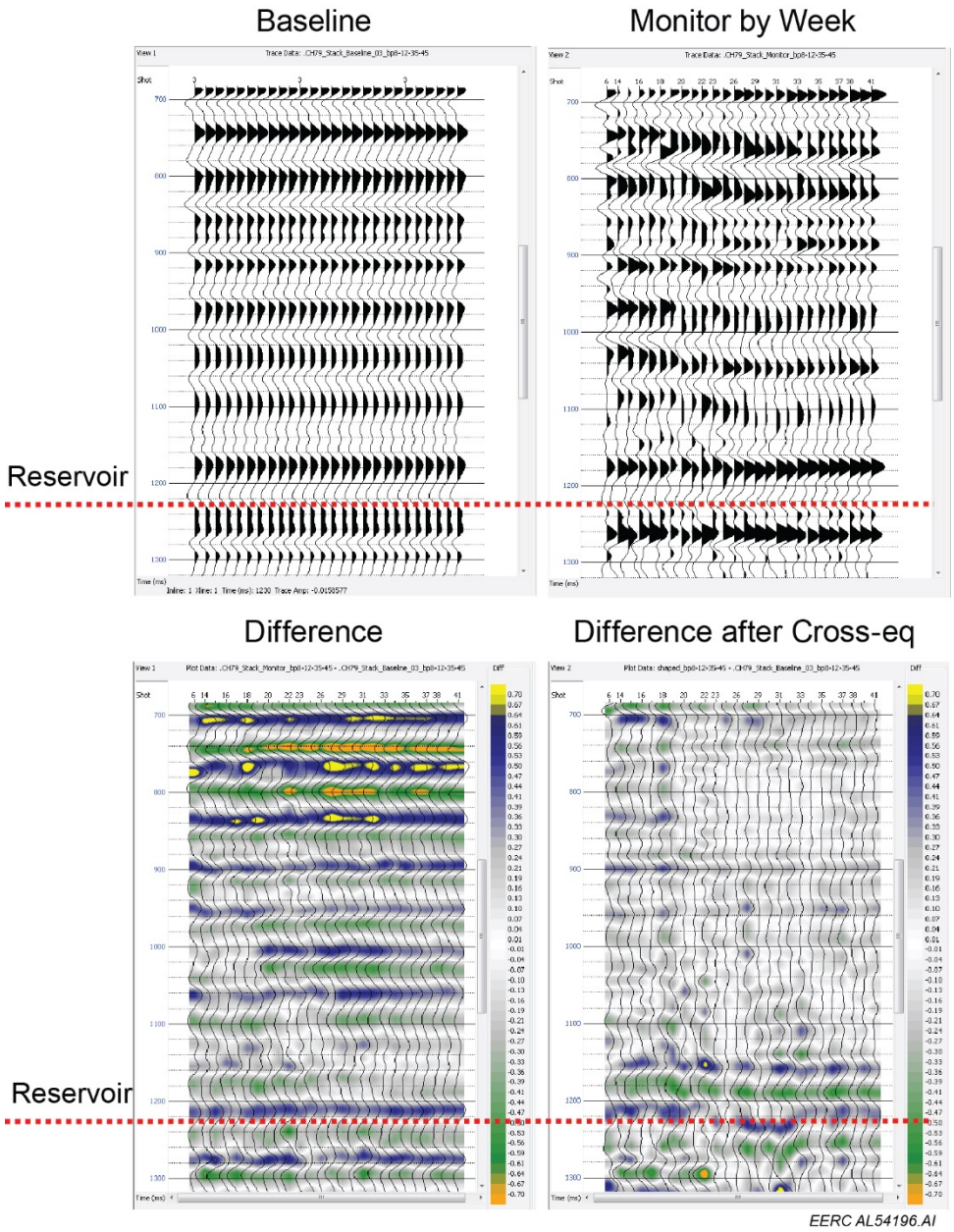

Figure E-19. Time-lapse difference results for Channel 79 before and after cross equalization.

Channel 81 (Figure E-20)

- Offset 2749 feet from the source with the monitor point located ~270 feet east of a CO_2 injection well that started injecting in January 2016, a CO_2 effect is expected at this location. Baseline 3 (November 29, 2015) is used as the reference.

- Prior to cross equalization, there are differences across all weeks on several reflection events. At the reservoir the change appears to increase starting at Week 20 (May 7, 2016). After cross equalization, the change remains at Week 20 (May 7, 2016) and has a variable amplitude.

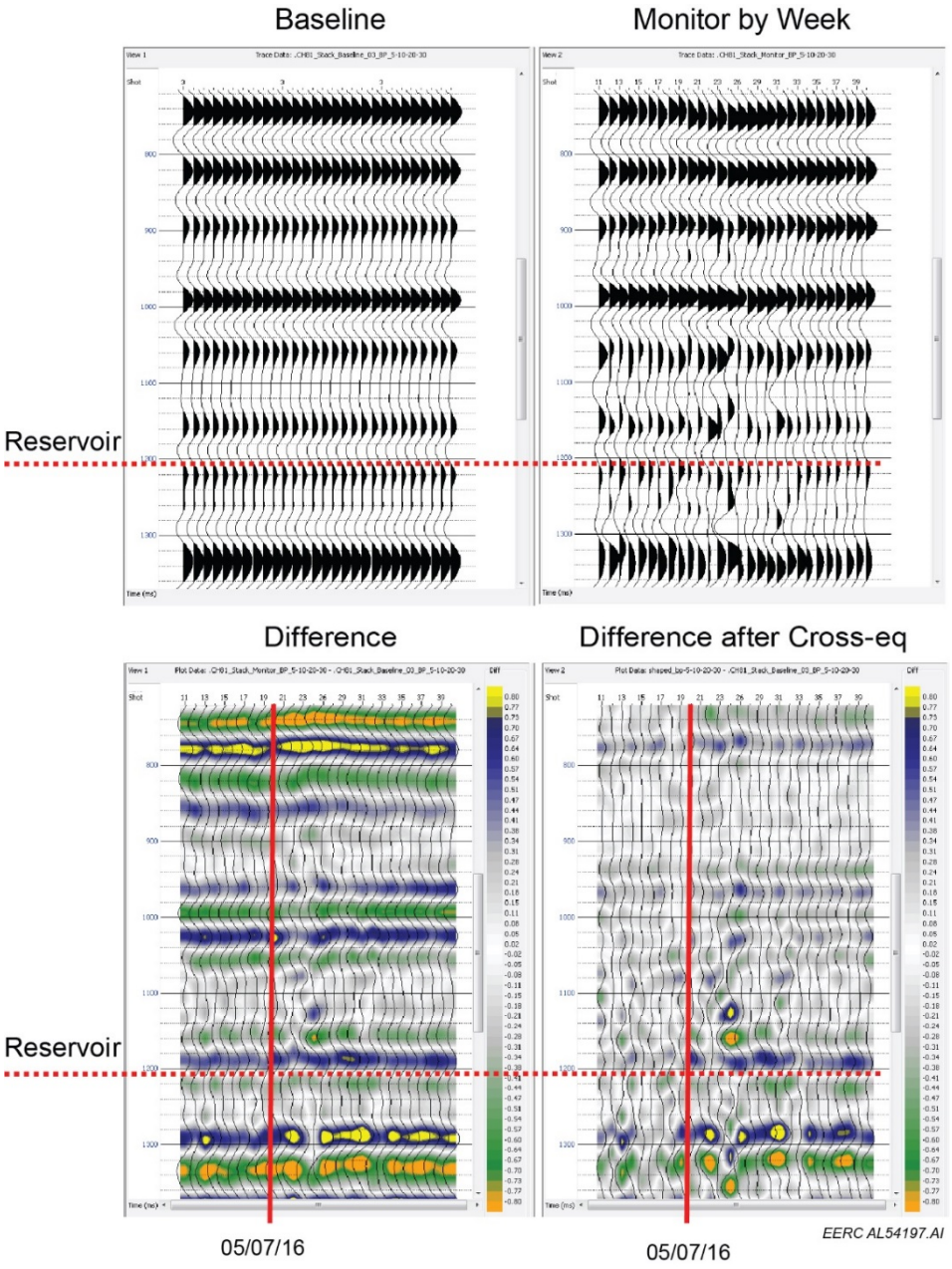

Figure E-20. Time-lapse difference results for Channel 81 before and after cross equalization.

Channel 85 (Figure E-21)

- Offset 3174 feet from the source with the monitor point located ~650 feet east of a CO_2 injection well that started injecting in January 2016, a CO_2 effect is expected at this location. Baseline 4 (December 13, 2015) is the reference.

- Prior to cross equalization, there are differences across all weeks on several reflection events. Below the reservoir the magnitude of change increases across Weeks 21–32 and then decreases, creating ambiguity. Unlike some other channels, after cross equalization, the change above and below the reservoir is not well corrected.

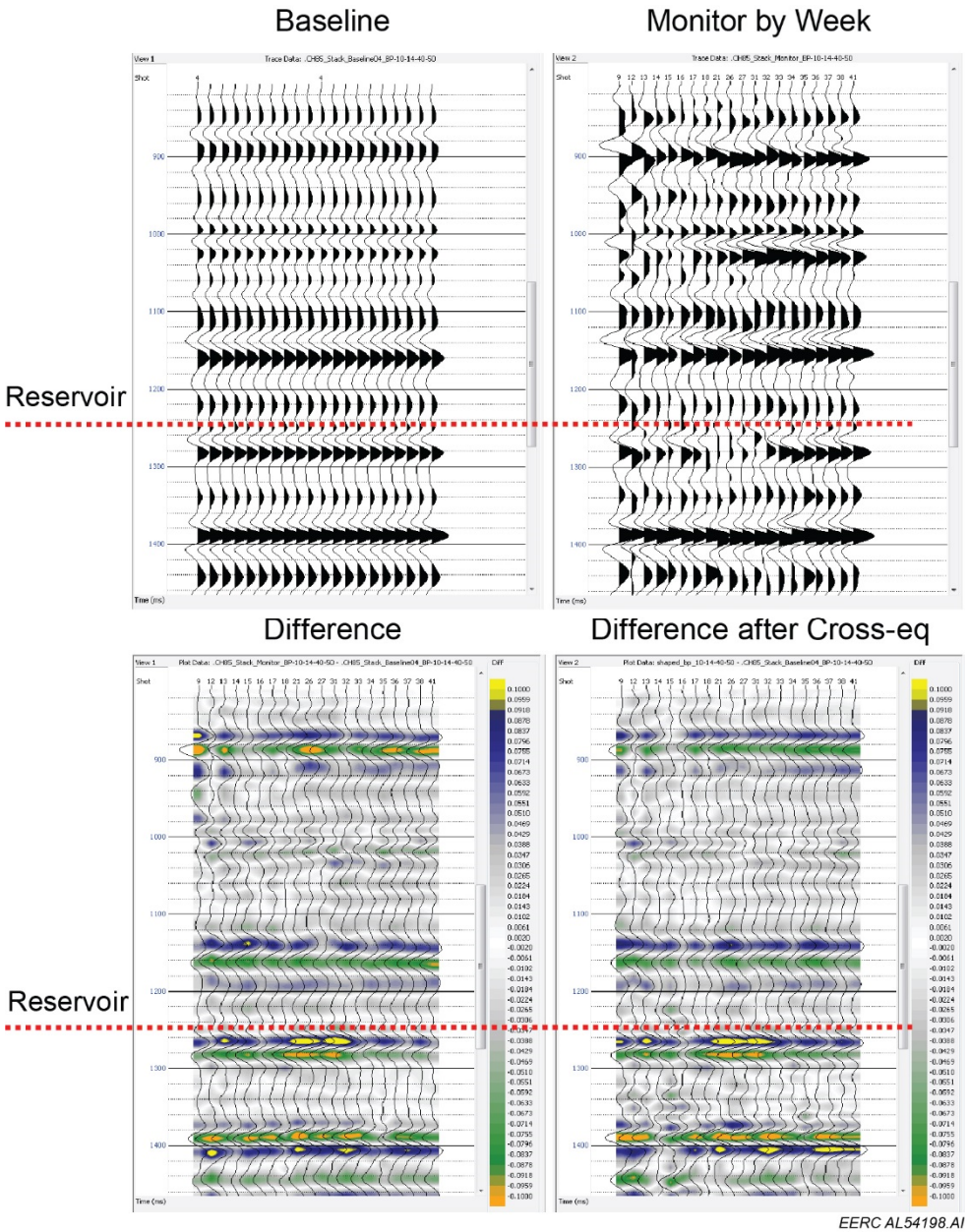

Figure E-21. Time-lapse difference results for Channel 85 before and after cross equalization.

Channel 86 (Figure E-22)

- Offset 3642 feet from the source with the monitor point located ~1030 feet east of a CO_2 injection well that started injecting in January 2016, a CO_2 effect is possible. Baseline 4 (December 13, 2015) is the reference.

- Prior to cross equalization, differences at the reservoir start Week 13 (February 28, 2016) and appear to increase in magnitude over time. After cross equalization, differences at the reservoir remain, but increased magnitude begins later at Week 32 (September 23, 2016). This is interpreted as a CO_2 effect.

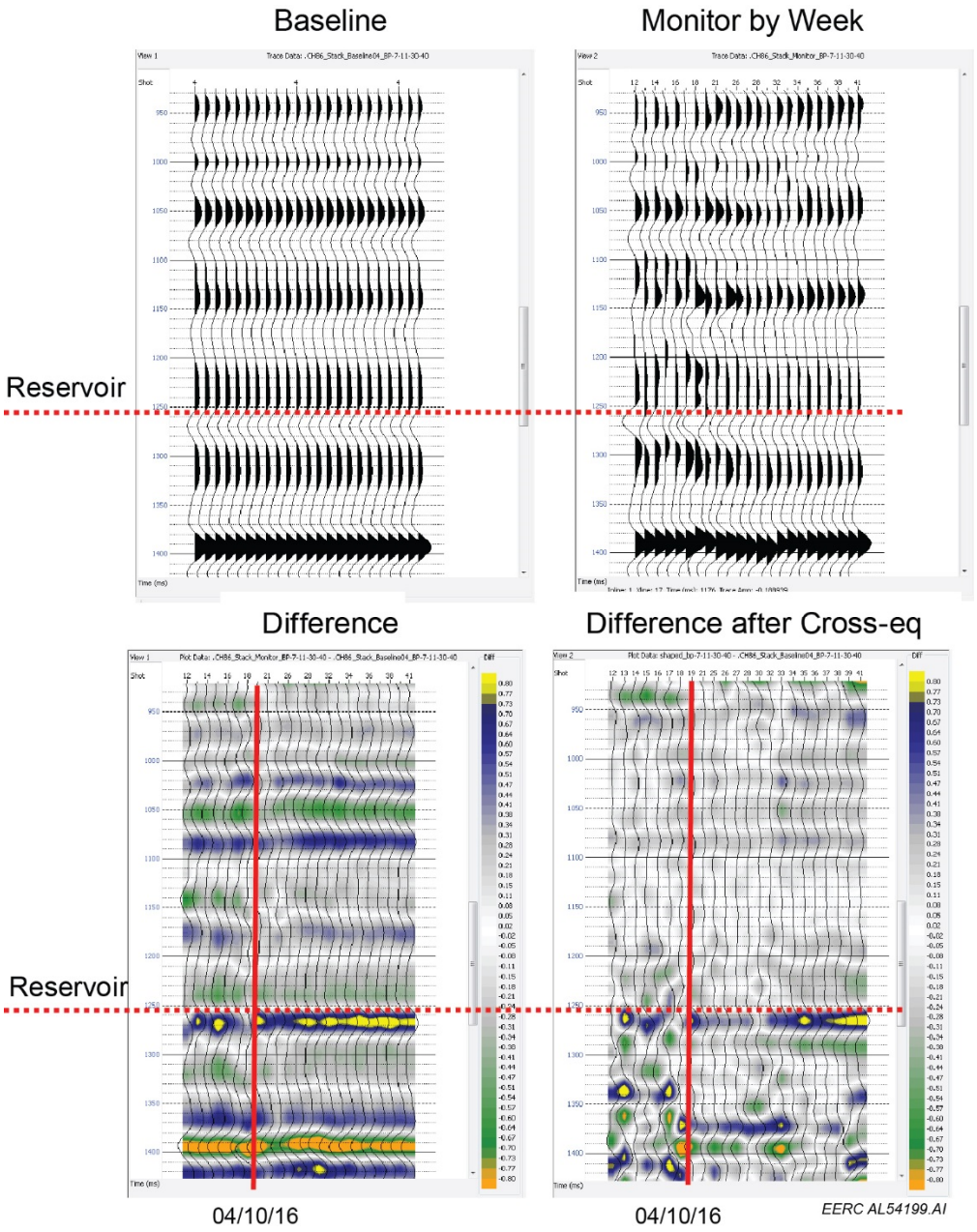

Figure E-22. Time-lapse difference results for Channel 86 before and after cross equalization.

Channel 87 (Figure E-23)

- Offset 3590 feet from the source with the monitor point located ~670 feet north of a CO_2 injection well that started injecting in January 2016, a CO_2 effect is unlikely at this location. Baseline 4 (December 13, 2015) is the reference.

- Prior to cross equalization, there are no significant differences at the reservoir. After cross equalization, there are still no significant differences at the reservoir. No CO_2 is indicated.

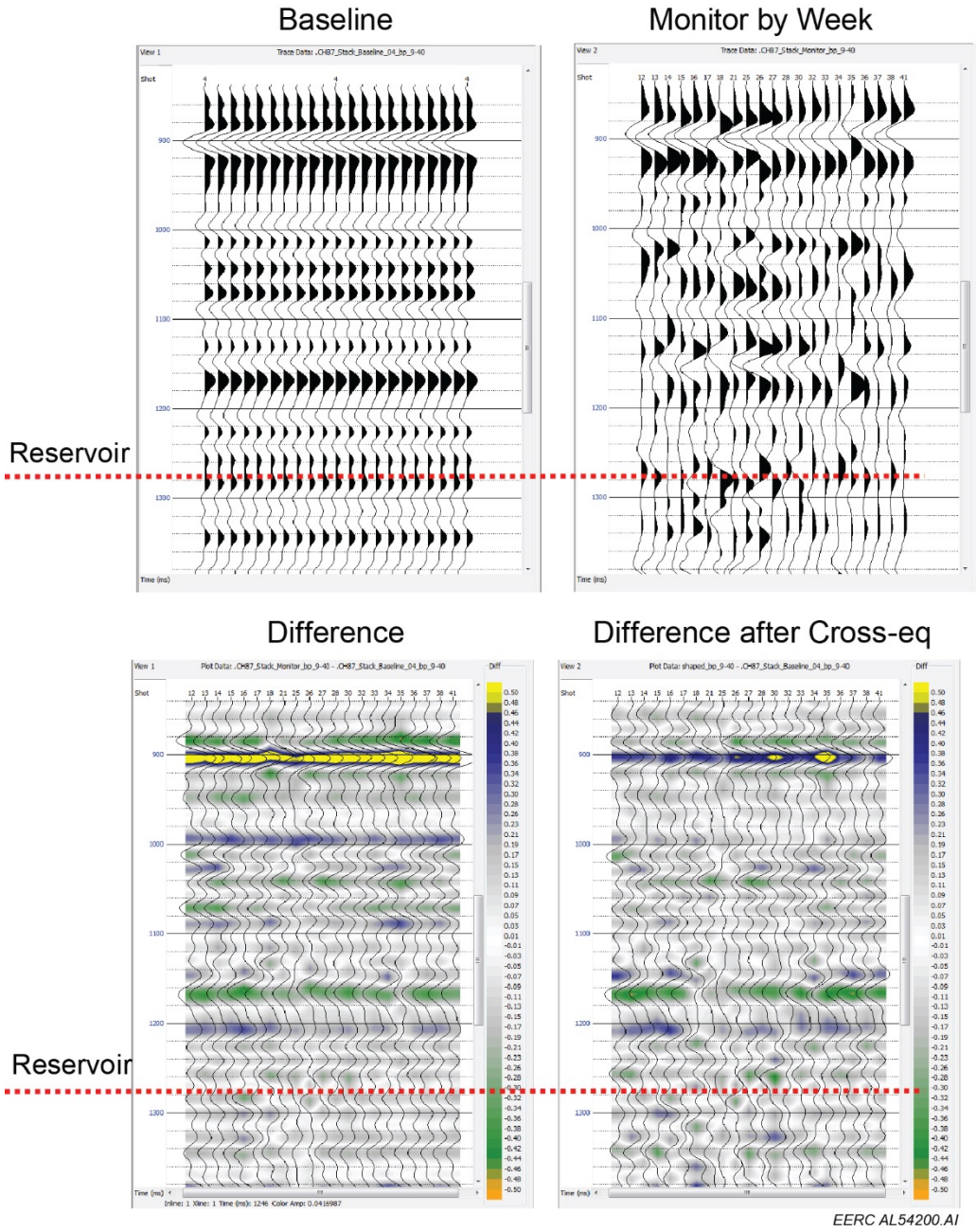

Figure E-23. Time-lapse difference results for Channel 87 before and after cross equalization.

APPENDIX F

RISK REGISTER WITH RISKS REALIZED

RISKS REALIZED

To help guide the technical design and implementation, a formal risk assessment was performed at the beginning of the project. A total of 48 risk items were identified and evaluated across four categories: 1) management, resources, and logistics; 2) equipment failure and field operation; 3) health, safety, environment, and security; and 4) seismic technical. For each risk, the likelihood of occurrence and potential cost and schedule impacts were estimated, and the risks were ranked in order of priority within each category. In order to ensure the highest probability of project success, the project team actively employed an ALARA (as low as reasonably achievable) approach to risk management, with active risks given extra attention throughout the project life cycle. The results of the risk management activities were used to help guide equipment selection and design, the source and surface receiver layout, systems testing, final source installation design (e.g., subgrade footing, etc.), and other activities and equipment configurations presented in the subsequent sections of this document. As the project is now over, the risk register was updated and closed. The risks that were active at project start are now designated as Realized or Not Realized. Eleven active risks were realized. Six were serious enough to impact data quality generally or caused a loss of data over an interval of time. All informed the lessons learned.

Scalable, Automated, Semipermanent Seismic Method for Detecting CO_2 Plume Extent During Geological CO_2 Injection

S/No.	STATUS	RISK	COST IMPACT	SCHEDULE IMPACT	LIKELIHOOD	SCORE	POSSIBLE MITIGATION
(A) MANAGEMENT, RESOURCES, AND LOGISTICS (MRL) ISSUES							
1	Resolved	Crew availability for 1 week each month	$	Week	Low	2	Training and cross-training of sufficient staff to ensure flexibility and redundancy, crew prescheduling.
2	Resolved	Hostile landowners impact site access	$$$	Month	Medium	18	Ensure good landowner relations with EERC. Information sharing and open communications based on care and respect. Negotiate site access agreements and payments to assure access. No-cost extension to project to operate in next development phase with different landowners.
3	Retired	Procurement delays impact project objectives	$$	Month	Medium	12	Awareness of procurement processes, lead times, close attention to order status, preplanning.
4	Resolved	Manufacturing delays impact project objectives	$$	Month	Medium	12	Timing of equipment orders for source and/or recording system adjusted. Alternate deployment locations possible.
5	Resolved	Training gap – insufficient trained staff cause acquisition errors	$$	Day	Low	2	Trained sufficient staff, created “cookbook” help files for field use.

Continued . . .

Scalable, Automated, Semipermanent Seismic Method for Detecting CO_2 Plume Extent During Geological CO_2 Injection (continued)

S/No.	STATUS	RISK	COST IMPACT	SCHEDULE IMPACT	LIKELIHOOD	SCORE	POSSIBLE MITIGATION
(B) EQUIPMENT FAILURE AND FIELD OPERATIONAL (EFFO) ISSUES							
1	Not realized	Difficult access to receiver nodes because of snowfall	$$	Month	Medium	12	Use nodes that have sufficient battery life to delay data harvest by weeks if weather issues make access impossible. Negotiate access using snow machines during winter if sufficient snowfall.
2	Realized	Source remote control failure	$$	Week	Low	8	Engineer redundancy into the system. Assemble components into a rack-mounted unit to minimize loose and open wiring and connections. Use high-quality components. Protect components from the elements, vermin, and environmental risks by proper installation. Overvoltage event damaged system.
3	Realized	Accidental deletion of data	$$$	Month	Low	6	Ensure redundancy of data and sufficient staff training: data remain in nodes until overwritten after months of acquisition, providing a natural backup. Data are auto-downloaded to the server on connection to charging rack. Data are automatically backed up from Derver. Overvoltage event corrupted data file; time stamps were lost. Better procedure would have file downloaded each weekend.
4	Realized	Electric power outage	$	Week	Medium	4	Have a backup source: independent battery power, 6-hour UPS on server and source control PC. A backup generator is available to the project and can be set up in 24 hours for prolonged outages. Overvoltage event destroyed source and remote control electronics.

Continued . . .

Scalable, Automated, Semipermanent Seismic Method for Detecting CO_2 Plume Extent During Geological CO_2 Injection (continued)

S/No.	STATUS	RISK	COST IMPACT	SCHEDULE IMPACT	LIKELIHOOD	SCORE	POSSIBLE MITIGATION
5	Not realized	Fuse blown on source signature recorder	$	Week	Medium	4	Ensure proper power hookup: consult with SSI, have spare fuses on hand. Train operators field staff on replacement.
6	Not realized	Receiver nodes frozen in place during winter	$$	Day	Medium	4	Devise in advance a method of removing nodes that prevents damage or alternate approach. Check node battery status and if possible leave in place to harvest on a later visit after milder weather.
7	Not realized	Rodents in the source building or server trailer	$	Week	Medium	4	Steel wool under shed walls to prevent tunneling, metal panels, poison, traps, dryer sheets.
8	Not realized	Hard drive failure in source control PC	$	Week	Low	2	Have a second drive: reboot option to backup second drive in computer with similar configuration.
9	Realized	Deep battery discharge on source	$	Week	Low	2	Proper trickle chargers connected to main power to ensure constant charge on batteries: heated shed, monthly check, and maintenance. Damaged during overvoltage event.
10	Realized	Handheld trimble unit failure, node failure, charge rack failure	$$	Day	Low	2	Incorporate redundancy of equipment. Online access to vendor engineers, including remote log-in. Online engineer reset node, but ~8 weeks of unrecorded data occurred.
11	Not realized	Source elastomer break	$	Week	Low	2	Spare elastomer on hand and stored with source. Staff trained on elastomer replacement and replacement standard operating procedure available onsite.
12	Realized	Loss of Internet service	$	Week	Low	2	Two mobilizations from Grand Forks were required to meet technician and reinstate service. One was weather-related, the other an overvoltage.

Continued . . .

Scalable, Automated, Semipermanent Seismic Method for Detecting CO_2 Plume Extent During Geological CO_2 Injection (continued)

S/No.	STATUS	RISK	COST IMPACT	SCHEDULE IMPACT	LIKELIHOOD	SCORE	POSSIBLE MITIGATION
13	Not realized	Dust and dirt accumulation in source control PC causes failure	$	Week	Low	2	Seal equipment rack with panels to minimize intrusion; put dryer sheets inside to repel rodents.
14	Not realized	Livestock interference on 2-D seismic line during data acquisition operation	$	Day	Medium	2	Strong preplanning, quick execution under 2 days to minimize interaction with livestock.
15	Not realized	Loss of nodes due to construction activities (bulldozed node)	$$	Day	Low	2	Coordinate and communicate with operator field staff, contractors, and landowners: Ensure locations of nodes are known by them and that the EERC is made aware of possible impactful activities.
16	Resolved	Lightning strike on source shed or EERC server trailer	$$$	Month	Low	9	Install lightning rods at both locations.
17	Resolved	Equipment damaged in transit	$$$	Month	Low	9	Use experienced driving staff, driver safety training, and compliance with traffic laws. Ensure equipment is insured for transit.
18	Resolved	Livestock and rodents chew on receiver system exposed wires	$$	Week	Medium	8	Choose a self-contained system without exposed wires, such as FairfieldNodal.

Continued . . .

Scalable, Automated, Semipermanent Seismic Method for Detecting CO_2 Plume Extent During Geological CO_2 Injection (continued)

S/No.	STATUS	RISK	COST IMPACT	SCHEDULE IMPACT	LIKELIHOOD	SCORE	POSSIBLE MITIGATION
(C) HEALTH, SAFETY, ENVIRONMENT, AND SECURITY (HSES) ISSUES							
1	Not realized	EERC crew involved in serious safety incident or injury	$$$	Month	Medium	18	Safety training and awareness of procedures, safety awareness through briefings, safety culture, proper PPE. Driver training, buddy system, check-in/checkout from field. Lock out, tag out procedure for maintenance. View source remotely prior to operation to ensure it is clear of personnel. Proper shielding of moving parts.
2	Not realized	EERC staff has OSHA reportable injury while performing field work	$$$	Month	Low	9	Comply with field operator and EERC safety requirements: Coordinate and communicate with field and safety staff immediately on occurrence. Use proper PPE, practice safety awareness, periodic safety training. Promote safety culture. Lockout, tagout procedure for maintenance. View source remotely prior to operation to ensure it is clear of personnel. Proper shielding of moving parts.
3	Not realized	Fire at source shed or EERC server trailer	$$$	Month	Low	9	Proper housekeeping: store fuel away from source and trailer, keep brush trimmed and a buffer zone. Fire extinguishers in all vehicles and locations. Staff training.
4	Not realized	Natural disaster, e.g., grass fire, tornado, flood at source shed or EERC server trailer	$$$	Month	Low	9	Install source on a higher elevation location. Have emergency health, safety, and environment (HSE) plan with location and contact information of nearest emergency services available in all locations and vehicles. Employ standard operating and emergency procedures that include muster and evacuation points. Crew training.

Continued . . .

Scalable, Automated, Semipermanent Seismic Method for Detecting CO_2 Plume Extent During Geological CO_2 Injection (continued)

S/No.	STATUS	RISK	COST IMPACT	SCHEDULE IMPACT	LIKELIHOOD	SCORE	POSSIBLE MITIGATION
5	Not realized	Field operator safety officer shuts down source operation	$$$	Week	Low	6	Comply with field operator requirements: coordinate and communicate with safety staff. Ensure safe install and operation of source, anticipating possible points of objection in advance. Provide effective and necessary signage and warnings on source shed - CAUTION - AUTO-OPERATING EQUIPMENT, etc. Ensure lock on shed. Install warning light to be activated prior to source activation.
6	Not realized	Source security, shed break-in, or stolen equipment	$$	Month	Low	6	Secure lock on shed. Coordination with field operator and contractors.
7	Not realized	Livestock injury due to trip on node or node hole	$$	Week	Low	4	Install nodes so top is at grade level. Cover hole when node is removed to avoid trip hazard.
8	Not realized	Theft of receiver nodes	$$	Week	Low	4	Ensure field workers are made aware of the project and equipment used: ID labels on units, notification of field operator workers and landowners, good relations with landowners.
9	Not realized	Node destruction due to vandalism or as firearm targets	$$	Week	Low	4	Install nodes so top is at grade level. Communicate with landowners regarding node appearance, install, and location.
10	Not realized	Hacking attack on networked systems	$	Week	Low	2	Firewall and network security. Secure passwords. Limited access to network information.
11	Not realized	Venomous snakebite during field work	$	Day	Low	1	Usage of proper PPE (snake chaps) and safety and environmental awareness.
12	Not realized	Crew member illness or other lack of availability	$	Day	Low	1	Crew flexibility, sufficient cross-training of staff to allow substitution. HSE plan with nearest emergency services, evacuation route, and contact information.
13	Realized	Vehicle breakdown, getting stuck, or flat tire in the field	$	Day	Low	1	Preventive maintenance, careful operation, safety awareness. 1) Vehicle slid off wet road, pulled back on by backhoe. 2) Vehicle slid off road, trees damaged fender.

Continued . . .

Scalable, Automated, Semipermanent Seismic Method for Detecting CO_2 Plume Extent During Geological CO_2 Injection (continued)

S/No.	STATUS	RISK	COST IMPACT	SCHEDULE IMPACT	LIKELIHOOD	SCORE	POSSIBLE MITIGATION
(D) SEISMIC TECHNICAL ISSUES							
1	Partially realized	CO_2 migration too slow; insufficient accumulation to be seismically visible during project data-gathering period	$$$	Month	Low	9	Coordinate with field operator and use proper array design to ensure monitoring of early injectors if injection development is phased over time. If possible and required to meet project objectives, request a no-cost extension to monitor for a longer period. Only a fraction of nodes encountered changes because of CO_2.
2	Not realized	Velocity model inaccuracies result in ambiguous results	$	Month	Medium	6	Continuous refinement of velocity model even after data acquisition starts. Use velocities from well logs and surface seismic. Acquire an array sonic log in a well in Phase 4. Generate a separate model using a different modeling application. Refine model to match physical measurements.
3	Realized	Data-processing challenges provide ambiguous results	$	Month	Medium	6	Assign processing to experienced geophysical staff. Still experienced interpretation challenges because of noise. Contract assistance from outside expertise if required.
4	Realized	Array single-fold geometry impacted by coherent noise (ground roll)	$	Week	Medium	4	Ensure sufficient offset of nodes from source: ensure ground roll attenuates enough to avoid swamping near offset nodes. Experiment with gain settings if strong ground roll overdrives receivers. Redesign array near source if necessary. Approximately 11 nodes less than 2200' offset from source that could have been affected by CO_2 were impacted beyond recovery.

Continued . . .

Scalable, Automated, Semipermanent Seismic Method for Detecting CO_2 Plume Extent During Geological CO_2 Injection (continued)

S/No.	STATUS	RISK	COST IMPACT	SCHEDULE IMPACT	LIKELIHOOD	SCORE	POSSIBLE MITIGATION
5	Not realized	Poor time-lapse seismic data repeatability due to inconsistent installation of receiver nodes at survey stations	$	Day	Medium	3	Train crew on proper installation practice to ensure consistent install; provide pocket level and compass to ensure proper leveling and orientation.
6	Realized	Environmental noise due to background activity impacting on seismic signal	$	Day	Medium	2	Acquire data during field quiet times – evenings or weekends. Night or dawn shooting would have minimized noise from wind.
7	Resolved	Injection starts before deployment of the array (Phase 4)	$$	Month	Medium	12	Install before injection: coordinate with field operator, maintain good landowner relations, acquire equipment, ensure training ahead of injection, preplan, and coordinate sequence of activities. If timing is close and installation is imminent, the mitigation is that it takes some time for sufficient gas volume percentage to build to impact p-wave velocity and be visible. If installation is delayed for weeks after injection starts, a no-cost extension to move project site to the subsequent field development phase may be required.
8	Realized/ resolved	Injection starts before deployment of the array (Phase 2)	$$	Month	High	18	Install before injection: coordinate with field operator, negotiate contract with seismic vendor for equipment and services ahead of injection, preplan and coordinate sequence of activities. No-cost extension to move project site to the subsequent field development phase was executed.

Continued . . .

Scalable, Automated, Semipermanent Seismic Method for Detecting CO_2 Plume Extent During Geological CO_2 Injection (continued)

S/No.	STATUS	RISK	COST IMPACT	SCHEDULE IMPACT	LIKELIHOOD	SCORE	POSSIBLE MITIGATION
9	Realized/ resolved	Injection starts before deployment of the array (Phase 3)	$$	Month	High	18	Install before injection: coordinate with field operator, acquire equipment, ensure training ahead of injection, preplan, and coordinate sequence of activities. If timing is not close and installation is delayed for weeks after injection starts, move project site to the subsequent field development phase.
10	Resolved	Source strength – offset limited energy	$$$	Month	Medium	18	Choose a strong source: use surface source, purchase largest model available (Gisco ESS-850). Source and recording system were tested during September 2015 training to provide signal to at least 1.5-mile offset.
11	Resolved	Repeated source firing digs a hole or otherwise impacts signal consistency	$$	Week	Medium	8	Design and install a broad and heavy source footing at grade to ensure consistent source signature over project period.
12	Resolved	Source signature varies with near-surface conditions, complicating recognition of true variations due to CO_2 migration	$	Day	Medium	2	Incorporate time-lapse calibration data-processing methodology to compensate for seasonal changes in source signature, as learned from the VSP acquisition and data-processing experience and from the surface 4-D processing methods.

Continued . . .

Scalable, Automated, Semipermanent Seismic Method for Detecting CO_2 Plume Extent During Geological CO_2 Injection (continued)

KEY			
STATUS			
	Active	Risk to the project that is possible.	
	Realized	Risk that has been realized and actions have been taken in response to it.	
	Resolved	Risk that is no longer applicable because of mitigation or intentional project changes.	
	Retired	Risk that is no longer applicable or overcome by events.	
COST			**FOR SCORE CALCULATION…**
	$	Hundreds of dollars	1
	$$	Thousands of dollars	2
	$$$	Tens of thousands of dollars	3
SCHEDULE			
	Day	Days of delay	1
	Week	Week or weeks of delay	2
	Month	Month or months of delay	3
LIKELIHOOD			
	Low	<20 % probability (typically much lower)	1
	Medium	20% to 50% probability	2
	High	greater than 50%	3

Scoring example: A risk marked as $$ = 2, day = 1, high = 3… scores as 2 × 1 × 3 = 6.